AD-A173 816 LIFE-CYCLE ANALYSIS OF CORRODING SHEET PILE STRUCTURES 1/2
FOR A LOCK AND DAM(U) CONSTRUCTION ENGINEERING RESEARCH
LAB (ARMY) CHAMPAIGN IL F W KEARNEY SEP 86

UNCLASSIFIED CERL-TR-M-86/12 F/G 13/2 NL

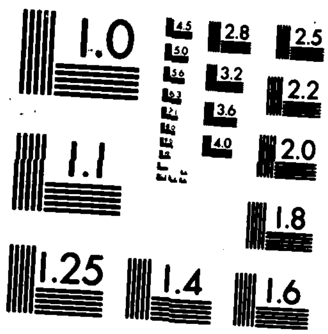

MICROCOPY RESOLUTION TEST CHART
NATIONAL BUREAU OF STANDARDS-1963-A

(2)

US Army Corps
of Engineers
Construction Engineering
Research Laboratory

USA-CERL

TECHNICAL REPORT M-86/12
September 1986

AD-A173 016

Life-Cycle Analysis of Corroding Sheet Pile Structures for a Lock and Dam

by
Frank W. Kearney

This report documents research conducted at the Thomas J. O'Brien Lock and Dam on the Illinois Waterway in Chicago to assess its structural condition, provide a structural quality-vs.-time prognosis, and develop an appropriate corrosion mitigation program. Although there is an abundance of design information for steel sheet pile structural design, including a program in the Corps of Engineers' computer-aided structural engineering (CASE) library, these programs are for new construction and do not consider the consequences of corrosion damage. To realistically determine the structural quality of the O'Brien Lock and to develop a credible projection of its usable life, a specialized analysis had to be developed for this particular structure; however, the analysis had to be general enough for use in other similar structures throughout the Corps.

Detailed field and laboratory analyses indicated that there is a large safety factor in the structure and that 0.25 in. of corrosion can be tolerated anywhere without catastrophic results. However, corrosion that exceeds 0.25 in. in highly stressed areas could cause catastrophic results.

The extreme value of corrosion calculated for the lock and dam is 0.0024 in. per year, which means that 83 years of corrosion must occur to achieve the 0.25 in. value.

It was found that cathodic protection could be used successfully at this structure to prevent additional corrosion damage. A deep well anode system is ideally suited for this project.

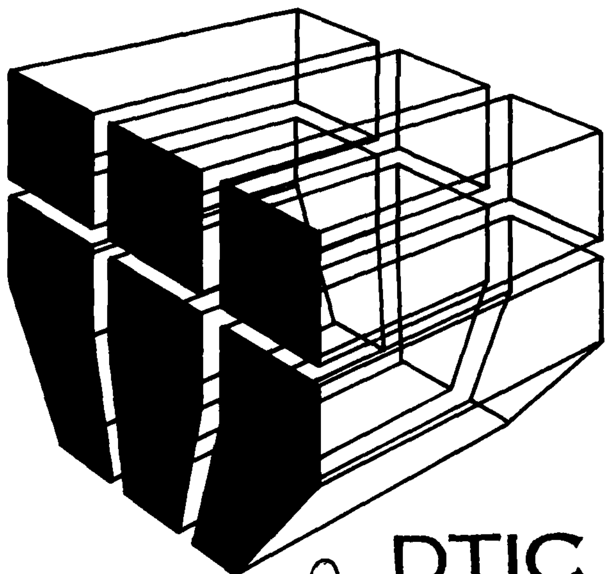

Approved for public release; distribution unlimited.

86 10 16 130
86 10 16 130

UNCLASSIFIED

SECURITY CLASSIFICATION OF THIS PAGE (When Data Entered)

REPORT DOCUMENTATION PAGE		READ INSTRUCTIONS BEFORE COMPLETING FORM
1. REPORT NUMBER CERL-TR-M-86/12	2. GOVT ACCESSION NO. A173 016	3. RECIPIENT'S CATALOG NUMBER
4. TITLE (and Subtitle) LIFE-CYCLE ANALYSIS OF CORRODING SHEET PILE STRUCTURES FOR A LOCK AND DAM		5. TYPE OF REPORT & PERIOD COVERED 6. PERFORMING ORG. REPORT NUMBER
7. AUTHOR(s) Frank W. Kearney		8. CONTRACT OR GRANT NUMBER(s)
9. PERFORMING ORGANIZATION NAME AND ADDRESS U.S. Army Construction Engr Research Laboratory P.O. Box 4005 Champaign, IL 61820-1305		10. PROGRAM ELEMENT, PROJECT, TASK AREA & WORK UNIT NUMBERS
11. CONTROLLING OFFICE NAME AND ADDRESS		12. REPORT DATE September 1986 13. NUMBER OF PAGES 119
14. MONITORING AGENCY NAME & ADDRESS(if different from Controlling Office)		15. SECURITY CLASS. (of this report) UNCLASSIFIED 15a. DECLASSIFICATION/DOWNGRADING SCHEDULE

16. DISTRIBUTION STATEMENT (of this Report)

Approved for public release; distribution unlimited.

17. DISTRIBUTION STATEMENT (of the abstract entered in Block 20, if different from Report)

18. SUPPLEMENTARY NOTES

Copies are available from the National Technical Information Service
Springfield, VA 22161

19. KEY WORDS (Continue on reverse side if necessary and identify by block number)

Thomas J. O'Brien Lock and Dam
corrosion
locks (waterways)
dams

20. ABSTRACT (Continue on reverse side if necessary and identify by block number)

This report documents research conducted at the Thomas J. O'Brien Lock and Dam on the Illinois Waterway in Chicago to assess its structural condition, provide a structural quality-vs.-time prognosis, and develop an appropriate corrosion mitigation program. Although there is an abundance of design information for steel sheet pile structural design, including a program in the Corps of Engineers' computer-aided structural engineering (CASE) library, these programs are for new construction and do not consider the consequences of corrosion damage. To realistically determine the structural quality

(cont'd)

DD FORM 1 JAN 73 1473 EDITION OF 1 NOV 65 IS OBSOLETE

UNCLASSIFIED

SECURITY CLASSIFICATION OF THIS PAGE (When Data Entered)

BLOCK 20. (Cont'd)

of the O'Brien Lock and to develop a credible projection of its usable life, a specialized analysis had to be developed for this particular structure; however, the analysis had to be general enough for use in other similar structures throughout the Corps.

Detailed field and laboratory analyses indicated that there is a large safety factor in the structure and that 0.25 in. of corrosion can be tolerated anywhere without catastrophic results. However, corrosion that exceeds 0.25 in. in highly stressed areas could cause catastrophic results.

The extreme value of corrosion calculated for the lock and dam is 0.0024 in. per year, which means that 83 years of corrosion must occur to achieve the 0.25 in. value.

It was found that cathodic protection could be used successfully at this structure to prevent additional corrosion damage. A deep well anode system is ideally suited for this project.

FOREWORD

This research was conducted for the U.S. Army Corps of Engineers' Chicago District under Intra-Army Order 79-16, dated December 1978. The work was performed by the Engineering and Materials Division (EM), U.S. Army Construction Engineering Research Laboratory (USA-CERL). The Chicago District Technical Monitor was Mr. I. Juzenas, NCC-DS.

Dr. R. Quattrone is Chief of USA-CERL-EM. COL Norman C. Hintz is Commander and Director of USA-CERL, and Dr. L. R. Shaffer is Technical Director.

CONTENTS

CONTENTS (Cont'd)

TABLES

FIGURES

Figures (Cont'd)

Figures (Cont'd)

LIFE-CYCLE ANALYSIS OF CORRODING SHEET PILE STRUCTURES FOR A LOCK AND DAM

1 INTRODUCTION

Background

In late 1977, the U.S. Army Corps of Engineers' Chicago District conducted a partial dewatering and inspection of the Thomas J. O'Brien Lock and Dam on the Illinois Waterway in Chicago.[1] The inspection revealed excessive corrosion and severe pitting. This observation came at about the same time that the full extent of the corrosion damage to the Lockport Lock and Dam (36 miles down the waterway from O'Brien) was recognized. The Chicago District asked the U.S. Army Construction Engineering Research Laboratory (USA-CERL) to analyze the corrosion damage, including its causes and extent, and to recommend remedial measures.

The lock walls, guide walls, and dam all have a sheet pile structural system. Although there is an abundance of design information for steel sheet pile structural design, including a program in the Corps of Engineers' computer-aided structural engineering (CASE) library, these programs are for new construction and do not consider the consequences of corrosion damage. To realistically determine the structural quality of the O'Brien Lock and to develop a credible projection of its usable life, a specialized analysis had to be developed for this particular structure; however, the analysis had to be general enough for use in other similar structures throughout the Corps.

Objective

The objectives of this study were to assess the present structural condition of the O'Brien Lock and Dam, delineate a structural quality-vs.-time prognosis based on predicted corrosion rates, and to develop the most appropriate corrosion mitigation program.

Approach

Carrying out these objectives required three major efforts: (1) establishing the present condition of the structure and appurtenances, (2) quantifying the ambient corrosion environment, and (3) developing a projection of structural performance.

Evaluation of Site Corrosion Characteristics

The nature and extent of existing corrosion damage were examined and correlated with environmental history. Three elements were involved:

1. Field survey data analysis

---

[1] *Thomas J. O'Brien Lock and Controlling Works*, Periodic Inspection Report No. 3 (U.S. Army Corps of Engineers, December 1978).

2. Inspection and analysis of test piles

3. Corrosion environmental history determination.

In-Situ Corrosion Rate Measurements

The variation in corrosion conditions was determined by installing a continuous corrosion monitoring system and measuring polarization current over several months.

Cathodic Protection System Development

This activity involved developing a comprehensive cathodic protection corrosion mitigation system, including design of cathodic protection for the land side of lock walls and guide walls, and design of cathodic protection for the water side of the lock walls, guide walls, and dam. Appendix A contains information on corrosion principles and cathodic protection. '

In addition, a structural analysis of the lock walls, guide walls, and dam was conducted. This was a two-phase effort consisting of analytical studies and in-situ tests. Based on the results of the site corrosion characteristics investigation, the present structural condition was assessed and a structural quality-vs.-time prognosis delineated. This included the following activities:

1. Determining the life-cycle of the lock and guide walls and of the anchor systems

2. Determining the structural integrity of the lock and guide walls in their present state of deterioration relative to original design requirements.

The in-situ measurements and tests, together with the laboratory testing, were conducted simultaneously with the analytical work, and extremely close interaction was maintained. As the analytical work progressed, the need for additional field data was noted, and elements of the ongoing analysis were used to determine the most appropriate test locations and procedures.

During the field investigation phase, there was only one dewatering (in November 1979); therefore, it was necessary to rely heavily on in-situ nondestructive evaluation techniques (see Appendix B) for most of the field measurements, particularly the polarization techniques. This investigation marked the first time that the Corps of Engineers used a continuous and instantaneous corrosion rate measurement system. This system was used to determine if there were any cyclical changes in the corrosivity of water flowing in the lock.

2 FIELD TEST AND RESULTS

In assessing the condition of a structure with corrosion damage, some type of measurement is usually made to determine the metal loss. The loss is then divided by the time it takes for this loss to occur; the resultant value is an average corrosion rate, usually in milli-inches per year. To project life expectancy, this corrosion rate is used to determine the specific time when the metal loss will reach the point that it renders the structure unusable. In the case of the O'Brien Lock and Dam, such a simplified approach could not be used, because the ambient corrosive conditions were changing during the structure's 20-year existence, with a resultant variation in corrosion rate from year to year. On the water side of the structure, the water quality changed as environmental protection procedures were implemented; on the land side, runoff of water from landfill operations near the project caused a variable electrolyte. It was therefore necessary to use innovative evaluation techniques to determine the corrosion mechanisms and their impact on various parts of the structure.

Fortunately, during construction, a series of H-beam piles had been placed adjacent to the lock structure; these piles were to be pulled out at 20-year intervals to indicate the amount of corrosion damage. Figure 1 shows the location of the test piles, labeled 1 through 4. These test piles were invaluable since they gave the corrosion indications for the various depths for the backfill pattern used. Figure 2 shows the pile extraction process conducted in June 1978. The test piles were taken to USA-CERL for evaluation; the analysis used was identical to that used in a previous study.[2] Figures 3 through 6 show the pattern of corrosion corresponding to various depths and backfill types. As expected, the corrosion pits are very severe in the region of coarse gravel backfill due to a crevice-type corrosion between the web and large stones. Analysis of this corrosion pattern served as valuable guidance for the ultrasonic measurements of the lock walls during the dewatering inspection in November 1979.

Soil resistivity is another parameter affecting the corrosion rate on the land side of the structure. Several measurements were made adjacent to the lock wall and the guide walls, as shown in Figure 7. Table 1 gives soil resistivity measurements. The extreme variation in soil resistivities was attributed to the nonuniformity of the backfill. The low values of resistivity obtained at points 5, 6, and 7 and at points 17, 18, and 19 were caused by septic tank effluent residue. These resistivity values, coupled with the landfill drainage water, indicate a severe corrosion problem.

Although water samples were taken to determine the corrosivity of the waterway water, results of these samples would not indicate any cyclic variation in water conductivity that might occur throughout the year due to increased barge traffic, heavy water runoff, etc. To determine if this might be occurring, USA-CERL installed a unique continuous and instantaneous recording corrosion rate instrument. This device provides an indirect corrosion current reading or corrosion rate measurement by taking advantage of the fact that there is a measurable relationship between the direct corrosion current and the effect of an externally applied current on a metal surface. The sensing probe assembly is shown in Figure 8. The three electrodes at the tip of the probe have the same carbon steel composition as the O'Brien structure's sheet piling. Analysis of data obtained over about 1 year indicated no extreme variations in the water's corrosivity.

---

[2] A. Kumar, R. Lampo, and F. Kearney, *Cathodic Protection of Civil Works Structures*, Technical Report M-276/ADA080057 (U.S. Army Construction Engineering Research Laboratory [USA-CERL], 1979).

To assist in cathodic protection, design polarization, current requirement, and IR drop tests were performed; these design curves are given in Figures 9, 10, and 11. USA-CERL Technical Report M-275 provides an extensive discussion of these types of measurements.[3]

In November 1979, the lock chamber was completely dewatered for the first time. There had been a partial dewatering in 1977, which was when it was determined that a corrosion problem existed. Figure 12 shows the dewatered lock. Besides the various corrosion products and contaminant buildup, there were numerous corrosion tubercles. Figure 13 is a close-up shot of a corrosion tubercle; Chapter 9 discusses how this type of corrosion forms. To ascertain what corrosive factors had affected the structure over the past 20 years, several tubercles were dissected and the laminations studied; results are provided on pp 49-55.

After the various corrosion formations had been analyzed, the entire lock wall surface was sandblasted to provide a clean metal surface for ultrasonic thickness measurements. These measurements were made with a state-of-the-art portable electronic system (Figure 14). To systematize the measurement pattern, the coffer cell numbers assigned in the construction drawings were used. Measurements were made starting at 1 ft from the top of the cell and continuing down to the bottom point at 13 ft below the top of the cell. Table 2 provides the thickness measurements. Overall values were: thickness--0.348 in.; standard deviation 0.008 in.*

To establish the pitting factor for the lock wall, a pit depth gauge was used (see Figure 15). Table 3 gives the pit depth and area. No statistical analysis can be used to simplify the interpretation of these data; rather, it requires a tedious point-by-point evaluation to determine the seriousness of this pitting corrosion. Essentially, a "worst case" analysis is used; that is, the deepest pit measured on the water side is coupled with the deepest pit measured on the test piles representing the land-side corrosion of the lock wall; this value represents the maximum web thickness deterioration. After these measurements were taken, suspect areas were re-examined; no incipient perforations were detected.

---

[3]F. Kearney, *Corrosion of Steel Pilings in Seawater: Buzzards Bay—1975-1978*, Interim Report M-275/ADA078626 (USA-CERL, 1979).

*Metric conversion factors are provided on p 97.

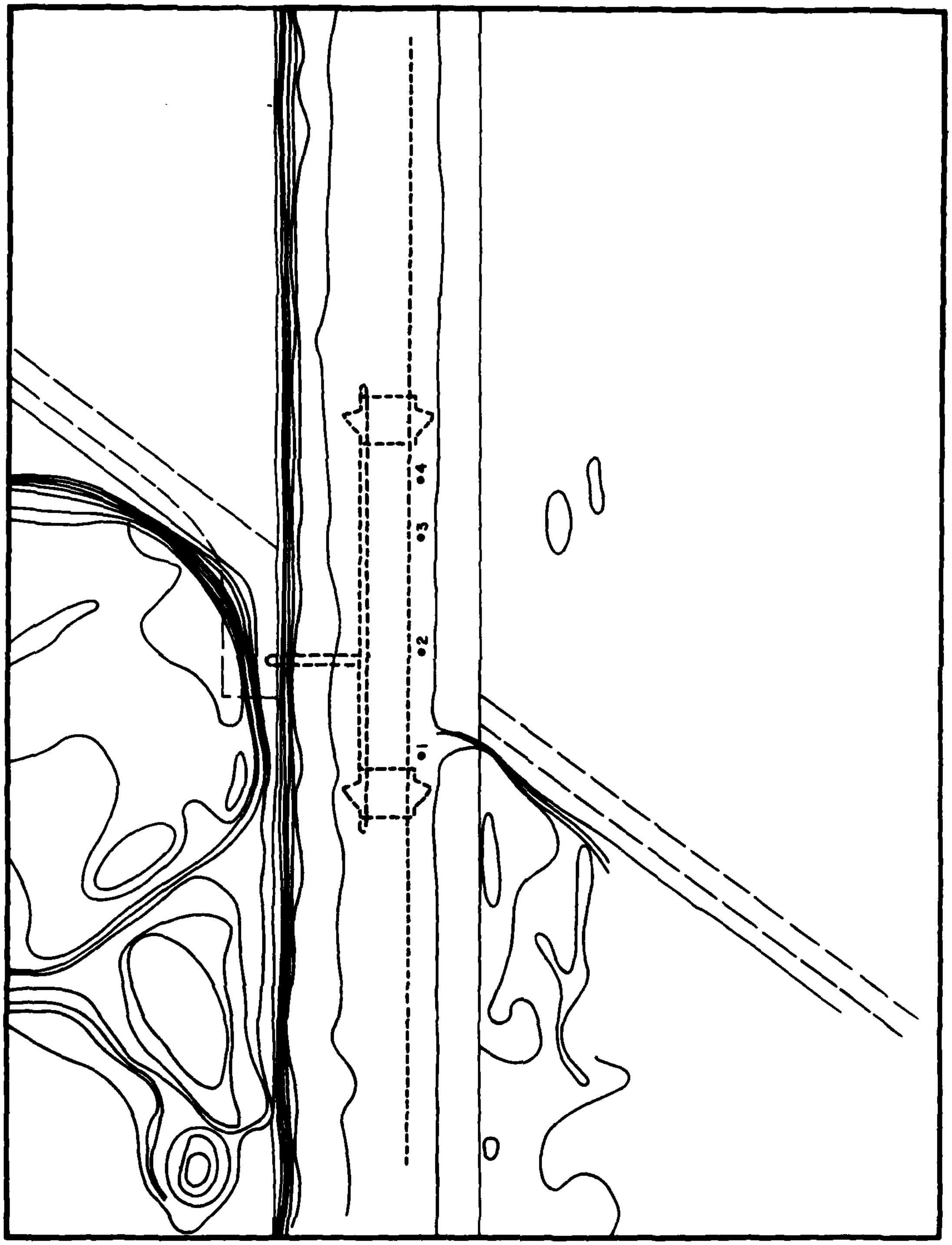

Figure 1. Four locations of test piles.

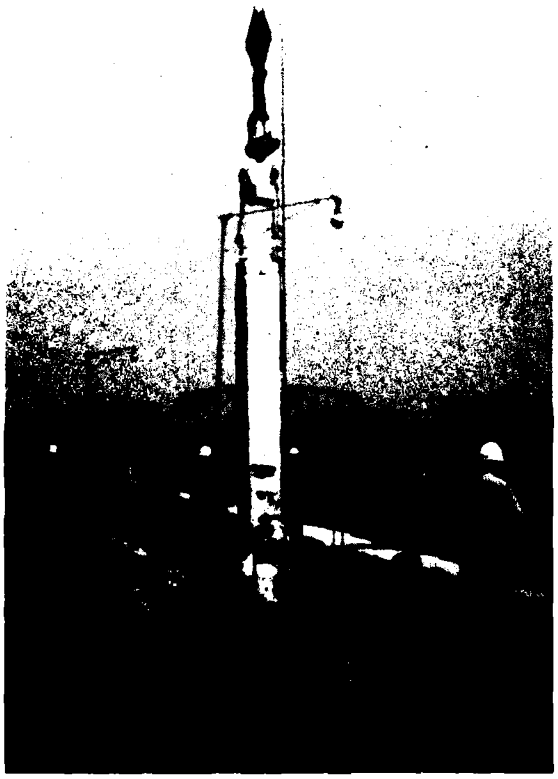

Figure 2. Pulling test piles.

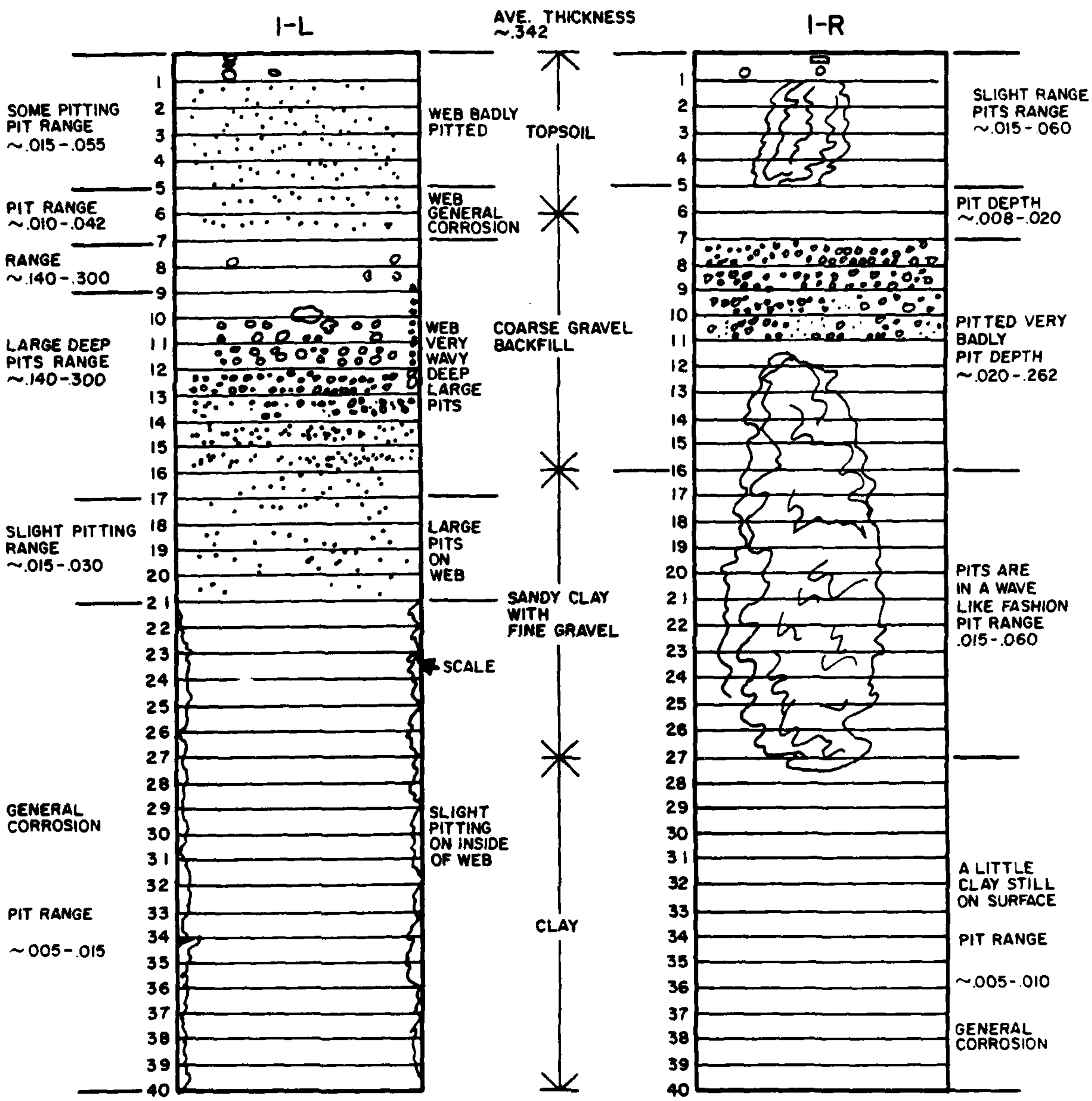

Figure 3. Corrosion pattern test pile No. 1.

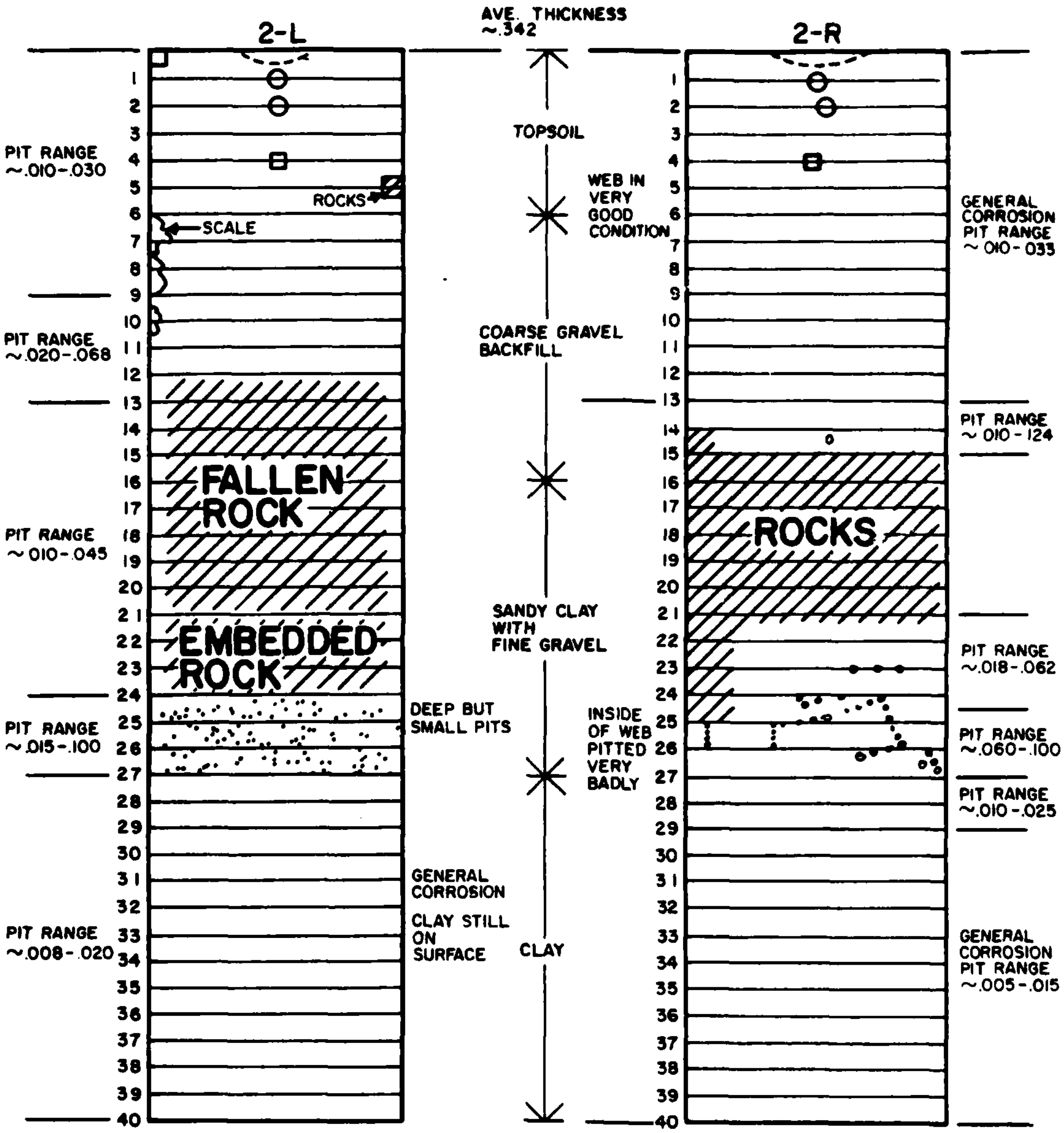

Figure 4. Corrosion pattern test pile No. 2.

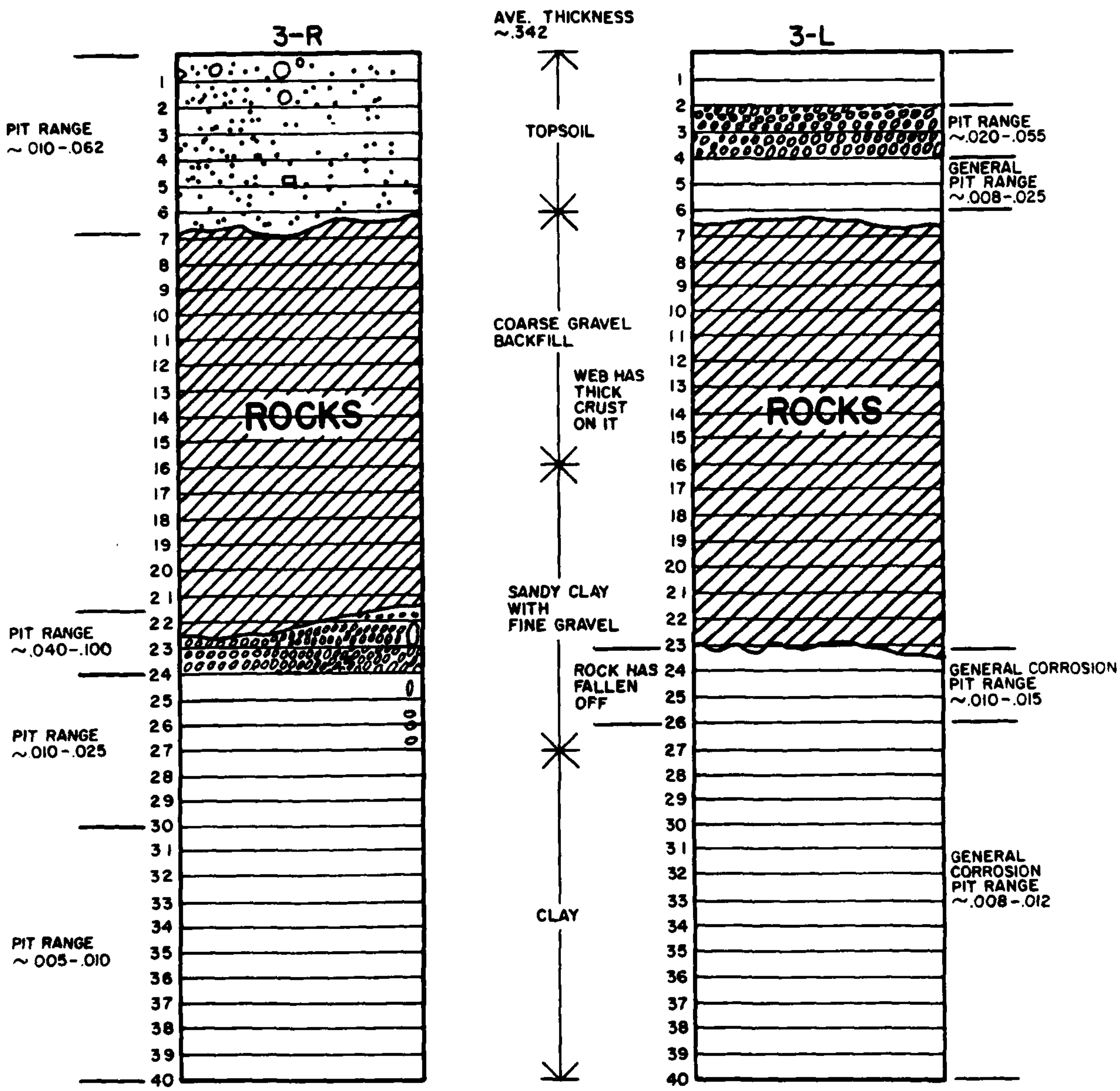

Figure 5. Corrosion pattern test pile No. 3.

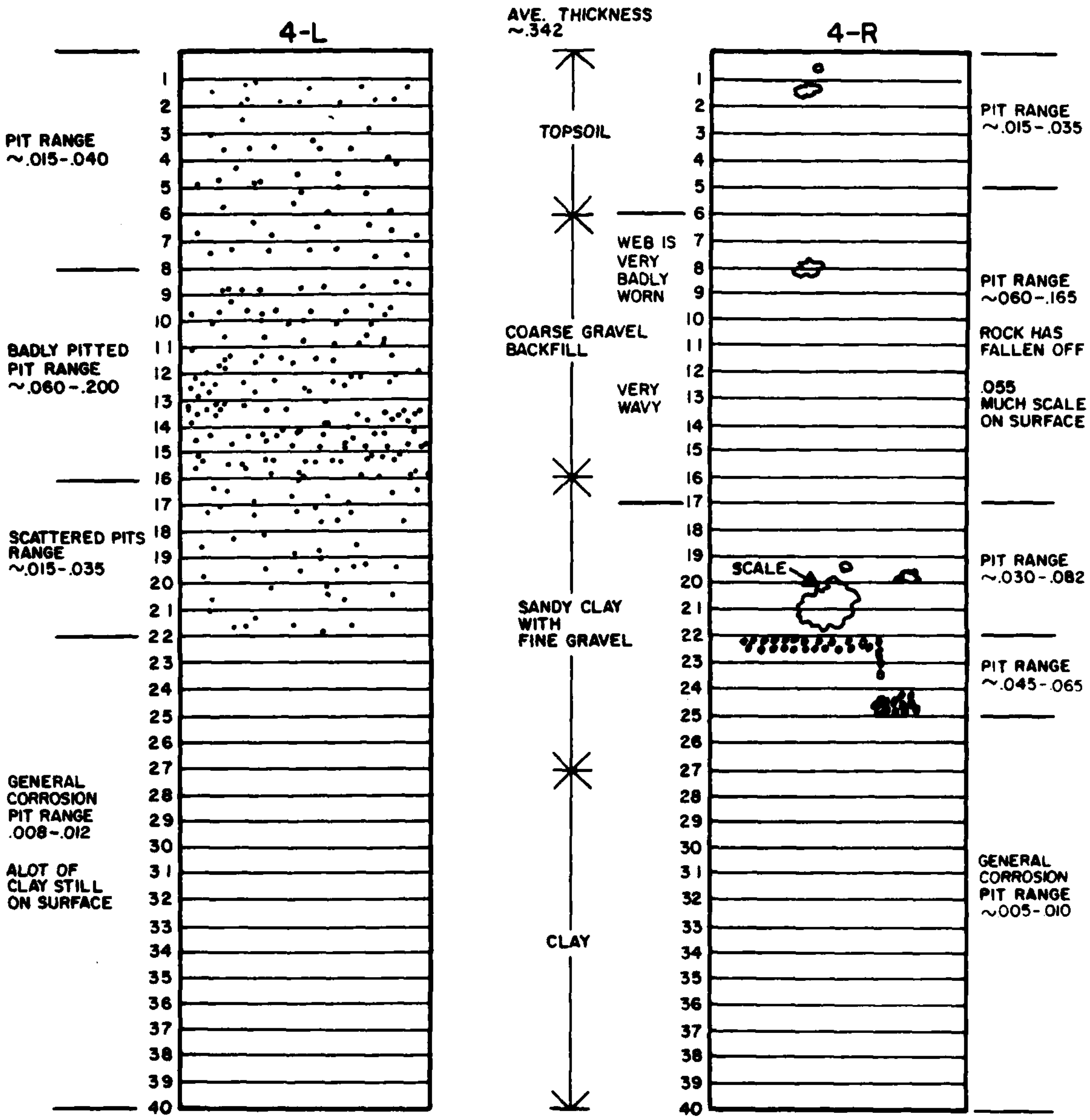

Figure 6. Corrosion pattern test pile No. 4.

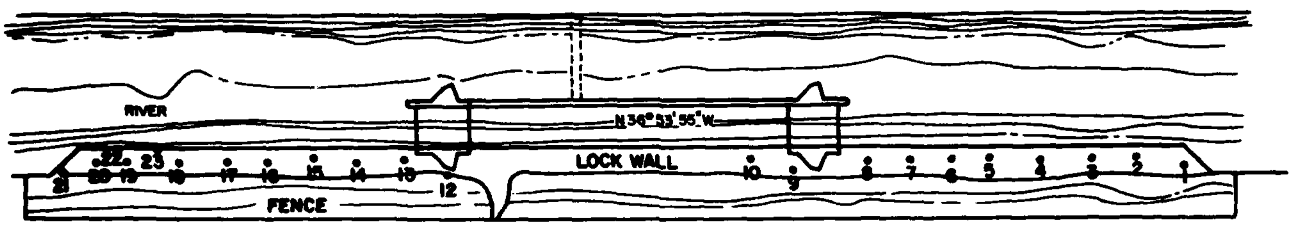

Figure 7. Soil resistivity test locations.

Figure 8. Polarization corrosion rate monitor.

Table 1

Soil Resistivity Measurements—O'Brien Lock and Dam (12-14 June 1979)

Position (100-ft Intervals)	5 ft	10 ft	15 ft	Location Comments
1	45,002	55,535	9,479	
2	4,213	3,830	3,447	
3	5,457	3,830	2,872	
4	3,159	2,872	2,870	
5	3,351	2,298	1,953	
6	4,596	2,872	1,723	
7	4,787	2,489	2,240	
8	10,532	18,192	10,915	
9	143,625	157,030	120,645	Opposite Gate Recess
10	172,350	178,095	129,262	Opposite Gate Recess
11	1,436	689	718	Along Fence
12	13,405	17,235	9,192	
13	5,074	3,830	2,298	
14	47,875	53,620	40,215	
15	25,852	45,960	43,087	
16	4,213	5,170	1,723	Opposite Metal Pile
17	7,085	6,511	6,606	
18	7,660	6,128	6,606	
19	4,787	3,447	3,734	
20	2,393	1,340	1,062	Opposite Brick Building
21	230,040	185,755	163,732	End of Sheet Piling
22	191,500	134,050	86,175	
23	210,650	180,010	109,155	

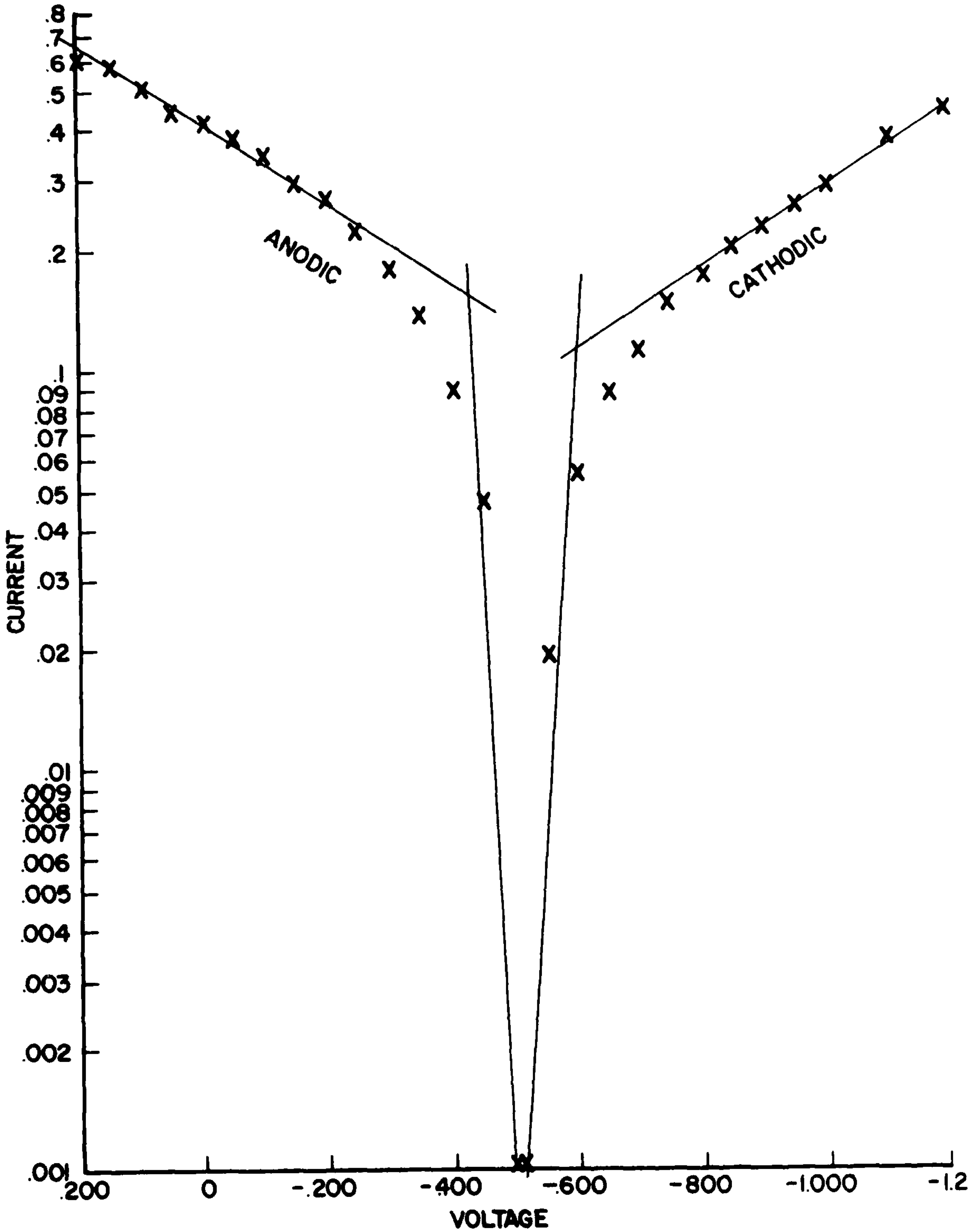

Figure 9. O'Brien Lock and Dam (I_p = 0.11A; I_Q = 0.15A; and I_c = 0.064).

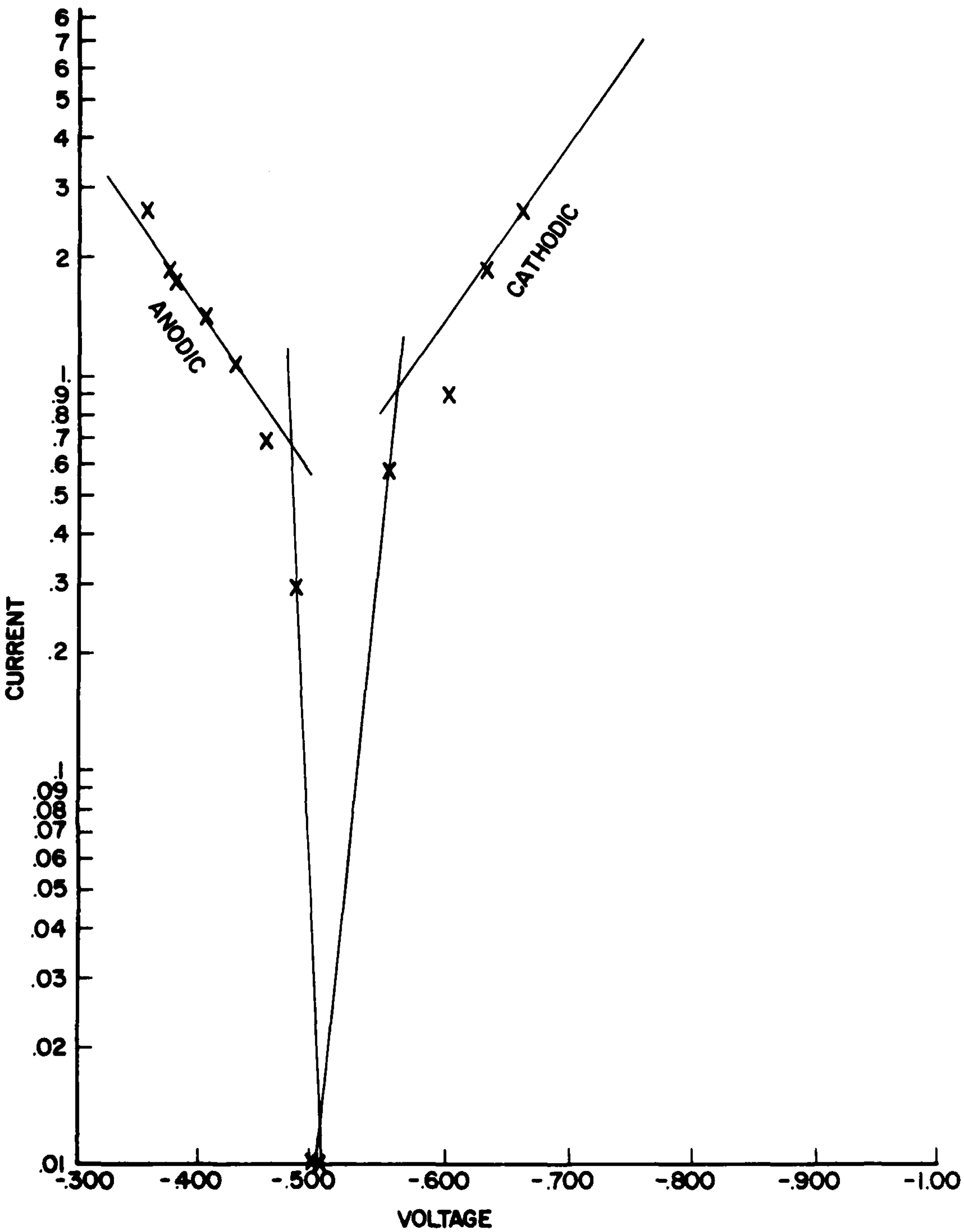

Figure 10. O'Brien Lock and Dam (I_p = 0.93A; I_Q = 0.67A; and I_c = 0.39).

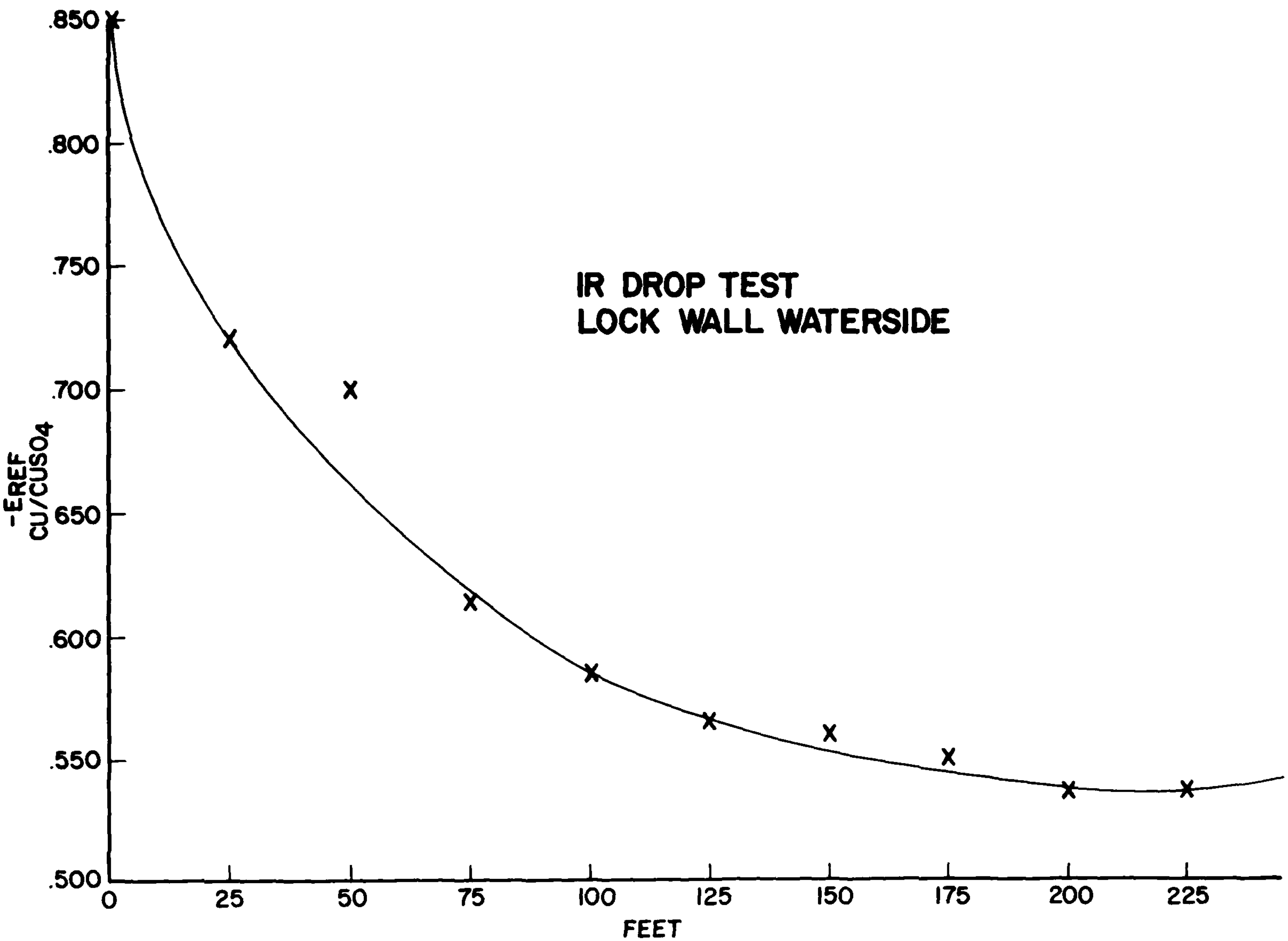

Figure 11. Lock wall waterside.

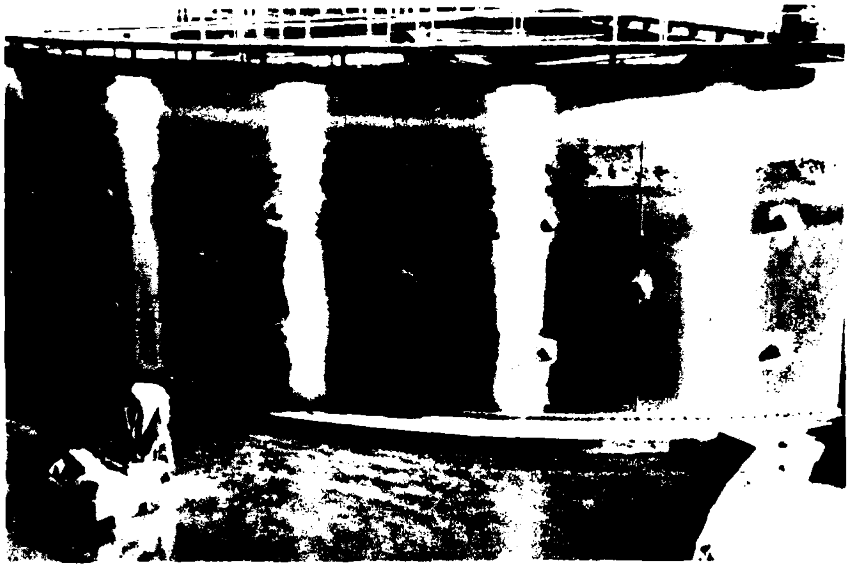

Figure 12. Dewatered lock.

Figure 13. Tubercle.

Figure 14. Ultrasound testing gauge.

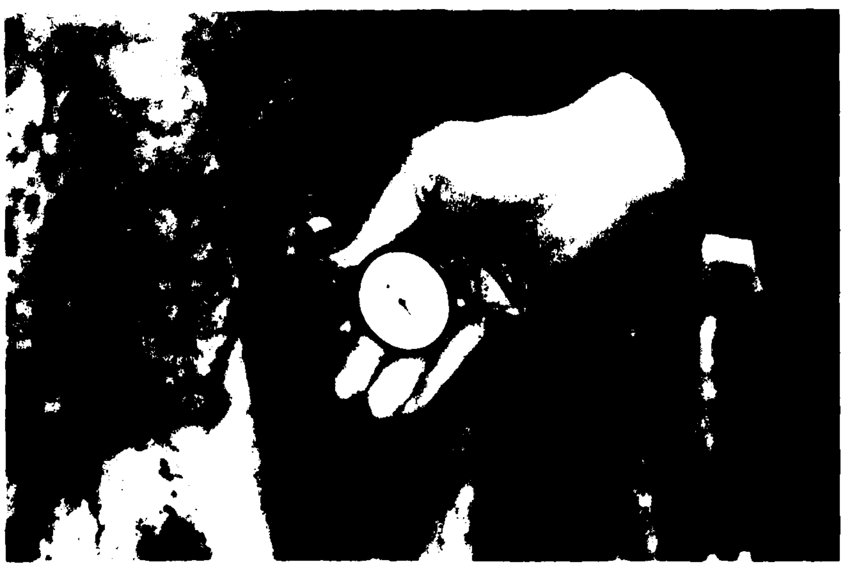

Figure 15. Pit depth gauge.

Table 2

Ultrasonic Thickness Measurements

Pile No.	1	2	3	4	5	6	7	8	9	10
1 ft	.368	.352	.350	.353	.358	.353	.362	.348	.342	.356
2 ft	.347	.364	.346	.355	.350	.357	.347	.348	.353	.351
3 ft	.330	.351	.353	.363	.360	.362	.350	.341	.353	.358
4 ft	.353	.327	.348	.353	.358	.349	.354	.359	.353	.351
5 ft	.330	.352	.335	.353	.355	.347	.342	.352	.348	.341
6 ft	.360	.347	.354	.348	.355	.340	.342	.344	.352	.329
7 ft	.355	.354	.353	.360	.357	.353	.344	.343	.362	.339
8 ft	.350	.333	.358	.346	.345	.330	.343	.336	.351	.353
9 ft	.333	.370	.355	.335	.354	.338	.350	.346	.350	.349
10 ft	.356	.357	.363	.354	.348	.337	.340	.346	.350	.335
11 ft	.349	.345	.352	.354	.344	.336	.347	.342	.345	.340
12 ft	.367	.360	.345	.355	.345	.346	.339	.351	.349	.341
13 ft	.367	.358	.347	.333	.363	.342	.346	.354	.341	.350
$\overline{X}$*	.351	.3515	.3506	.3509	.3532	.3453	.3466	.3469	.3499	.3456
SD**	.013	.012	.0068	.0086	.0062	.0092	.0063	.0060	.0054	.0087

Pile No.	11	12	13	14	15	16	17	18	19	20
1 ft	.360	.356	.352	.359						.353
2 ft	.353	.356	.337	.349						.348
3 ft	.346	.335	.352							
4 ft	.350	.346	.347							
5 ft	.342	.348	.351							
6 ft	.353	.327	.346							
7 ft	.340	.354	.347	.348						.347
8 ft	.347	.346	.341	.344						.352
9 ft	.344	.342	.342							
10 ft	.339	.348	.347							
11 ft	.342	.347	.339							
12 ft	.334	.348	.347	.347	.349	.351	.354	.347	.352	.346
13 ft	.352	.353	.354	.350	.352	.347	.346	.352	.347	.352
$\overline{X}$	.3463	.3466	.3463	.3495	.3505	.3490	.350	.3495	.3495	.3496
SD	.0071	.0082	.0079	.0050	.0021	.0028	.0056	.0035	.0035	.0030

*$\overline{X}$ = mean.
**SD = standard deviation.

Table 2 (Cont'd)

Pile No.	21	22	23	24	25	26	27	28	29	30
1 ft	.346	.340	.357	.353	.363			.351	.358	.351
2 ft	.347	.349	.346	.344	.351			.351	.355	.351
3 ft										
4 ft										
5 ft										
6 ft										
7 ft	.352	.339	.351	.344	.345	.345	.340	.338	.358	.340
8 ft	.348	.340	.347	.353	.349	.347	.350	.349	.346	.357
9 ft										
10 ft										
11 ft										
12 ft	.340	.345	.346	.355	.349	.348	.351	.349	.348	.345
13 ft	Not Blasted	.346	.342	.349	.340	.347	.347	.351	.351	.351
$\overline{X}$	.3466	.3431	.3481	.3496	.3495	.3467	.347	.3481	.3526	.3491
SD	.0043	.0040	.0051	.0048	.0076	.0012	.0049	.0050	.0051	.0058

Pile No.	31	32	33	34	35	36	37	38	39	40
1 ft	.353	*	.355	*	*	.357	.358			
2 ft	.350	*	.348	*	*	.354	.347			
3 ft										
4 ft										
5 ft										
6 ft										
7 ft	.345	*	.347	.347	.339	.353	.347			
8 ft	.345	.345	.344	.352	.345	.348	.342			
9 ft										
10 ft										
11 ft										
12 ft	.347	.348	.356	.350	*	.352	.350			
13 ft	.340	.350	.342	.350	*	.348	.355			
$\overline{X}$	.3466	.3476	.3486	.3497	.342	.352	.3498			
SD	.0045	.0025	.0057	.0020	.0042	.0035	.0058			

* = Too rough.

Table 2 (Cont'd)

Pile No.	41	42	43	44	45	46	47	48	49	50
1 ft		*	*	*	*	*	*	*	*	*
2 ft		*	*	*	*	*	*	*	*	*
3 ft										
4 ft										
5 ft										
6 ft										
7 ft		*	*	*	*	.340	*	*	*	.361
8 ft		*	*	*	*	.352	.359	*	.361	.351
9 ft										
10 ft										
11 ft										
12 ft		.350	.360	.346	.366	.348	.354	.349	.342	.344
13 ft		.347	.348	.330	.358	.343	.347	.351	.354	.342
$\bar{X}$		.3485	.354	.338	.362	.3457	.3533	.3500	.348	.3495
SD		.0021	.0084	.0133	.0056	.0053	.0060	.0014	.0084	.0085

Pile No.	51	52	53	54	55	56	57	58	59	60
1 ft	.359	*	.352	*	*	*	*	*	*	*
2 ft	.348	*	.350	*	*	*	*	.349	*	*
3 ft										
4 ft										
5 ft										
6 ft										
7 ft	.359	.357	*	.363	*	.345	.340	.348	*	.354
8 ft	.351	.361	*	.349	*	.339	.363	.349	*	.350
9 ft										
10 ft										
11 ft										
12 ft	.362	.355	.348	.343	*	.361	.363	*	.334	.348
13 ft	.339	.333	.347	.347	.341	.357	.363	*	.343	.350
$\bar{X}$	.353	.3515	.3492	.3505	.341	.3505	.3572	.3486	.3385	.3505
SD	.0086	.1258	.0022	.0086	0	.1024	.0115	.0005	.0063	.0025

* = Too rough.

Table 2 (Cont'd)

Pile No.	61	62	63	64	65	66	67	68	69	70
1 ft	*	*	*	*	*	*	.347	*	*	*
2 ft	*	*	*	*	*	*	.351	*	*	*
3 ft										
4 ft										
5 ft										
6 ft										
7 ft	*	*	.355	.363	*	.350	.346	.353	.351	*
8 ft	*	*	.357	.364	.347	.351	.344	.354	.343	*
9 ft										
10 ft										
11 ft										
12 ft	*	.352	.336	.339	.359	.351	.330	.351	.355	.345
13 ft	*	.340	.345	.346	.354	.346	.346	.342	.349	.355
$\bar{X}$		.346	.3482	.353	.3533	.3495	.344	.350	.3495	.350
SD		.0084	.0097	.0124	.0060	.0023	.0072	.0054	.005	.0070

Pile No.	71	72	73	74	75	76	77	78	79	80
1 ft	.347	*	*	*	*	*	*	*	*	*
2 ft	.351	*	*	*	*	*	*	*	*	*
3 ft										
4 ft										
5 ft										
6 ft										
7 ft	.352	.355	.333	*	.349	*	.337	*	*	.353
8 ft	.346	*	.338	*	.348	*	.356	*	*	.347
9 ft										
10 ft										
11 ft										
12 ft	.354	.346	.327	.348	*	.346	.344	.333	.347	*
13 ft	.353	353	.342	.335	.347	.351	.339	.342	.358	.344
$\bar{X}$	.3505	.3513	.335	.3415	.348	.3485	.344	.3375	.3525	.348
SD	.0032	.0047	.0064	.0091	.001	.0035	.0085	.0063	.0077	.0045

* = Too rough.

Table 2 (Cont'd)

Pile No.	81	82	83	84	85	86	87	88	89	90
1 ft	.356	*	*	*	*	*	*			
2 ft	*	*	*	.358	*	*	*			
3 ft										
4 ft										
5 ft										
6 ft										
7 ft	*	.352	*	.353	*	.344	.354			
8 ft	*	.349	*	.351	*	.348	.348			
9 ft										
10 ft										
11 ft										
12 ft	.348	.351	.355	.354	.348	*	.350			
13 ft	.351	.351	.348	.348	.347	.344	.347			
$\bar{X}$	.3516	.3507	.3515	.3528	.3475	.3453	.3497			
SD	.0040	.0012	.0049	.0037	.0007	.0023	.0030			

* = Too rough.

Table 3

Pit Depth and Area of Depth Measurements

Cell No.	1			2			3			4			5		
	Area Size	No. of Areas	Depth	Area Size	No. of Areas	Depth	Area Size	No. of Areas	Depth	Area Size	No. of Areas	Depth	Area Size	No. of Areas	Depth
1 ft							1	2	.090	1/4	1	.080	1/4	1	.070
2 ft							1	1	.085	1/2	1	.100	1/4	3	.110
3 ft							1/2	1	.065	1/4	2	.060	1/8	3	.083
4 ft							1	2	.100	3/4	1	.070	1/16	1	.090
5 ft							1/2	1	.075	1/2	1	.060	1/2	1	.070
6 ft							3/4	2	.060	1/2	1	.060	1/4	2	.050
7 ft							1/4	3	.080	1/4	2	.040	1/4	1	.080
8 ft							1	1	.100	1/4	1	.060	1/4	1	.060
9 ft							1/4	1	.070	1/8	1	.060	1/2 3/4	1 1	.070 .100
10 ft							1/4	1	.050	1/8	1	.080	1/4	1	.050
11 ft							3/4	1	.065	1/4	1	.055	1/4	3	.050
12 ft							1/4	1	.050	1/4	1	.040	1/4	1	.050
13 ft							1	1	.050	1/4	1	.045	1/4	1	.030

Note: * = Scattered pits.
All areas are square inches.
All depths are inches.
Blanks = No data obtained.
+ = Reinforced plates.
- = Not blasted.

Table 3 (Cont'd)

Cell No.	6			7			8			9			10		
	Area Size	No. of Areas	Depth	Area Size	No. of Areas	Depth	Area Size	No. of Areas	Depth	Area Size	No. of Areas	Depth	Area Size	No. of Areas	Depth
1 ft	1/4	1	.070	1/2	1	.040	1/2	1	.080	1/16	4	.060	1/8	2	.060
2 ft	1/4	2	.110	3/8	1	.060	1/4	2	.075	1/16	1	.100	1/4	1	.130
	1/4	1	.090				1/2	1	.080		1	.110			
3 ft	1/8	1	.085	1/4	1	.070	3/4	1	.110	1/16	1	.080	1/16	2	.060
	1/8	2	.080												
4 ft	1/16	1	.090	1	1	.055	2	1	.040	1/16	1	.070	1/4	3	.050
5 ft	1/2	1	.070	1/2	1	.065	2	1	.040	1/4	1	.110	1/16	2	.050
6 ft	1/4	2	.050	1/2	1	.060	3/4	1	.040	3/4	1	.075	*	*	.040
7 ft	1/4	1	.080	1/4	1	.110	1/4	1	.070	*	*	.040	*	*	.040
8 ft	1/4	1	.060	1/4	2	.060	1/4	1	.060	*	*	.040	1/4	1	.070
9 ft	1/2	1	.070	1/16	1	.050	1/4	2	.050	1/8	1	.060	1/8	1	.070
	3/4	1	.100												
10 ft	1/4	1	.050	1/16	1	.050	1/4	4	.050	1/4	1	.060	1/4	1	.070
11 ft	1/4	3	.050	1/16	2	.050	1/4	2	.050	1/4	1	.050	1/4	3	.060
12 ft	1/4	1	.050	1/4	1	.050	1/4	1	.050	1/4	1	.050	1/4	2	.050
13 ft	1/4	1	.030	1/5	1	.050	*	*	.030	1/4	1	.050	1/8	1	.060

Table 3 (Cont'd)

Cell No.	11			12			13			14			15		
	Area Size	No. of Areas	Depth	Area Size	No. of Areas	Depth	Area Size	No. of Areas	Depth	Area Size	No. of Areas	Depth	Area Size	No. of Areas	Depth
1 ft	1/4	2	.100	1/4	2	.090	1/8	2	.060	1/4	2	.110	1/8	2	.060
	1/2	1	.130	1/8	4	.060							1/8	2	.050
2 ft	1/4	1	.130	1/2	1	.125	1/4	4	.080	1/8	4	.050	1/4	3	.050
				1/4	1	.090									
3 ft	1/16	2	.060	1/4	2	.080	1/8	4	.060	1/2	2	.080	1/4	3	.065
													1/2	3	.050
4 ft	1/4	3	.050	*	*	.040	*	*	.040	1/2	1	.050	1/8	1	.060
5 ft	1/16	2	.050	*	*	.040	*	*	.040	1/4	3	.080	1/8	4	.048
6 ft	*	*	.040	*	*	.040	*	*	.040	1/8	1	.090	1/16	2	.060
													1/16	1	.080
7 ft	*	*	.040	1/16	1	.060	1/16	2	.050	1/8	1	.050	1/2	2	.060
													1/8	2	.050
8 ft	1/4	1	.070	*	*	.040	1/8	1	.050	1/4	1	.090	1/4	2	.060
9 ft	1/8	1	.070	1/16	1	.060	1/8	1	.060	1/4	2	.060	1/4	1	.070
													1/8	1	.050
10 ft	1/4	1	.070	*	*	.040	1/8	2	.050	1/4	1	.065	1/4	2	.070
													1/8	1	.060
11 ft	1/4	3	.060	*	*	.040	*	*	.040	1/8	1	.060	1/4	5	.060
12 ft	1/4	2	.050	*	*	.040	1/8	1	.090	1/8	2	.050	1/4	2	.065
13 ft	1/8	1	.060	*	*	.040	*	*	.040	*	*	.040	*	*	.040

Table 3 (Cont'd)

Cell No.	16			17			18			19			20		
	Area Size	No. of Areas	Depth	Area Size	No. of Areas	Depth	Area Size	No. of Areas	Depth	Area Size	No. of Areas	Depth	Area Size	No. of Areas	Depth
1 ft	1/2	3	.095	1/2	4	.075	1/4	3	.090	1/8	1	.075	1/4	3	.090
	1/4	1	.070	1/8	2	.050	1/4	1	.085	1/4	2	.070	1/8	1	.120
2 ft	1/4	2	.090	1/8	7	.080	1/4	3	.100	1/16	2	.095	1/4	3	.080
	1/8	1	.080				1/8	2	.070	1/16	1	.080			
3 ft	1/8	1	.075	1/8	2	.085	1/8	1	.065	1/8	1	.060	1/4	1	.080
	1/8	1	.060	1/8	2	.065	1/8	1	.075	1/8	1	.055	1/8	2	.090
4 ft	1/16	2	.060	1/4	2	.100	*	*	.050	*	*	.050	3/8	1	.080
				1/4	2	.075									
5 ft	*	*	.050	1/4	2	.070	1/4	1	.125	*	*	.040	1/2	1	.090
				1/6	2	.060	1/8	3	.070						
6 ft	1/8	4	.050	1/4	2	.090	1/16	1	.080	1/8	1	.080	1/16	1	.120
				1/16	1	.060	1/4	2	.050	1/8	2	.060	1	1	.060
7 ft	1/8	1	.090	1/4	2	.070	1/16	1	.065	1/8	1	.120	1/16	2	.070
	1/16	2	.055	1/8	2	.060	1/16	5	.050	1/16	1	.075	1/16	1	.090
8 ft	3/8	1	.090	1/8	1	.140	*	*	.040	*	*	.040	1/16	10	.075
	1/16	1	.055	1/4	2	.050							1/16	1	.100
9 ft	1/16	2	.050	1/16	1	.075	1/16	3	.050	1/8	1	.070	1/8	2	.070
	1/8	1	.060	1/8	2	.050				1/16	1	.060	1/8	1	.125
10 ft	1/4	3	.070	*	*	.040	*	*	.040	3/8	1	.140	1/16	1	.110
	1/16	2	.060							1/16	2	.050	1/16	3	.090
11 ft	1/4	2	.075	1/16	1	.060	*	*	.040	1/8	1	.070	1/8	3	.060
	1/16	1	.065	1/16	1	.050				1/16	1	.055	1/8	1	.090
12 ft	1/16	2	.065	*	*	.055	*	*	.040	1/8	1	.080	1/8	4	.060
	1/8	2	.060							1/8	1	.075	1/16	1	.100
13 ft	*	*	.050	*	*	.050	*	*	.040	*	*	.040	1/14	8	.080
													1/16	.1	.090

Table 3 (Cont'd)

Cell No.	21			22			23			24			25		
	Area Size	No. of Areas	Depth	Area Size	No. of Areas	Depth	Area Size	No. of Areas	Depth	Area Size	No. of Areas	Depth	Area Size	No. of Areas	Depth
1 ft	1/4	1	.100		2	.070	1/4	2	.070	1	3	.080	1/16	3	.070
	1/2	1	.120	1/4						1/4	2	.090	3/8	1	.090
2 ft	1/4	1	.090	1/4	2	.070	3/8	1	.080	1/8	2	.080	1/2	1	.070
	1/4	1	.100							1/8	2	.090			
3 ft	+	+	+	1/2	1	.060	1/2	1	.100	1/4	3	.060	+	+	+
										1/8	1	.070			
4 ft	*	*	.040	1/4	3	.050	1/4	1	.065	1/8	2	.090	1/4	1	.060
										1/8	1	.100			
5 ft	1/4	1	.095	3/8	1	.095	1/2	1	.060	1/4	2	.060	1/4	1	.080
	1/4	1	.120												
6 ft	1/8	1	.060	*	*	.040	*	*	.040	*	*	.040	*	*	.040
7 ft	*	*	.040	*	*	.030	1/16	2	.060	*	*	.040	*	*	.040
8 ft	*	*	.040	1/4	2	.060	1/4	1	.060	*	*	.040	1/2	3	.050
				1/8	1	.090									
9 ft	1/4	1	.060	*	*	.040	1/4	1	.060	*	*	.040	1/4	1	.070
10 ft	1/16	2	.070	1/4	2	.050	*	*	.040	*	*	.040	*	*	.040
	1/8	1	.080												
11 ft	*	*	.040	1/4	3	.050	*	*	.040	1/2	1	.060	*	*	.040
12 ft	*	*	.040	1/4	1	.050	*	*	.040	*	*	.040	*	*	.040
13 ft	-	-	-	*	*	.040	1/4	1	.060	*	*	.040	*	*	.040

Table 3 (Cont'd)

Cell No.	26			27			28			29			30		
	Area Size	No. of Areas	Depth	Area Size	No. of Areas	Depth	Area Size	No. of Areas	Depth	Area Size	No. of Areas	Depth	Area Size	No. of Areas	Depth
1 ft	1/4	1	.095	1/4	1	.060	1/16	1	.095	1/2	1	.070	1/4	1	.090
							1/8	1	.115	3/8	2	.090	1/2	1	.110
2 ft	1/8	1	.070	1/8	1	.080	1/8	1	.095	1/4	3	.070	1/4	2	.060
	1/8	1	.090	1/8	1	.130									
3 ft				1/8	1	.070	1/16	1	.080	+	+	+	1/8	1	.090
				1/16	1	.080									
4 ft	*	*	.040	*	*	.040	1/8	1	.110	1/4	1	.060	*	*	.040
5 ft	*	*	.040	*	*	.040	1/16	1	.075	*	*	.040	1/2	1	.110
							1/16	1	.110						
6 ft	*	*	.040	*	*	.040	1/4	1	.050	*	*	.040	*	*	.040
7 ft	1/8	1	.050	1/16	1	.090	*	*	.040	*	*	.040	1/64	4	.090
8 ft	1/16	1	.060	1/16	1	.090	1/8	1	.065	3/8	1	.080	*	*	.040
	1/8	1	.070												
9 ft	1/16	1	.100	1/16	1	.065	1/16	1	.050	1/8	2	.060	1/8	1	.070
10 ft	1/4	1	.130	*	*	.040	1/16	1	.060	*	*	.040	*	*	.040
11 ft	*	*	.040	1/8	2	.060	1/8	1	.050	*	*	.040	*	*	.040
12 ft	*	*	.040	1/8	1	.050	1/4	1	.055	*	*	.040	*	*	.040
13 ft	*	*	.040	1/16	5	.050	*	*	.040	*	*	.040	*	*	.040
				1/8	5	.050									

Table 3 (Cont'd)

Cell No.	31			32			33			34			35		
	Area Size	No. of Areas	Depth	Area Size	No. of Areas	Depth	Area Size	No. of Areas	Depth	Area Size	No. of Areas	Depth	Area Size	No. of Areas	Depth
1 ft	1/4	2	.070	1/2	1	.070	1/2	2	.170	1/4	2	.080	1/4	1	.090
	1/4	1	.085	1/4	1	.080				1/2	2	.075	1	1	.060
	1/4	1	.090												
2 ft	1/4	2	.070	3/8	1	.060	1/4	1	.100	1/8	1	.085	3/8	1	.140
	1/4	1	.100		*	.050	1/64	10	.090	1/8	2	.080	1	1	.090
3 ft	1/4	2	.080	*			1/8	1	.070	1/8	1	.060	1/8	2	.060
	1/8	1	.090												
4 ft	1/4	1	.060	1/64	15	.070	1/8	1	.060	1/4	1	.080	*	*	.050
										1/8	1	.170			
										1/16	1	.1060			
5 ft	1/8	2	.070	*	*	.040	1/64	8	.110	1/8	3	.060	1/8	1	.070
	1/64	4	.080				1/64	2	.070						
6 ft	1/64	10	.090	1/64	8	.080	1/16	2	.065	1/8	1	.090	1/16	1	.065
	1/4	1	.100							1/4	1	.060	1/64	10	.060
7 ft	1/64	5	.090	1/64	10	.080	1/64	1	.100	*	*	.050	1/64	4	.070
							1/64	2	.110				1/16	2	.060
8 ft	1/8	1	.070	1/64	8	.080	1/8	1	.175	1/8	1	.065	1/64	10	.080
	1/4	1	.090				1/16	2	.080	1/16	1	.060			
	1/4	1	.120												
9 ft	*	*	.040	1/64	25	.080	1/64	1	.065	1/8	1	.065	1/64	10	.080
										1/16	1	.060			
10 ft	*	*	.040	1/64	25	.080	1/16	2	.060	1/16	1	.065	1/64	10	.080
										1/16	1	.060			
11 ft	*	*	.040	1/64	10	.060	1/16	1	.070	1/64	1	.115	1/16	3	.075
							1/16	1	.060	1/16	1	.060	1/64	10	.080
12 ft	1/64	3	.080	1/64	10	.060	*	*	.060	1/16	1	.085	*	*	.030
										1/8	2	.060			
13 ft	*	*	.040	1/64	10	.060	*	*	.050	1/64	1	.075			
										1/16	1	.060			

Table 3 (Cont'd)

Cell No.	36			37			38			39			40		
	Area Size	No. of Areas	Depth	Area Size	No. of Areas	Depth	Area Size	No. of Areas	Depth	Area Size	No. of Areas	Depth	Area Size	No. of Areas	Depth
1 ft	-	-	.030	1/2	1	.085									
				1/4	1	.060									
2 ft	-	-	.030	3/8	1	.100									
				1/64	8	.080									
3 ft	-	-	.030	1/4	1	.095									
4 ft	1/4	1	.100	1/64	6	.080									
5 ft	-	-	.040	*	*	.030									
6 ft	-	-	.040	*	*	.040									
7 ft	-	-	.040	*	*	.040									
8 ft	-	-	.040	*	*	.040									
9 ft	1/64	1	.080	*	*	.040									
10 ft	*	*	.040	*	*	.040									
11 ft	*	*	.040	*	*	.040									
12 ft	*	*	.040	*	*	.040									
13 ft	*	*	.040	1/64	8	.060									

Table 3 (Cont'd)

Cell No.	41			42			43			44			45		
	Area Size	No. of Areas	Depth	Area Size	No. of Areas	Depth	Area Size	No. of Areas	Depth	Area Size	No. of Areas	Depth	Area Size	No. of Areas	Depth
1 ft				*	*	.040	*	*	.040	*	*	.040	*	*	.040
										1/4	1	.085	1/2	1	.090
2 ft				*	*	.040	*	*	.040	*	*	.040	+	+	+
				3/8	2	.080				1/4	1	.080	*	*	.040
3 ft															
4 ft															
5 ft															
6 ft															
7 ft				*	*	.03	*	*	.030	*	*	.035	*	*	.035
				1/4	1	.050									
8 ft				*	*	.030	*	*	.030	*	*	.040	*	*	.030
				1/2	1	.060				1 1/2	1	.060			
9 ft															
10 ft															
11 ft															
12 ft				*	*	.035	*	*	.040	*	*	.030	*	*	.030
				1/64	6	.080	1/4	2	.065	1/64	10	.080			
13 ft				*	*	.025	*	*	.040	*	*	.030	*	*	.030
				1/64	3	.080	1/8	3	.063				3/8	1	.100

Table 3 (Cont'd)

Cell No.	46			47			48			49			50		
	Area Size	No. of Areas	Depth	Area Size	No. of Areas	Depth	Area Size	No. of Areas	Depth	Area Size	No. of Areas	Depth	Area Size	No. of Areas	Depth
1 ft	1/4	4	.100	*	*	.035	*	*	.080	*	*	.040	*	*	.040
	1/4	2	.100				1/4	1	.100						
2 ft	1/16	3	.080	*	*	.035	*	*	.030	*	*	.040	*	*	.040
	1/8	1	.080	1/8	2	.075									
3 ft															
4 ft															
5 ft															
6 ft															
7 ft	*	*	.040	*	*	.030	*	*	.025	*	*	.035	*	*	.030
				1/4	1	.080							1/8	1	.060
8 ft	*	*	.040	*	*	.040	*	*	.025	*	*	.030	*	*	.030
													1/2	2	.055
9 ft															
10 ft															
11 ft															
12 ft	*	*	.040	*	*	.040	*	*	.025	*	*	.030	*	*	.035
							1/64	20	.060						
13 ft	*	*	.040	*	*	.030	*	*	.025	*	*	.030	*	*	.040
													1/64	10	.060

Table 3 (Cont'd)

Cell No.	51			52			53			54			55		
	Area Size	No. of Areas	Depth	Area Size	No. of Areas	Depth	Area Size	No. of Areas	Depth	Area Size	No. of Areas	Depth	Area Size	No. of Areas	Depth
1 ft	*	*	.025	*	*	.040	*	*	.030	*	*	.040	*	*	.040
				1/4	1	.120									
2 ft	*	*	.025	*	*	.050	+	+	+	*	*	.040	*	*	.040
				1/4	1	.070	*	*	.040	1/4	1	.070			
3 ft															
4 ft															
5 ft															
6 ft															
7 ft	*	*	.025	*	*	.080	*	*	.030	*	*	.030	*	*	.040
8 ft	*	*	.025	*	*	.030	*	*	.030	*	*	.040	*	*	.040
	1/8	2	.050												
9 ft															
10 ft															
11 ft															
12 ft	*	*	.040	*	*	.030	*	*	.040	*	*	.030	*	*	.040
13 ft	*	*	.040	*	*	.030	*	*	.040	*	*	.030	1/64	10	.050
													1/64	12	.070

Table 3 (Cont'd)

Cell No.	56			57			58			59			60		
	Area Size	No. of Areas	Depth	Area Size	No. of Areas	Depth	Area Size	No. of Areas	Depth	Area Size	No. of Areas	Depth	Area Size	No. of Areas	Depth
1 ft	1/4	1	.060	3/8	1	.080	*	*	.040	3/8	3	.100	1/4	1	.070
	1/8	1	.080	1/8	1	.145	3/8	1	.100	1/4	3	.085	3/8	1	.150
2 ft	3/8	2	.085	+	+	+	1/8	2	.060	3/8	1	.130	1	1	.065
	1/4	2	.100	1/4	1	.130	1/4	1	.140						
3 ft															
4 ft															
5 ft															
6 ft															
7 ft	1/64	10	.060	*	*	.030	1/64	10	.080	*	*	.040	1/64	6	.090
	1/64	6	.090	1/4	10	.090	1/64	10	.060				1/64	2	.110
8 ft	*	*	.030	*	*	.030	1/8	1	.080	*	*	.040	1/32	12	.090
							1/64	15	.080						
9 ft															
10 ft															
11 ft															
12 ft	*	*	.030	*	*	.050	*	*	.040	*	*	.030	*	*	.040
	1/64	24	.060				1/64	10	.080						
13 ft	1/4	1	.110	*	*	.040	*	*	.040	*	*	.030	*	*	.040
	3/8	1	.085	1/64	12	.080									

Table 3 (Cont'd)

Cell No.	61			62			63			64			65		
	Area Size	No. of Areas	Depth	Area Size	No. of Areas	Depth	Area Size	No. of Areas	Depth	Area Size	No. of Areas	Depth	Area Size	No. of Areas	Depth
1 ft	3/8	2	.070	1/4	2	.080	1/4	1	.085	*	*	.040	1	1	.070
	1/4	4	.085	1/2	1	.110	3/8	1	.100				1/8	1	.100
2 ft	*	*	.050	*	*	.040	*	*	.040	*	*	.040	+	+	+
	1/2	1	.080	3/8	1	.060	1/8	1	.080						
3 ft															
4 ft															
5 ft															
6 ft															
7 ft	*	*	.040	1/4	1	.060	*	*	.050	*	*	.040	*	*	.040
							1/8	1	.080	3/8	4	.060			
8 ft	*	*	.040	*	*	.040	*	*	.040	*	*	.050	1/8	1	.070
							1/8	2	.065				*	*	.040
9 ft															
10 ft															
11 ft															
12 ft	*	*	.040	*	*	.040	*	*	.040	1/64	25	.050	*	*	.040
	3/8	1	.070							1/4	1	.060			
13 ft	*	*	.040	1/64	25	.070	*	*	.040	*	*	.030	*	*	.040
													1/64	3	.090

Table 3 (Cont'd)

Cell No.	66			67			68			69			70		
	Area Size	No. of Areas	Depth	Area Size	No. of Areas	Depth	Area Size	No. of Areas	Depth	Area Size	No. of Areas	Depth	Area Size	No. of Areas	Depth
1 ft	*	*	.040	*	*	.040	*	*	.050	1/8	1	.125	*	*	.050
				3/8	1	.075	1/4	2	.050	1/4	2	.110	1/8	1	.100
2 ft	*	*	.040	*	*	.040	3/8	3	.050	3/8	1	.060	1/4	1	.070
				1/16	1	.080	3/8	1	.060	1/4	1	.080	1/8	2	.060
3 ft															
4 ft															
5 ft															
6 ft															
7 ft	1/4	2	.080	*	*	.040	1/2	2	.050	1/64	2	.080	*	*	.040
	1/4	2	.060				3/8	2	.060	3/8	1	.090	1/4	3	.060
8 ft	1/2	2	.060	*	*	.040	3/8	2	.050	3/8	2	.050	1/64	12	.080
													1/4	1	.100
9 ft															
10 ft															
11 ft															
12 ft	*	*	.040	*	*	.040	*	*	.050	*	*	.040	*	*	.040
													1/4	1	.080
13 ft	*	*	.040	*	*	.040	*	*	.050	*	*	.040	*	*	.040

Table 3 (Cont'd)

Cell No.	71			72			73			74			75		
	Area Size	No. of Areas	Depth	Area Size	No. of Areas	Depth	Area Size	No. of Areas	Depth	Area Size	No. of Areas	Depth	Area Size	No. of Areas	Depth
1 ft	1/8	1	.110	*	*	.050	*	*	.060	*	*	.050	*	*	.050
	1/4	3	.085	1/4	4	.060	1	1	.070	1/16	1	.070			
2 ft	*	*	.040	*	*	.050	+	+	+	*	*	.050	1/8	2	.060
	3/8	1	.150							1/4	2	.065	1/4	1	.070
3 ft															
4 ft															
5 ft															
6 ft															
7 ft	*	*	.050	*	*	.050	*	*	.050	*	*	.040	1/8	3	.060
	1	1	.070				1/64	20	.075	3/8	1	.060	1/4	1	.070
8 ft	*	*	.040	+	+	+	1/64	25	.060	*	*	.050	*	*	.050
	1/64	12	.060				1/64	12	.080						
9 ft															
10 ft															
11 ft															
12 ft	*	*	.040	*	*	.040	1/4	10	.050	1/2	1	.070	*	*	.050
	1/4	1	.080	1/4	1	.050	1/4	1	.064	1/8	1	.100			
13 ft	*	*	.040	*	*	.040	1/64	8	.060	*	*	.040	*	*	.040
	2	1	.060	1/8	1	.060				1/4	1	.070	1/8	1	.080

Table 3 (Cont'd)

Cell No.	76			77			78			79			80		
	Area Size	No. of Areas	Depth	Area Size	No. of Areas	Depth	Area Size	No. of Areas	Depth	Area Size	No. of Areas	Depth	Area Size	No. of Areas	Depth
1 ft	*	*	.050	*	*	.040	*	*	.050	*	*	.050	*	*	.050
	1/4	1	.060	1/8	1	.060									
2 ft	*	*	.050	+	+	+	*	*	.050	1/4	1	.070	*	*	.050
	1/4	1	.060							1 1/2	1	.060			
3 ft															
4 ft															
5 ft															
6 ft															
7 ft	*	*	.040	1/64	20	.060	*	*	.040			.050	*	*	.040
							3/8	1	.070	1	2	.070			
8 ft	1/4	1	.055	1/8	2	.075	*	*	.040	*	*	.040	*	*	.040
	1/2	1	.060	1/64	10	.060				1	3	.070			
9 ft															
10 ft															
11 ft															
12 ft	1/4	3	.050	*	*	.040	*	*	.040	1/16	8	.060	*	*	.040
	3/8	1	.125				1/4	1	.120						
13 ft	*	*	.040	*	*	.040	*	*	.040	1/64	10	.060	*	*	.040

Table 3 (Cont'd)

Cell No.	81			82			83			84			85		
	Area Size	No. of Areas	Depth	Area Size	No. of Areas	Depth	Area Size	No. of Areas	Depth	Area Size	No. of Areas	Depth	Area Size	No. of Areas	Depth
1 ft	2	1	.050	*	*	.050	*	*	.040	*	*	.040	*	*	.050
	3/8	1	.070	3/8	1	.120									
2 ft	+	+	+	*	*	.040	*	*	.050	1/64	15	.060	*	*	.040
				1/4	1	.060									
3 ft															
4 ft															
5 ft															
6 ft															
7 ft	*	*	.050	*	*	.040	*	*	.060	1/4	4	.060	1/4	6	.060
							3/8	1	.070	1/8	1	.080			
8 ft	*	*	.040	*	*	.050	*	*	.060	1/2	3	.060	1/64	15	.060
	1/4	1	.075	1/4	2	.060	1/2	1	.070						
9 ft															
10 ft															
11 ft															
12 ft	*	*	.040	*	*	.040	*	*	.050	*	*	.040	*	*	.040
				3/8	1	.050									
13 ft	*	*	.040	*	*	.040	*	*	.050	*	*	.040	*	*	.040
				1/2	1	.055	1/64	30	.080						

Table 3 (Cont'd)

Cell No.	86			87			88			89			90		
	Area Size	No. of Areas	Depth	Area Size	No. of Areas	Depth	Area Size	No. of Areas	Depth	Area Size	No. of Areas	Depth	Area Size	No. of Areas	Depth
1 ft	1/16	1	.090	1/64	1	.070									
	1/16	1	.055												
2 ft	1/8	1	.090	1/64	4	.65									
	1/8	1	.100												
3 ft															
4 ft															
5 ft															
6 ft															
7 ft	*	*	.050	1/2	1	.110									
8 ft	1/64	1	.060	*	*	.040									
9 ft															
10 ft															
11 ft															
12 ft	*	*	.040	1/4	1	.070									
13 ft	*	*	.040	*	*	.040									

3 LABORATORY TESTS AND RESULTS

To complement the field tests, several types of tests were performed in the laboratory. The tests were designed to measure material properties, such as tensile and interlock strength, compare the strength of corroded and uncorroded components, assess the structure's integrity, and provide constant values for use in later analysis. The testing was done on specimens obtained during the field testing. Figures 16 and 17 and Tables 4 through 8 provide results of the laboratory tests.

Figure 16. Tensile testing.

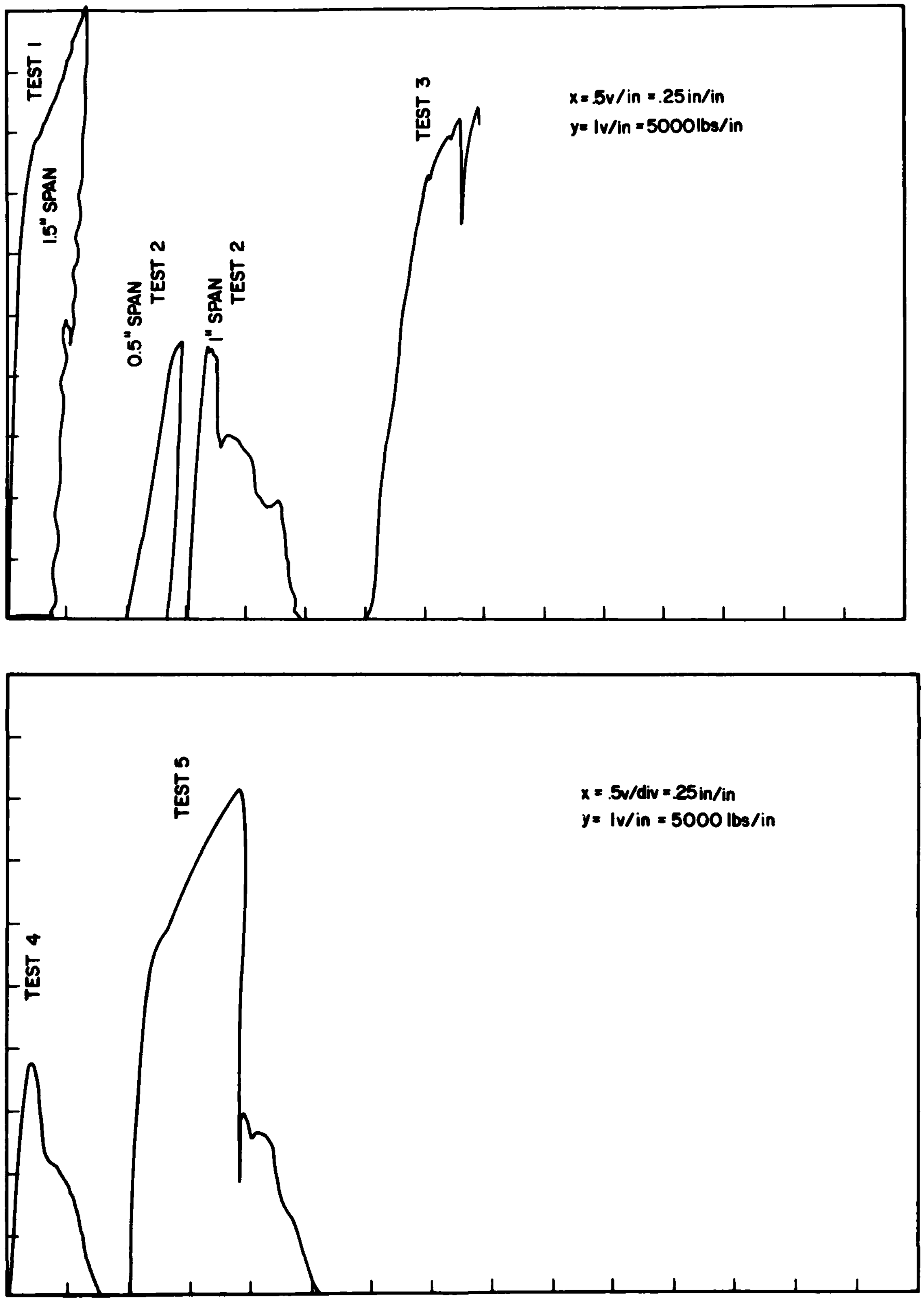

Figure 17. Typical plot of interlock tensile tests.

Table 4

Tensile Specimens—Uncorroded Lock Wall

Specimen	Initial Area (in.^{2})	Yield (psi)	Ultimate (PSI)
A	.251 x .503 = .1264	43,547	74,443
B	.251 x .503 = .1263	44,338	74,426
1	.504 x .3755 = .1893	43,547	74,443
2	.504 x .375 = .1890	44,339	74,426
3	.504 x .377 = .1900	43,684	73,158
4	.504 x .376 = .1895	40,633	72,296

Table 5

Spectrographic Analysis of Test Pile

Sample Number: 3	
Carbon	0.36%
Manganese	0.82
Phosphorus	0.006
Sulfur	0.021
Silicon	0.06
Nickel	0.01
Chromium	0.04
Molybdenum	<0.01
Copper	0.03

Table 6

Spectrographic Analysis of Tubercles*

<u>Sample Number: 1</u>

CO_3	3.45%
NO_3	0.12
SO_4	1.44
Chlorides	Present

<u>Qualitative Spectrochemical Analysis and Concentrational Estimates of Detected Constituents</u>

Iron	Major Constituent	
Silicon	0.3 - 3%	
Aluminum	0.05 - .5	
Zinc	0.03 - .3	
Magnesium, Calcium	0.02 - .2	each
Sodium, Manganese	0.01 - .1	each
Titanium	0.003 - .03	
Lead	0.002 - .02	
Molybdenum, Zirconium, Tin	0.001 - .01	each
Copper, Nickel	0.0003 - .003	each
Chromium	0.0002 - .002	
Vanadium, Cobalt	0.0001 - .001	each
Ash	73.25	

<u>Sample Number: 2</u>

CO_3	4.80%
NO_3	0.13
SO_4	1.98
Chlorides	Present

<u>Qualitative Spectrochemical Analysis and Concentrational Estimates of Detected Constituents</u>

Identical to No. 1 except for:

Sodium	0.02 - .2%
Ash	52.12

*Analysis is based on the recovered ash.

Table 7

Lock Wall Specimen Pitting Summary
(Specimen Plate Size--8 x 11 in.)

Cell Sample No. 2

Average thickness 0.349 in. (14 data points around edge; ultrasound testing in same locations.)

Depth	Number	Total Area	Average Area
.030	4	1.7875	.4468
.035	5	.4375	.0875
.040	6	.5625	.0937
.045	1	.0625	.0625
.050	2	.4375	.2187
.055	1	.125	.125
.065	1	.250	.250
.085	1	.125	.125

Cell Sample No. 17

Average thickness: 0.340 (10 data points)

Depth	Number	Total Area	Average Area
.030	2	.375	.1875
.035	4	1.250	.312
.040	2	.375	.1875
.045	6	1.500	.250
.000	-	.000	.000
.110	1	.375	.375

Cell Sample No. 34

Average thickness: 0.3398 (16 data points)

Depth	Number	Total Area	Average Area
.030	17	4.7187	.2775
.035	4	.625	.156
.040	6	2.125	.354
.045	2	.375	.1875
.000	-	.000	.000
.100	1	.0625	.0625

Table 7 (Cont'd).

Cell Sample No. 35

Average thickness: 0.3365 (16 data points)

Depth	Number	Total Area	Average Area
.030	19	3.999	.210
.035	5	.875	.0175
.040	13	1.575	.121
.045	4	.500	.125
.050	21	2.1874	.104
.055	2	.125	.0625
.060	12	1.3125	.109
.065	1	.0625	.0625
.070	12	.8279	.0689
.075	2	.0625	.0312
.080	1	.0625	.0625
.085	1	.0625	.0625
.000	-	.000	.000
.100	1	.0625	.0625

Cell Sample No. 60

Average thickness: 0.340 (10 data points)

Depth	Number	Total Area	Average Area
.030	6	1.875	.312
.035	6	.0937	.0156
.045	1	.500	.500
.050	3	.750	.250
.060	2	.375	.1875
.000	-	.000	.000
.090	1	.375	.375

Table 8

O'Brien Water Samples From Lock Wall Cell Interior (19 November 1979)

Chloride Samples 12/13/79

Sample No. (Cell No.)	Chloride Content Mole Equivalent/Liter	Ave
6	6	
	7	6
	6	
41	5	5
	5	
	10	
23	10	10
	9	
	10	
2	10	10
	10	
57	5	5
	6	
57 2nd Sample	5	5
	5	
6 2nd Sample	6	6
	6	

4 STRUCTURAL ANALYSIS OVERVIEW

The purpose of the structural analyses provided in Chapters 5, 6, and 7 was to estimate how long the sheet pile structural systems of the lock walls, guide walls, and dam would function satisfactorily without major repairs, and to provide a basis for developing a corrosion mitigation procedure. The life of a lock and dam depends on the corrosion rates in critical areas of the structure, but the stress analysis concentrates on minimum allowable thicknesses of sheet piles. The life of a sheet pile is the time it takes for corrosion to reduce the pile's thickness to its minimum allowable value.

Although pitting is harmful, it is not easily accounted for mathematically, except by statistical estimates of how much the pits reduce the mean thicknesses. Small, isolated, reduced sections in the sheet piling are not dangerous; also, corrosion reduces thicknesses rather uniformly. For example, Figure 18 is a profile of two interlocked test specimens cut from a test pile that had been underground for 21 years. Rust on the specimens was sand-blasted off. Corrosion had reduced the web thickness by about 33 percent, but this was an extreme case. The claws of the specimens are bent because they were pulled apart in laboratory testing. Figure 19 shows a specimen that is practically uncorroded; it had been embedded in clay near the bottom of a test pile for 21 years.

The analyses given in Chapters 5, 6, and 7 are based on assumptions that render the stresses on the piles statically determinant. The factor, C, by which the hydrostatic pressure of the soil is to be multiplied to provide the pressure on a sheet-pile wall is not well established. Rankine[4] derived the formula:*

$$C = \tan^2 (45^\circ - \frac{\theta}{2}) \qquad \text{[Eq 1]}$$

where θ is the angle of friction of the soil. A formula of Coulomb[5] sometimes is recommended in preference to Rankine's formula, because it involves an additional parameter--the friction of the soil on the wall. Terzaghi[6] suggested that $\theta = 34^\circ$ for gravel, but argued that determination of C is a matter of engineering judgment. For this analysis, the value C = 0.45 is used, in conformity with Coulomb. If Eq 1 is roughly correct, the value C = 0.45 is quite conservative.

The density of the fill at O'Brien Lock and Dam is not exactly the same as the density of the clay subsoil. Also, the variable C for the fill need not be the same as that of the subsoil. However, due to the uncertainty in the value of C, these differences are ignored.

All elevations except these quoted from referenced reports were measured from the bottom of the relevant sheet piles.

---

[4] S. Timoshenko and S. Woinowsky-Krieger, *Theory of Plates and Shells*, 2nd ed. (McGraw-Hill, 1959).

*Appendix C summarizes and defines the variables of all equations provided in this report.

[5] D. W. Taylor, *Fundamentals of Soil Mechanics* (John Wiley and Sons, 1948).

[6] K. Terzaghi, "Stability and Stiffness of Cellular Cofferdams," *Trans. ASCE*, Paper 2253 (September 1944), pp 1083-1202.

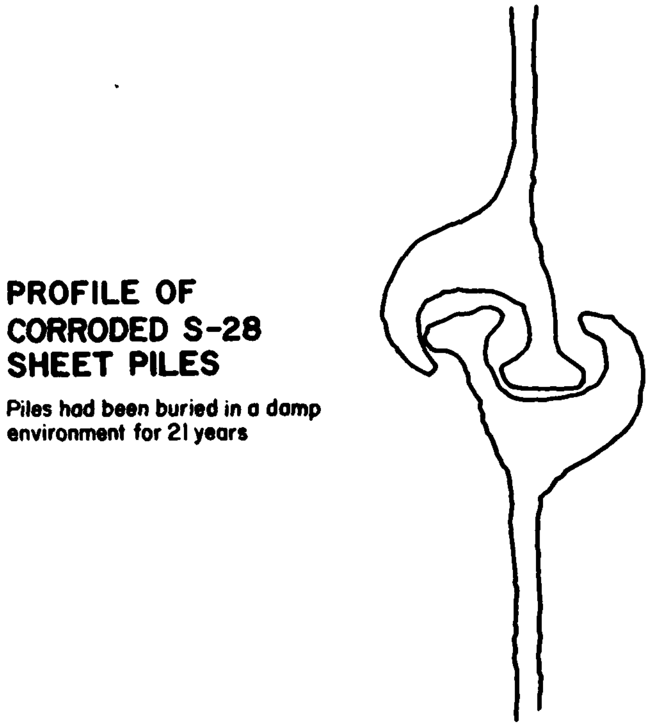

Figure 18. Corroded sheet piles.

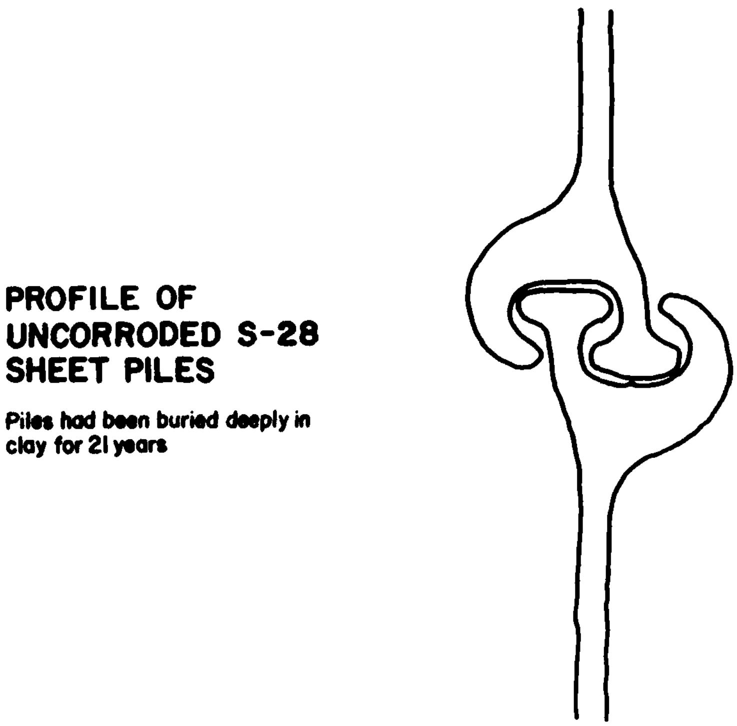

Figure 19. Uncorroded sheet piles.

5 INTERLOCK FAILURE MODE ANALYSIS

Variation of Interlock Strength With Corrosion

Hoop tension in the walls of a cellular cofferdam may damage the sheet piling, either by rupturing the webs or by pulling the claws apart. The hoop tension required to rupture the webs is $t\sigma_u$.

Figure 19 is a profile of two interlocked segments of sheet piles with little apparent damage, although this specimen had been buried deeply in clay for 21 years. A possible eventual mode of failure would be simultaneous tensile rupture of the shanks of the two bulbs. Before such a failure could occur, there would be considerable elongation of the shanks, as illustrated by Figure 20. It is apparent that the load, N_u, per inch required to cause this type of failure is

$$N_u = 2t_1\sigma_u \qquad \text{[Eq 2]}$$

If the shank thickness, t_1, is reduced greatly by corrosion, this type of failure may occur. Certainly, $N_u = 0$ if $t_1 = 0$. Usually, however, the shanks must bend before the claws part. Bending of the shanks causes the bulbs to pull on the hooks, and the hooks must also bend before the claws part. This behavior was illustrated in Figure 18.

The shanks and the hooks are subjected to combined tension and bending. Before shanks and hooks analysis, combined tension and bending of a ductile rectangular bar of thickness t and width w should be considered. The bar is subjected to a tension N and a bending moment M. Then N_w is the load per inch of width, and M_w is the bending moment per inch of width. Consequently, the dimension of N_w is $[F\ L^{-1}]$ and the dimension of M_w is [F]. With the usual assumption that plane cross sections remain plane, the axial strain ε_y is a linear function of the transverse coordinate x, that is,

$$\varepsilon_y = ax + b,$$

as illustrated by Figure 21. Consequently, the distribution of stress σ on the cross section is identical in form to the stress-strain curve of the material (Figure 21). The tension N and the bending moment M are determined by

$$N = \int_{-t/2}^{t/2} \sigma\, dx, \quad M = -\int_{t/2}^{t/2} x\sigma\, dx \qquad \text{[Eq 3]}$$

The stress-strain relationship is represented by

$$\sigma = f(\varepsilon_y) = f(ax+b)$$

If the function f is given, the integrals in Eq 3 can be evaluated, and then a and b can be expressed algebraically in terms of M and N. Then the abscissa c of the point of zero stress and strain can be determined by the equation

$$\varepsilon_y = ac+b = 0 \qquad \text{[Eq 4]}$$

In general, c depends on M and N.

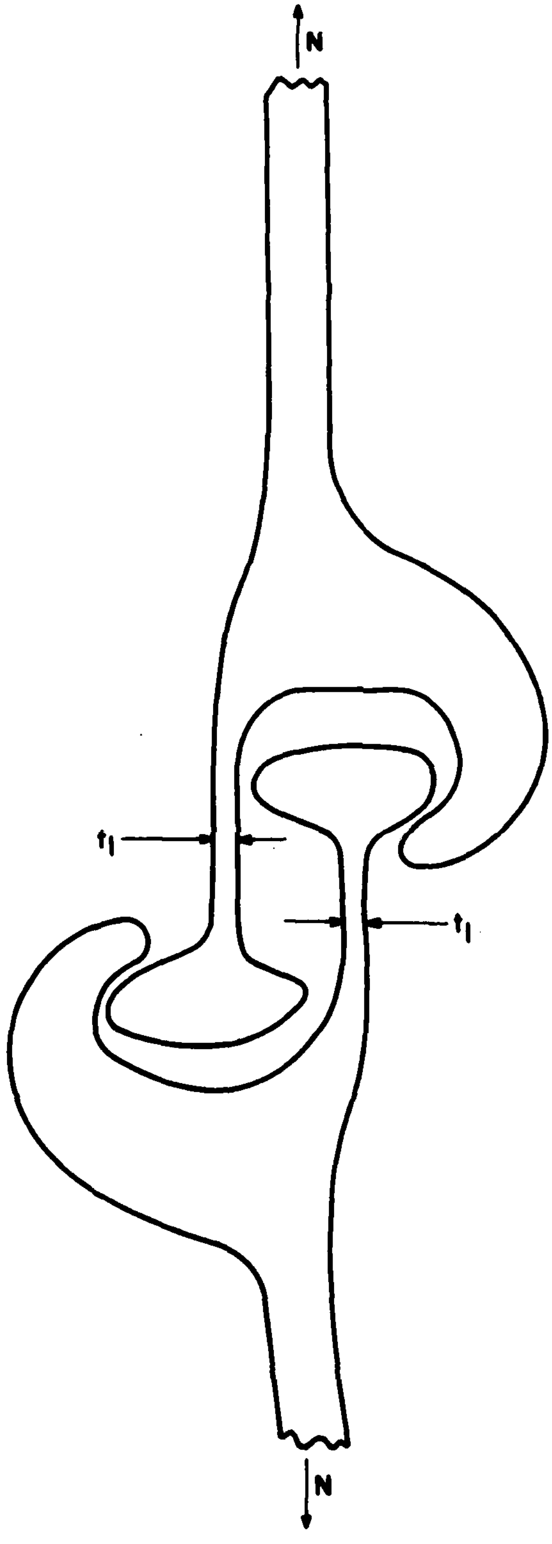

Figure 20. Exaggerated illustration of tensile yielding of the shanks.

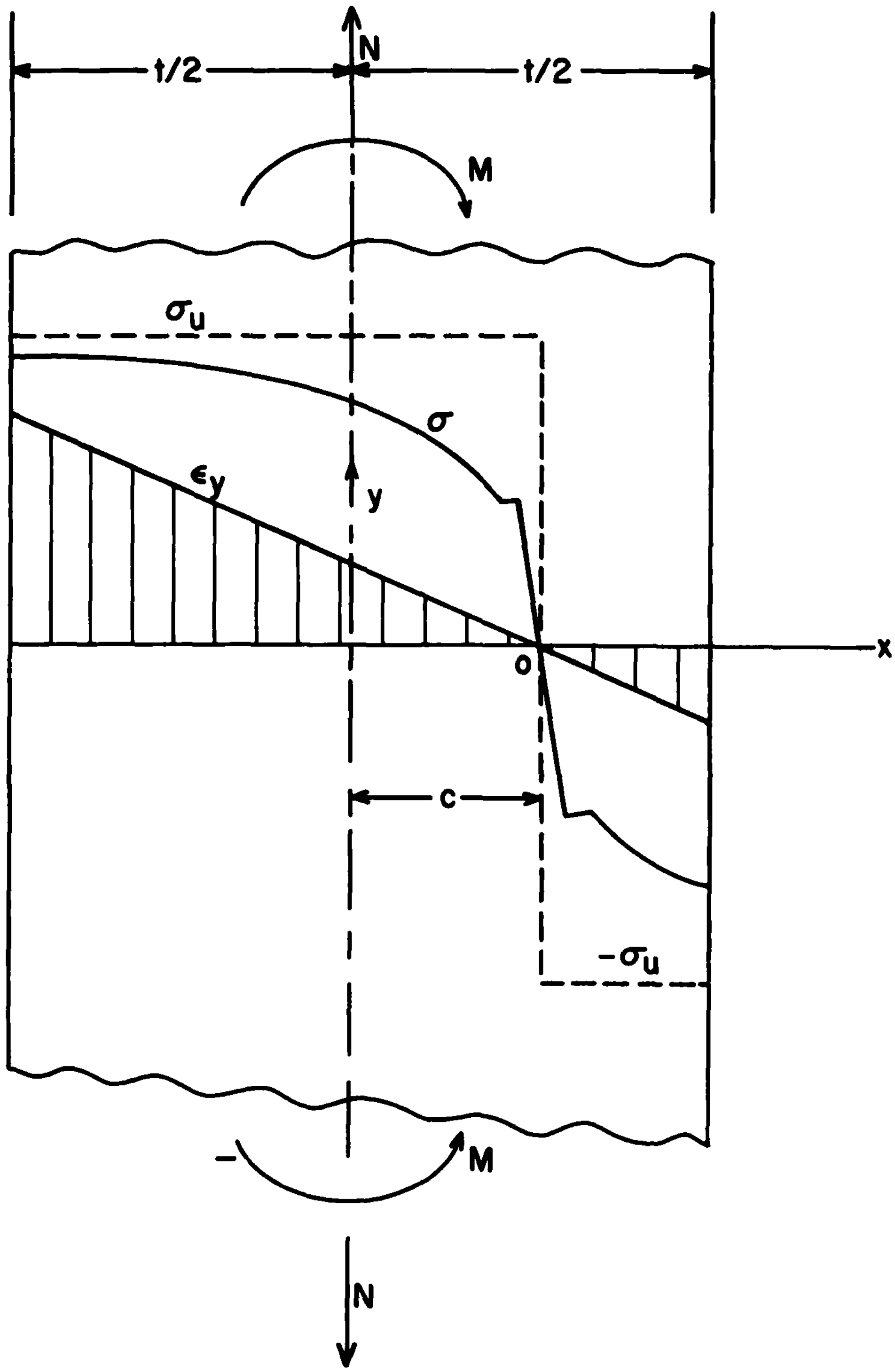

Figure 21. Combined tension and bending of a ductile bar.

The limiting case is reached if all the material is stressed to the ultimate value of σ_u. Then the stress distribution is as indicated by the dashed line in Figure 21, and a fully plastic hinge is said to exist. For this case, it is seen from Figure 21 that

$$N - (\frac{1}{2}t + c)\,\sigma_u + (\frac{1}{2}t - c)\,\sigma_u = 0 \qquad \text{[Eq 5]}$$

This equation reduces to:

$$N - 2\,c\sigma_u = 0. \qquad \text{[Eq 6]}$$

Also, equilibrium of moments about points 0 requires that

$$N\,c + M - \frac{1}{2}\sigma_u\,(\frac{1}{2}t + c)^2 - \frac{1}{2}\sigma_u\,(\frac{1}{2}t - c)^2 = 0 \qquad \text{[Eq 7]}$$

or

$$N\,c + M - \sigma_u\,(\frac{1}{4}\,t^2 + c^2) = 0 \qquad \text{[Eq 8]}$$

Elimination of c from Eqs 6 and 7 yields

$$M = \frac{1}{4}\,(t^2\sigma_u - \frac{N^2}{\sigma_u}) \qquad \text{[Eq 9]}$$

Equation 9 is to be applied to the shanks and hooks of an interlock.

When a claw is under tension, the right-hand bulb exerts a force, N_2, on the left-hand bulb. If the claw deforms symmetrically, this force acts along the center line of the webs, as illustrated by Figure 22. The left-hand hook exerts a downward force, N_1, on the left-hand bulb. The total tension in the shank of the left-hand bulb is $N_1 + N_2$. The bending moment in the shank of the left-hand bulb is

$$M = N_2e_2 - N_1e_1 \qquad \text{[Eq 10]}$$

When a fully plastic hinge develops in the shank of the left-hand bulb, Eqs 9 and 10 show that

$$4(N_2e_2 - N_1e_1) = t_1^2\sigma_u - \frac{(N_1 + N_2)^2}{\sigma_u} \qquad \text{[Eq 11]}$$

From Figure 22, the bending moment in the left-hand hook is N_1e_3. Consequently, by Eq 9, a fully plastic hinge develops in the left-hand hook when

$$4N_1e_3 = t_2^2\sigma_u - \frac{N_1^2}{\sigma_u} \qquad \text{[Eq 12]}$$

Eq 12 yields

$$N_1 = 2e_3\sigma_u\,(-1 + [1 + \frac{t_2^2}{4\,e_3^2}]^{1/2}) \qquad \text{[Eq 13]}$$

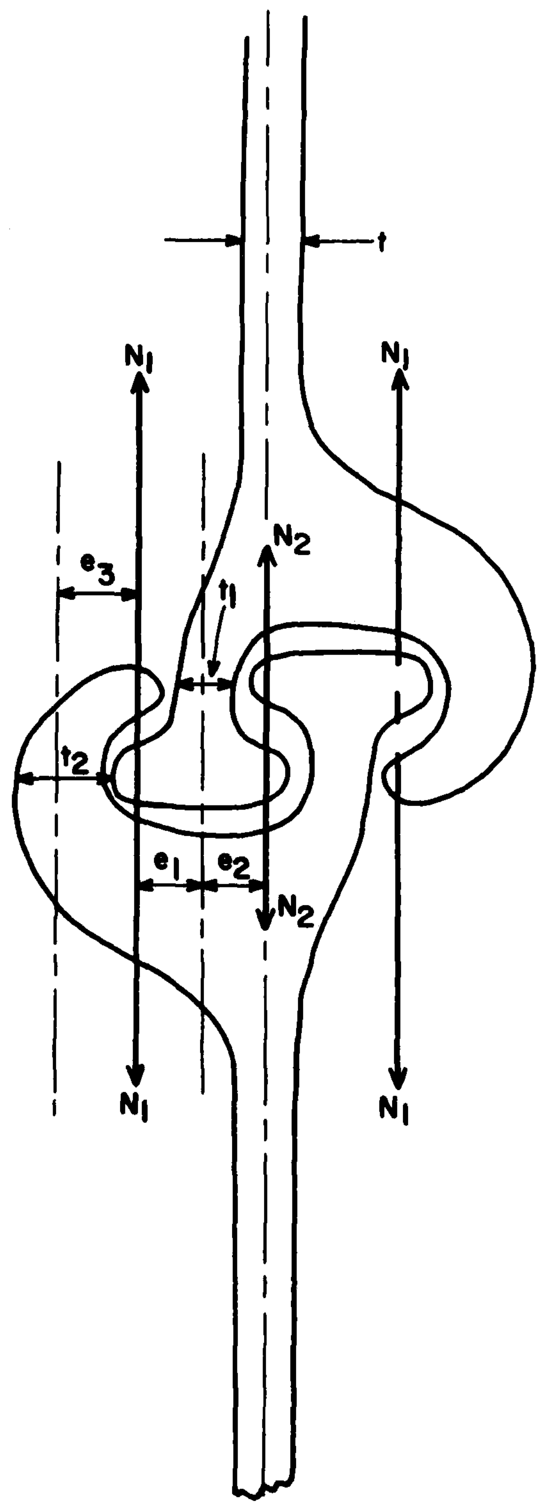

Figure 22. Trace of sheet piles interlock.

Eqs 11 and 13 determine N_1 and N_2. Generally, $N_2 > N_1$, since the shanks bend outward. It is convenient to write Eq 11 as follows:

$$(N_1 + N_2)^2 + 4(N_1 + N_2)e_2\sigma_u - 4N_1(e_1 + e_2)\sigma_u - t_1^2\sigma_u^2 = 0 \qquad \text{[Eq 14]}$$

Figure 22 shows that the total tension carried by a claw is

$$N_u = 2N_1 + N_2 \qquad \text{[Eq 15]}$$

Both N_1 and N_2 are directly proportional to σ_u.

The distances e_1 and e_2 are not known exactly. In view of this uncertainty, it is reasonable to assume that $e_1 = e_2$. Since $e_1 + e_3$ is the distance between the centerlines of the shank and the hook, e_3 is then determined. Corrosion does not affect the eccentricities e_1, e_2, e_3, but it reduces the thicknesses t_1 and t_2, as well as the web thickness t. It is assumed that t_1 and t_2 are reduced by the same amount, ε.

Numerical Calculations of Strengths of Corroded Sheet Piles

Piles in the land wall, the river wall, and the dam are made of U.S. Steel No. S-28. The initial web thickness is t = 0.375 in. Figure 22 is a tracing of an interlock of S-28 piles. Initially, the shank thickness is t_1 = 0.35 in., and the hook thickness is t_2 = 0.50 in., as determined by measurements of uncorroded specimens. After uniform corrosion, these thicknesses are reduced to

$$t = 0.375-\varepsilon, \quad t_1 = 0.35 - \varepsilon, \quad t_2 = 0.50 - \varepsilon$$

where ε is the reduction of the thicknesses caused by corrosion. Also, by measurements of the specimens,

$$e_1 = e_2 = 0.48 \text{ in.}, \quad e_3 = 0.56 \text{ in.}$$

For the following computations, σ_u is taken to be 60,000 lb/sq in., although this value may be low.

With these numbers, Eq 13 determines N_1. Then Eq 14 is a quadratic equation that determines $N_1 + N_2$. Finally, N_u is determined by Eq 15. This value of N_u is superseded by the value given by Eq 2, if it is lower. In turn, both of these values are superseded by $t\sigma_u$, if it is the lowest value. However, according to the present calculations, S-28 piles fail because the claws part, rather than because of shank fracture or web fracture, unless the corrosion is extremely severe.

Table 9 presents computed stresses N_u (lb/in.) required to pull the claws apart. These values are less than the web-rupture stress $t\sigma_u$ or the shank-rupture stress $2t_1\sigma_u$. A graph of the data in Table 9 is roughly a straight line. Although Table 9 was computed with σ_u = 60,000 lb/sq in., the stresses N_u corresponding to any other value of σ_u can be computed by proportioning the values in Table 9 directly as σ_u.

Table 9

Stress Required To Separate Claws of S-28 Sheet Piles

(σ_u = 60,000 lb/sq in.)

ϵ (in.)	N_u (lb/in.)
0	21120
0.01	20320
0.02	19530
0.03	18740
0.04	17980
0.05	17220
0.06	16480
0.07	15750
0.08	15030
0.09	14330
0.10	13640
0.11	12960
0.12	12300
0.13	11660
0.14	11030
0.15	10410
0.16	9820
0.17	9230
0.18	8660
0.19	8100
0.20	7570
0.21	7060
0.22	6560
0.23	6080
0.24	5610
0.25	5160
0.26	4730

6 ANALYSIS OF THE LOCK WALLS AND DAM

Probable Modes of Failure

The lock walls and dam are cellular cofferdams formed from interlocked S-28 sheet piles driven into clay and hard glacial till. Figure 23 shows a plan view of a lock wall. Where a cross wall joins the cylindrical walls, there is a Y-shaped pile; the other sheet piles are flat. The cells are filled with gravel.

A cellular cofferdam may fail in several ways. One type of failure is general heaving or tilting of the whole structure. However, this is not a hazard at the O'Brien Dam, since heaving has not occurred in the past, and the tendency for heaving is not aggravated by corrosion.

Terzaghi[7] regarded sliding in the interlocks of the cross walls as a potential type of failure. Corrosion actually mitigates this problem, since it tends to prevent slipping in the sheet-pile interlocks. Since slipping has not already damaged the cofferdams, it is unlikely that it will do so in the future. However, it is possible that the webs in the cross walls will become so corroded that they will rupture in shear.

The cell walls carry considerable horizontal tension due to the pressure of the fill and the water in the cells. If corrosion proceeds too far, this tension will cause the cells to burst. Since hoop tension is transmitted to the Y-piles at the junctions between the cylindrical walls and the cross walls, horizontal tension develops in the cross walls.

For studies of general stability of cellular cofferdams, the actual structure often is replaced by a box structuring with rectangular cells, as indicated by the dashed lines in Figure 23. For cofferdams with conventional proportions, the width b' of a rectangular cell is taken to be 0.9b, where b is the outside width of the cofferdam.

Figure 24 is a cross section of the lock's land wall. The 4-ft elevation is the assumed height of the surface of pore water in the backfill. The elevation -4 ft* is the height of the surface of the pool in the lock chamber.

Shear in a Cross Wall

The land wall of the lock carries greater shear than the river wall due to the pressure of the backfill. The greatest shear occurs at the bottom of the lock chamber. From Figure 24, the net pressure, ρ, tending to overturn the land wall is

$$\rho = C\gamma(H - x)\ , \quad x > s$$

$$\rho = C\gamma(H - s) + (C\gamma' + \gamma_w)(s - x), \quad h < x < s \qquad \text{[Eq 16]}$$

$$\rho = C\gamma(H - s) + (C\gamma' + \gamma_w)(s - x), \quad d < x < h$$

[7] K. Terzaghi (1944).
*4 ft below the top of the piles.

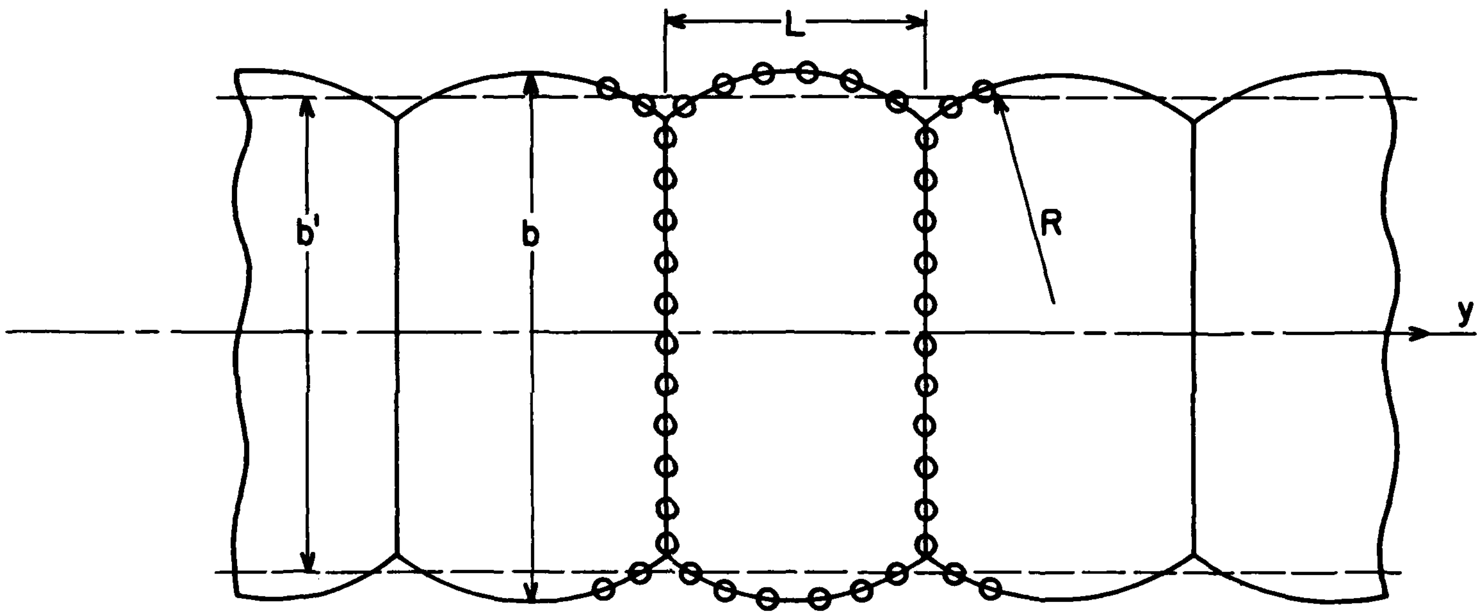

Figure 23. Cellular cofferdam.

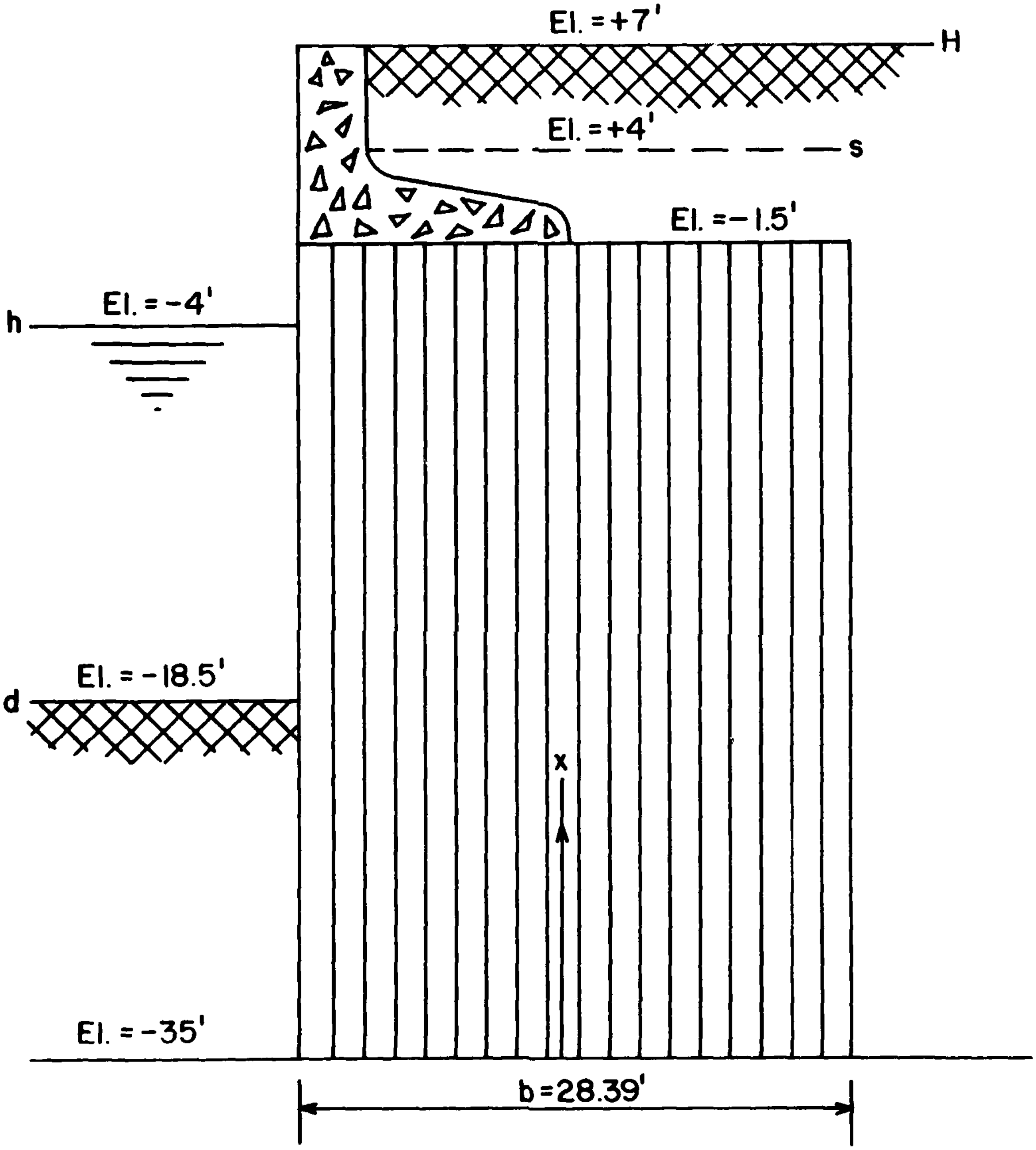

Figure 24. Cross section of land wall of lock.

The total shear in a cross wall at the bottom of the chamber is

$$F = L \int_{d}^{H} \rho \, dx$$

Consequently,

$$F = C\gamma L(H - s)(s - d) + \frac{1}{2}(C\gamma' + \gamma_w)L(s - d)^2$$
$$-\frac{1}{2}\gamma_w L(h - d)^2 + \frac{1}{2}C\gamma(H - s)^2 L \qquad \text{[Eq 17]}$$

From Figure 24, the following values are obtained for the land wall: H = 504 in., s = 468 in., h = 372 in., d = 198 in. From U.S. Army Corps of Engineers information,[8] L = 316 in. For fresh water, γ_w = 0.0361 lb/cu in. Also, γ = 0.0723 lb/cu in, γ' = 0.0376 lb/cu in., and C = 0.45.[9] With these numbers, Eq 17 yields F = 544,600 lb.

It is not correct to assume that all the shear, F, is carried by the cross wall, since some of it is carried by the fill in the cells.[10] However, lacking any reliable theory to estimate how much of the shear is carried by the fill, it is assumed that all of it is carried by the cross wall. A segment of the cofferdam lying between the middle planes of adjacent cells is similar to a big I-beam (Figure 25). The segments of the cylindrical walls from the flanges of the beam and the cross wall forms the web. For I-beams with heavy flanges, the shearing stress is nearly constant on a cross section of the web. Consequently, since b = 28.39 ft (see Figure 24), the shear flow (lb/in.) in the cross wall at x = d is

$$S = F/b' = 544{,}600/307 = 17{,}741 \text{ lb/in.}$$

This is the maximum shear flow expected in the cross wall under normal operating conditions for the lock.

When the lock is dewatered, the shearing force in the cross wall is higher. Then h = d, and Eq 17 yields F = 717,000 lb. Hence, for the dewatered condition, S = F/b' = 717,000/307 = 2335 lb/in.

At a Y-pile junction, half of the shear flow, S, passes into each of the contracting cylindrical walls. Consequently, the shear flow in the cross wall is twice that in either cylindrical wall at the junction.

Hoop Tension in a Cell of the Land Wall

The hoop tension in a cylindrical wall is determined by the membrane theory of shells:

$$N = Rq(x) \qquad \text{[Eq 18]}$$

where q(x) denotes the difference between the internal and external pressures on the cylindrical wall.

---

[8] *Plans for the Construction of Calumet River Lock and Controlling Works* (Chicago District, U.S. Army Corps of Engineers, November 1957).

[9] *Analysis of Calumet Sag Navigation Project-Lock* (M.J.M., August 1956).

[10] K. Terzaghi.

By statics, the horizontal tension transmitted to a cross wall at its junction with the cylindrical walls is

$$T = 2N\cos\alpha \qquad \text{[Eq 19]}$$

where α is half the angle between legs of the Y-pile. For the O'Brien Lock, $\alpha = 60°$. Consequently, $T = N$; i.e., the horizontal tension in a cross wall at its junction in the cylindrical walls is equal to the hoop tension in the cylindrical walls.

There is no danger of bursting the cylindrical shells on the land side of the land wall, since the sheet piles there are completely buried. For the chamber side, the pressure $q(x)$ in the range $x > d$ is the same as the function $p(x)$ defined by Eq 16. Consequently, for the cylindrical walls on the chamber side of the land wall, Eq 18 yields

$$N(x) = R[C\gamma(H - s) + (C\gamma' + \gamma_w)(s - x)], \quad h < x < s \qquad \text{[Eq 20]}$$

$$N(x) = R[C\gamma(H - s) + (C\gamma' + \gamma_w)(s - x) - \gamma_w(h - x)], \quad d < x < h$$

Eq 20 applies only up to X = 402 in., which is the top of the piles. The largest hoop tension occurs at the bottom of the chamber (i.e., at x = d). Consequently, the maximum hoop tension in the land wall is

$$N_{max} = R[C\gamma(H - s) + (C\gamma' + \gamma_w)(s - d) - \gamma_w(h - d)] \qquad \text{[Eq 21]}$$

For the land wall, R = 316 in. As in the preceding computations, H = 504 in., s = 468 in., h = 372 in., d = 198 in., γ_w = 0.0361 lb/cu in., γ = 0.0723 lb/cu in., γ' = 0.0376 lb/cu in., C = 0.45. With these values, Eq 21 yields N_{max} = 2909 lb/in. This is the maximum tension transmitted by the claws of the sheet piles under normal operating conditions. For the dewatered condition, h = d, and N_{max} = 4894 lb/in. The value s = 468 in. is somewhat arbitrary. After heavy precipitation, the fill might be saturated to the top; in this case, s = H. Then, for the normal operating condition, N_{max} = 3142 lb/in., and for the dewatered condition, N_{max} = 5127 lb/in. It is apparent that the height, s, of the surface of the pore water in the fill is quite influential.

An element of the web of a cross wall near the junction with the Y-pile is subjected to shear S and tension N, as illustrated by Figure 26. By the Mohr circle, the maximum shear in the cross wall is

$$S_{max} = (S^2 + \frac{1}{2} N^2_{max})^{1/2} \qquad \text{[Eq 22]}$$

For the normal operating condition, S = 1774 lb/in. and N_{max} = 2909 lb/in. Consequently, S_{max} = 2294 lb/in. For the dewatered condition, S = 2335 lb/in. and N_{max} = 4894 lb/in. Then S_{max} = 3382 lb/in. These results are on the high side, since shear carried by the fill in a cell has been neglected. However, they indicate that the point of highest stress in the lock wall is in a cross wall near its junction with the cylindrical walls on the chamber side of the land wall, and at the elevation of the bottom of the chamber.

The ultimate shearing stress of the steel is probably greater than 30,000 lb/sq in. The maximum shear in a cross wall is that for the dewatered condition (in this case, 3382 lb/in). Accordingly, the minimum allowable thickness of a web in the cross wall is

$$t = \frac{3,382}{30,000} = 0.11 \text{ in.}$$

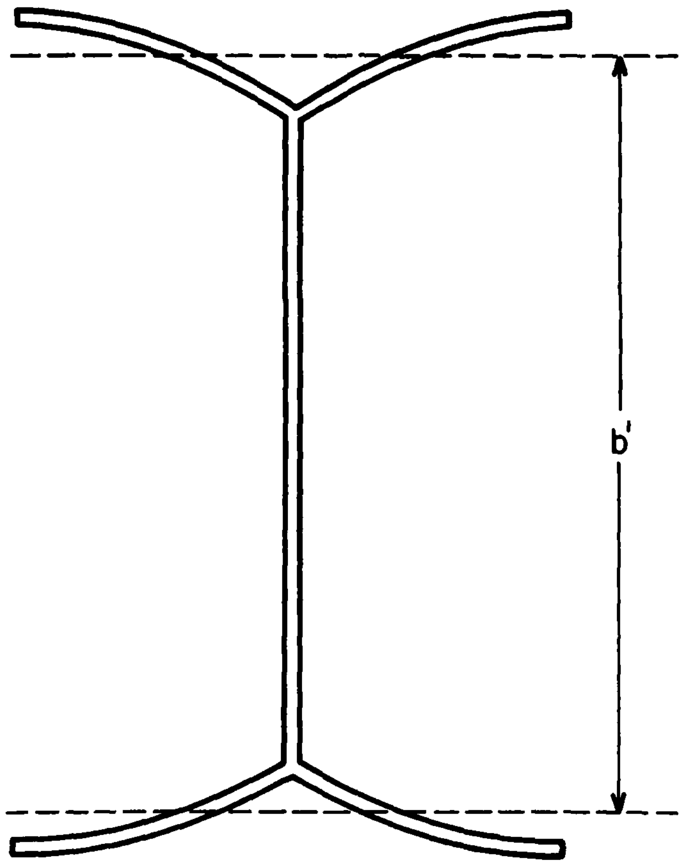

Figure 25. Segment of a cofferdam represented as an I-beam.

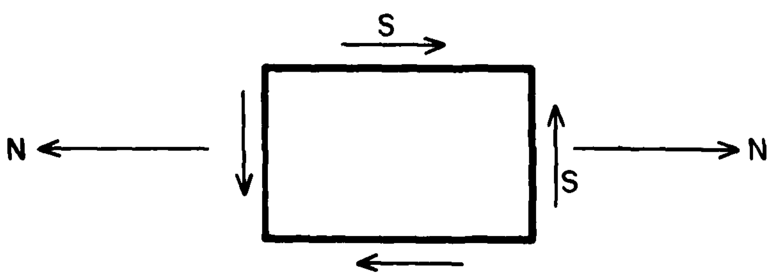

Figure 26. Stress in an element of a web of a cross wall.

Since the initial thickness is 0.375 in., severe corrosion can develop before the cross walls are in danger of failure.

The maximum tension in the claws of the sheet piles has been determined to be about 5100 lb/in. Table 9 showed that the reduction, ε, of thickness due to corrosion may be 0.25 in. before there is danger of pulling the claws apart.

Hoop Tension in River Wall Cells and Dam Cells

Figure 27 is a cross section of the river wall. It shows that H = 504 in., h = 372 in., s = 456 in., and d = 252 in. on the river side, and that d = 198 in. on the chamber side. Also, for the river wall, R = 244 in. The maximum hoop tension occurs at the bottom of the lock chamber, at x = d = 198 in. Consequently, Eq 21 again applies, yielding

$$N_{max} = 2186 \text{ lb/in.}$$

There is no appreciable transverse shear in a cross wall of the river wall. Consequently, under normal operating conditions, N_{max} = 2186 lb/in. is the maximum principal stress both in the cross wall and in the cylindrical walls on the chamber side of the river wall. For the dewatered condition, h = d, and Eq 21 yields

$$N_{max} = 3719 \text{ lb/in. for the dewatered condition.}$$

Eq 21 also applies for the river side of the river wall, with d = 252 in. The chamber side of the river wall is stressed somewhat more than the river side.

The dam is similar to the river wall. Data for the dam are:[11]

$$L = R = 201.5 \text{ in.},\ H = 312 \text{ in.},\ d = 138 \text{ in.}$$

If the elevation of the water surface downstream from the dam is -4 ft, as for the downstream guide wall, h is 198 in. If, as for the river wall, the surface of the pore water in the cells is taken to be 4 ft below the top of the piles, s = 264 in. Then, by Eq 21, N_{max} = 1220 lb/in. in the dam. This is the hoop tension in the downstream side of the dam at the level of the bottom of the river. It is also the horizontal tension in the cross wall at that point.

[11] *Plans for the Construction of Calumet River Lock and Controlling Works.*

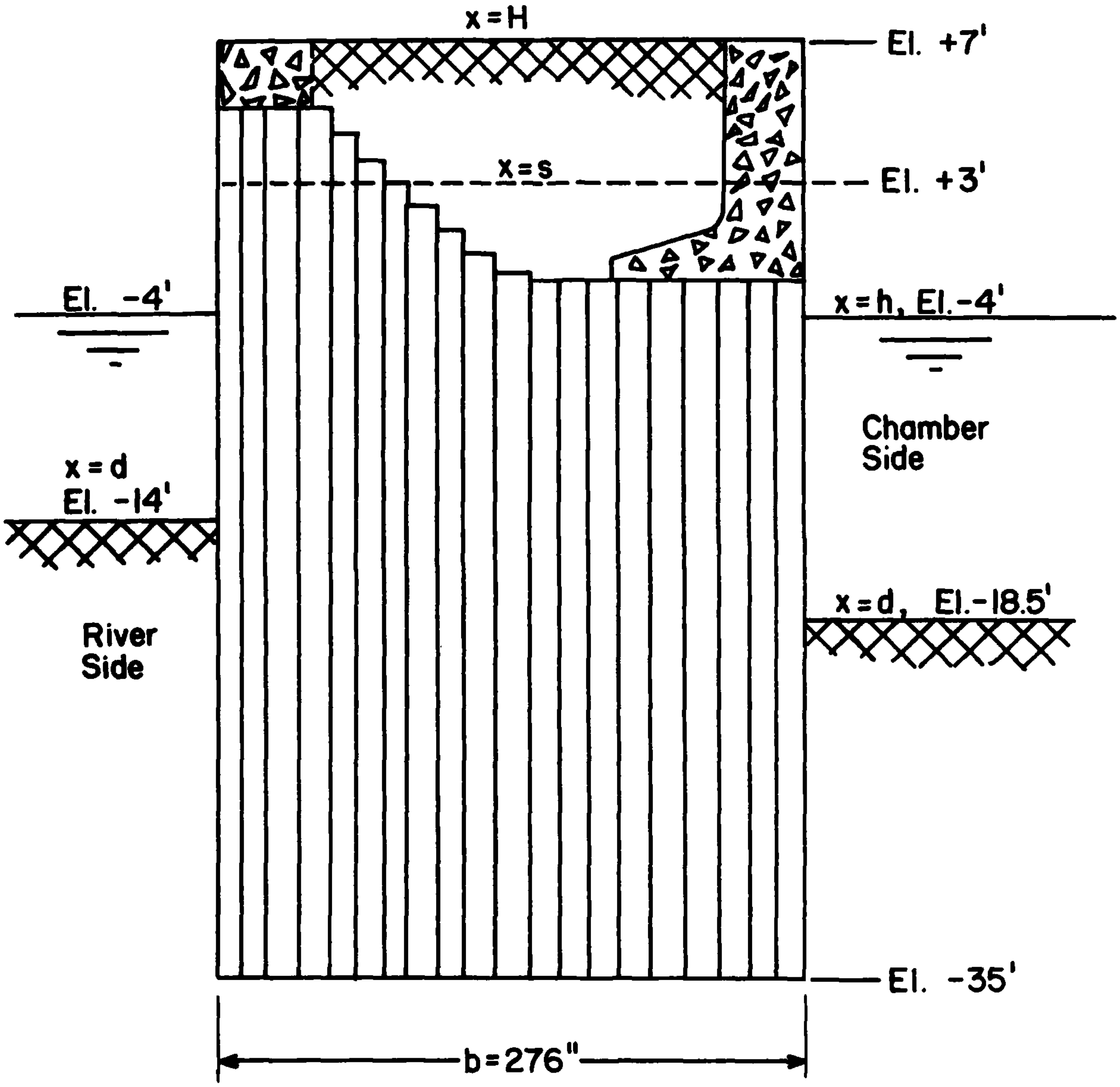

Figure 27. Cross section of river wall.

7 ANALYSIS OF THE GUIDE WALLS

Configuration of Walls and Tie Back Systems

A guide wall is essentially a corrugated plate formed by interlocking z-shaped sheet piles driven into clay and glacial till. Figure 28 shows a plan view of the wall. A capping plate on top of the piles with a lip on one side is attached to the top of the piles by short pieces of welded-on rolled angles. A wale consisting of two rolled channels back-to-back, several yards below the pile cap (Figures 28 and 29) is connected by buried tie rods to a buried sheet-pile wall located at some distance behind the guide wall. The tie rods are several yards apart. There are 8- x 12-in. wooden fenders bolted to the guide wall. These fenders tend to strengthen the wall, but high localized stresses in the sheet piling may occur when barges or boats bump into them. Only stresses caused by earth pressure and water pressure on the walls are considered in the following analysis. The fenders are disregarded.

Pressure on the Wall

The corrugated guide wall is regarded as a flat orthotropic plate. Rectangular coordinates (x,y) are set up in the plane of the plate, such that the y-axis coincides with the bottom edge of the wall, and the x-axis is directed vertically upward. One bay of the wall between successive tie rods is considered. The tie rods are attached to the wale at $y = 0$ and $y = L$. The bottom of the river adjacent to the wall lies at $x = d$; the level of the water in the river is at $x = h$; the wale lies at $x = a$, and the top of the wall lies at H. The backfill is saturated with water to the level $x = s$ (Figure 29). Although the backfill does not rise quite to the top of the wall, it is close to it. As a conservative estimate, the level of the top of the backfill is taken to be $x = H$.

Below the level of the river bottom, the soil pressures on the two sides of the sheet pilings are generally unequal. The wall deflects, and, where it is embedded in the subsoil, the passive soil pressure acts at any given point on one side of the wall, and the active soil pressure acts at the adjacent point on the other side.[12] It is reasonable to assume that the deflection has a constant sign everywhere on a horizontal line along the wall. Thus, the net pressure, q, that the backfill, the water, and the subsoil exert on the wall depends only on the vertical coordinate x; it does not depend on y.

Since the piles penetrate deeply into the subsoil, there is no appreciable horizontal movement at the foot of a pile. Consequently, the deflection is believed to have a constant sign over the entire wall (i.e., everywhere the deflection has the same sense [is consistent in direction]). The net pressure q is the algebraic sum of the pressures on the front and back sides of the wall. Consequently, as Figure 29 indicates, the pressure is given by the following equations:

$$q = C\gamma(H - x), \quad x > s \qquad \text{[Eq 23]}$$

$$q = C\gamma(H - s) + (C\gamma' + \gamma_w)(s - x), \quad h < x < s$$

$$q = C\gamma(H - s) + (C\gamma' + \gamma_w)(s - x) - \gamma_w (h - x), \quad d < x < h$$

[12] K. Terzaghi.

$$q = C\gamma(H - s) + (C\gamma' + \gamma_w)(s - x) - \gamma_w(h - x) - \bar{C}\gamma'(d - x), \quad x < d$$

in which C is the coefficient of active earth pressure and $\bar{C}$ is the coefficient of passive earth pressure. Eq 23 complies with the condition that q(x) is continuous in the entire range $0 < x > H$.

Beam Analysis of the Guide Wall

The guide wall will carry little horizontal tension, since such tension would flatten the corrugations. The equilibrium equations for plates[13] then indicate that all the membrane stresses (N_x, N_y, N_{xy}) are small. Also, the bending moment M_y is practically zero because the interlocks in the piles act like hinges. Furthermore, the transverse shear Q_y on any vertical section is small because the webs in the sheet piles are thin. It may be concluded from the equilibrium equations for moments in a plate[14] that the twisting moment M_{xy} is small. The significant reactions are consequently the bending moment M_x and the shear Q_x on a horizontal section. For brevity, M_x is denoted simply by M.

In view of these simplifications, a vertical strip of the guide wall of unit width acts like a uniform beam carrying the lateral load q(x). At the top, the beam carries a concentrated reaction, F_2, from the capping plate (Figure 2). There is no bending moment at the top, if torsional stiffness of the capping plate is neglected (i.e., M = 0 at x = H). At the point x = a, the beam carries a concentrated force, F_1, from the wale. Since F_1 and F_2 are forces per unit width in the y-direction, their dimension is [F L^{-1}]. Likewise, since M is a bending moment per unit width, its dimension is [F].

Since any vertical strip of the wall is in equilibrium, and since there is no shear at the bottom of a sheet pile.

$$F_1 + F_2 = \int_0^H q(x)\, dx \qquad \text{[Eq 24]}$$

Eqs 23 and 24 yield

$$2(F_1 + F_2) = C\gamma(H^2 - s^2) + (C\gamma' + \gamma_w)s^2 - \gamma_w h^2 - \bar{C}\gamma' d^2 \qquad \text{[Eq 25]}$$

Also, moments must balance about the axis of the wale. Since there is no shear or bending moment at the foot of a pile, this condition yields

$$- F_2(H - a) + \int_0^H (x - a)q(x)\, dx = 0 \qquad \text{[Eq 26]}$$

Eqs 23 and 26 yield

$$\begin{aligned} &- C\gamma(H^3 - s^3) - (C\gamma' + \gamma_w)s^3 + \gamma_w h^3 + \bar{C}\gamma' d^3 + 3C\gamma a(H^2 - s^2) \\ &+ 3(C\gamma' + \gamma_w)as^2 - 3\gamma_w ah^2 - 3\bar{C}\gamma' ad^2 + 6F_2(H - a) = 0 \end{aligned} \qquad \text{[Eq 27]}$$

Eq 27 shows that F_2 does not depend on y. Consequently, Eq 25 shows that F_1 also does not depend on y.

---

[13]S. Timoshenko and S. Woinowsky-Krieger.
[14]S. Timoshenko and S. Woinowsky-Krieger.

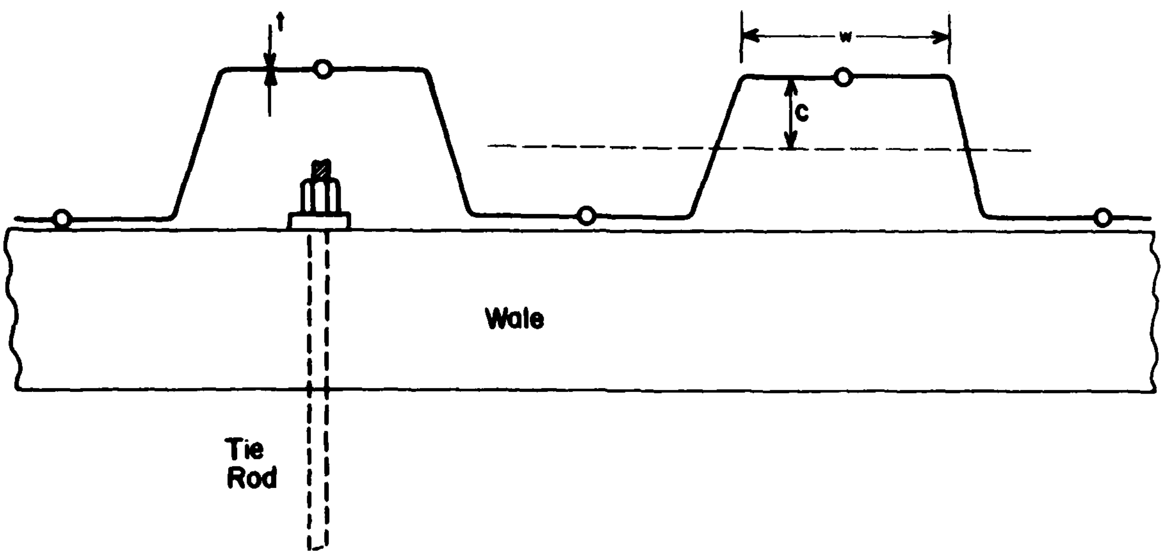

Figure 28. Horizontal section of sheet piling guide wall.

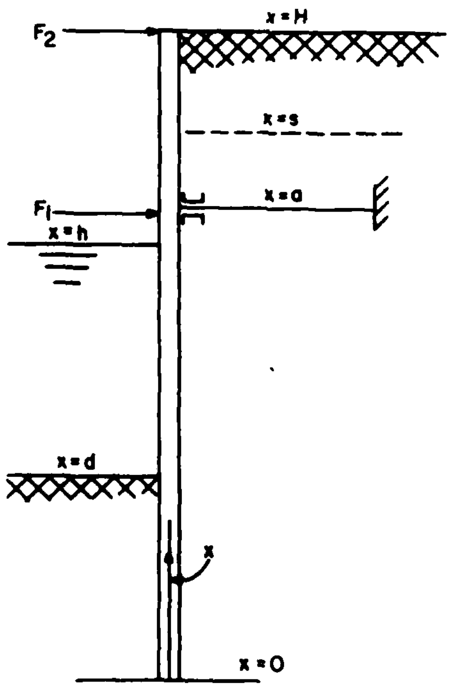

Figure 29. Guide wall.

The tension, P, in a tie rod must balance the forces on one bay of the wall. Since there is no shear in the wale or the pile cap at y = 0 or y = L,

$$P = \int_0^H \int_0^L q(x)\, dx\, dy = L \int_0^H q(x)\, dx \qquad \text{[Eq 28]}$$

Consequently, by Eq 24,

$$P = (F_1 + F_2)L \qquad \text{[Eq 29]}$$

Eqs 25 and 29 determine P.

Treating a unit vertical strip of the guide wall as a beam, the data in Figure 29 gives

$$M = F_2(H - x) - \int_x^H (u - x)q(u)du, \quad x > a \qquad \text{[Eq 30]}$$

$$M = F_1(a - x) + F_2(H - x) - \int_x^H (u - x)q(u)du, \quad x < a$$

where u is a variable of integration. With Eq 23, the integrals in Eq 30 can be evaluated. Thus,

$$M = F_2(h - x) - \frac{1}{6} C\gamma(H - x)^3, \text{ in } x > s \qquad \text{[Eq 31]}$$

$$M = F_2(h - x) - \frac{1}{6} (C\gamma' + \gamma_w - C\gamma)(s - x)^3 - \frac{1}{6}C\gamma(H - x)^3$$

$$\text{in } a < x < s$$

$$M = F_1(a - x) + F_2(H - x) - \frac{1}{6}(C\gamma' + \gamma_w - C\gamma)(s - x)^3$$
$$- \frac{1}{6} C\gamma(H - x)^3, \text{ in } h < x < a$$

$$M = F_1(a - x) + F_2(H - x) - \frac{1}{6}(C\gamma' + \gamma_w - C\gamma)(s - x)^3$$
$$- \frac{1}{6}C\gamma\, (H - x)^3 + \frac{1}{6}\gamma_w(h - x)^3, \text{ in } d < x < h$$

$$M = F_1(a - x) + F_2(H - x) - \frac{1}{6}(C\gamma' + \gamma_w - C\gamma)(s - x)^3$$
$$- \frac{1}{6} C\gamma(H - x)^3 + \frac{1}{6} \gamma_w(h - x)^3 + \frac{1}{6} \bar{C}\gamma'(d - x)^3, \text{ in } x < d$$

By Eq 31, M is continuous in the range $0 < x < H$. Because of Eqs 25 and 27, the last of Eq 31 complies with the requirement that M = 0 at x = H. Also, M = 0 at x = H, and Q_x = 0 at x = 0.

Ordinarily, the maximum moment M_{max} occurs in the interval $x < d$. Consequently, by Eq 31, M_{max} occurs at the point x, determined by

$$2\frac{dM}{dx} = - 2(F_1 + F_2) + (C\gamma' + \gamma_w - C\gamma)(s - x)^2 + C\gamma(H - x)^2$$
$$- \gamma_w(h - x)^2 - \bar{C}\gamma'(d - x)^2 = 0$$

With Eq 25, this yields

$$x = \frac{2[-(C\gamma' + \gamma_w - C\gamma)s - C\gamma H + \gamma_w h + \bar{C}\gamma' d]}{(\bar{C} - c)\gamma'} \qquad \text{[Eq 32]}$$

The value of x given by Eq 32 is to be substituted into the last of Eq 31 to yield M_{max}.

Eqs 25 and 27 determined F_1 and F_2, if C and $\bar{C}$ are known. However, $\bar{C}$, in particular, is hard to estimate. If the capping plate is eliminated, $F_2 = 0$. The capping plate imposes less restraint on the sheet piles than the wale, since it is not connected directly to the tie rods; consequently, it may undergo appreciable deflection at the stations of the tie rods. Using the assumption $F_2 = 0$, Eq 27 determines the value of $\bar{C}$ that is statically consistent with the value of C. Eq 25 then determines F_1.

Crumpling of the Sheet Piles

The bending moment, M, given by Eq 31, causes compression and tension stresses in the sheet piling, which are defined by the well-known beam equation.

$$\sigma = \frac{M\ c}{I} \qquad \text{[Eq 33]}$$

It is unlikely that this stress will rupture the piles, even though corrosion is severe, since local buckling, called "crumpling" or "crippling," will occur on the compression side before rupture occurs on the tension side.

On the basis of the effective-modulus theory, there is a method[15] for simultaneously plotting buckling curves for plates and columns. With column data only, it permits compression buckling stresses for plates with various edge conditions to be estimated, when these stresses exceed the material's compression proportional limit. This method may be used to compute the crumpling stress of the compression side of the sheet piling.

Beedle et al.,[16] have given extensive data for structural steel columns. Their results show that the well-known parabolic approximation is quite accurate for mild steel columns; i.e.,

$$\sigma_{cr} = \sigma_y \left[1 - \frac{\sigma_y L^2}{4\pi^2\ CE\rho^2} \right], \quad \frac{L}{\pi\rho\sqrt{C}} \leq \left(2\ \frac{E}{\sigma_y}\right)^{1/2} \qquad \text{[Eq 34]}$$

$$\sigma_{cr} = C\pi^2\ E \left(\frac{\rho}{L}^2\right), \quad \frac{L}{\pi\rho\sqrt{C}} \geq \left(2\ \frac{E}{\sigma_y}\right)^{1/2}$$

where L/ρ is the slenderness ratio of the column, σ_y is the compression yield stress, and C is the end fixity factor; i.e., $L/\ C$ is the reduced length. The second part of Eq 34, which applies for sufficiently large L/ρ, is the Euler formula.

---

[15] H. L. Langhaar, "Buckling of Aluminum-Alloy Columns and Plates," *Jour. Aero. Sci.*, Vol 10, No. 7 (July 1943), pp 218-222.

[16] L. S. Beedle, T. V. Galambos, and L. Tall, *Column Strength of Constructional Steels*,

By the method described in Langhaar,[17] Eq 34 is modified to cover inelastic buckling of axially compressed plates. The abscissa $L/\pi\rho\sqrt{C}$ of the column curve is merely replaced by $w/t\sqrt{K}$, where w is the width of the plate, t is the thickness of the plate, and K is the edge fixity factor. Accordingly, the crumpling stress of the steel piling (modulus of rupture) is

$$\sigma_{cr} = \sigma_y \left(1 - \frac{\sigma_y w^2}{4KEt^2}\right), \quad \frac{w}{t\sqrt{K}} \leq \left(2\,\frac{E}{\sigma_y}\right)^{1/2} \qquad \text{[Eq 35]}$$

$$\sigma_{cr} = K\,E\,\left(4\,\frac{K}{w^2}\right)^2, \quad \frac{w}{t\sqrt{K}} \geq \left(\frac{1}{2}\,\frac{E}{\sigma_y}\right)^{1/2}$$

For hat-type stringers,[18] w is interpreted to be the width of the hat between the centroids of the cross sections of the filleted areas. This interpretation will also be used for the sheet piles (Figure 28). The value of K is questionable, but for axially compressed square tubes with rounded edges, the value K = 6.25 conforms well with experimental data.[19] No doubt, the sheet piling will carry a greater stress than a uniformly compressed square tube with width w and thickness t, since the sloping walls in the sheet piling tend to support the highly stressed flanges. However, the value of X (the elevation of surface of pore water in the fill) is not very important, and the value K = 6.25 is used in the following computations.

Due to corrosion of the sheet piling, the thickness, t, gradually diminishes with time. Eq 35 determines the crumpling stress, and hence, the maximum bending moment, M, corresponding to any given thickness, t. After some time, the thickness of a sheet pile at a critical section is reduced by an amount, ε, due to corrosion; i.e., the thickness at that time is $t_0 - \varepsilon$, where t_0 is the initial thickness. Then the mean moment of inertia of the pile, per unit width in the y-direction, is

$$I = I_0 - k\varepsilon \qquad \text{[Eq 36]}$$

where I_0 is the initial value of the moment of inertia, and k is a constant determined by the shape of the cross section. The value of ε at which the pile will crumple is determined by equating the bending stress Mc/I to the stress σ_{cr} in Eq 35. Thus, with K = 6.25,

$$M\,\frac{c}{I_0 - k\varepsilon} = \sigma_y\left(1 - \frac{\sigma_y w^2}{25E(t_0 - \varepsilon)^2}\right) \qquad \text{[Eq 37]}$$

This equation may be written as follows:

$$\varepsilon = \frac{I_0}{K} - \frac{Mc}{K\sigma\left(1 - \dfrac{\sigma_y w^2}{25\varepsilon(t_0 - \varepsilon)^2}\right)} \qquad \text{[Eq 38]}$$

Fritz Lab. Reprint No. 177 (U.S. Steel Co.).

[17] H. L. Langhaar.

[18] H. L. Langhaar.

[19] L. S. Beedle, T. V. Galambos, and L. Tall.

Eq 38 is to be solved for ε. A first approximation is

$$\varepsilon_1 = \frac{I_0}{k} - \frac{M\ c}{k\sigma_y} \qquad \text{[Eq 39]}$$

The value ε_1 may be substituted into the right side of Eq 38 to provide a second approximation, ε_2. Then ε_2 may be substituted into the right side of Eq 38 to provide a third approximation, ε_3, and so on. Instead of Eq 39, any starting value ε based on engineering judgment may be used.

ε_{all} = 0.20 in. is a reasonable working value; however, in regions of low or moderate stress, this number could be greatly exceeded. To translate the number ε_{all} = 0.20 in. into projected years of service requires detailed knowledge of the corrosion rates at critical places in the lock. Measurements taken during dewatering of the lock chamber in 1979 indicated that the mean thickness of the webs of sheet piles in the cofferdam is 0.348 in. Initially, the thickness of these webs was nominally 0.375 in. The reduction occurred over 21 years. (The standard deviation of the measurements was 0.008 in.)

The probability that a normally distributed random variable will lie within one standard deviation of the mean is 0.682; the probability that it will lie within two standard deviations of the mean is 0.954, and the probability that it will lie within three standard deviations of the mean is 0.997. Consequently, on the basis of the cited measurements, there should be very few places where the web thickness is less than 0.324 in. (which is three standard deviations from the mean). Accordingly, a likely upper bound for the present amount of corrosion of the lock wall is

$$\varepsilon = 0.375 - 0.324 = 0.051 \text{ in.}$$

Since this reduction is considered to have occurred over 21 years, an extreme value of the corrosion rate is then

$$\varepsilon = 0.051/21 = 0.0024 \text{ in. per year}$$

Consequently, the time required for the allowable amount of corrosion (ε_{all} = 0.20 in.) to be reached is

$$0.20/0.0024 = 83 \text{ years}$$

This period began when the lock opened (1958). Accordingly, the webs of the sheet piles in the lock walls should serve until 2041. This is also true for the claws of the interlocks in the cofferdam walls, if the shanks and hooks in the claws corrode at the same rate as the webs. However, crevice corrosion rates for parts of the claws are not as well known as those of the webs. Thus, more data about the corrosion rates of the claws are desirable.

Failure of the Wale or a Tie Rod

A possible mode of failure is a tension rupture of a tie rod, as given by Eqs 25 and 29.

The wale can fail in several ways. Lateral buckling might be a mode of failure, but such a collapse is unlikely because of the resistance provided by the sheet piling and the backfill.

A shear failure of a channel's web is another possibility. The shearing stress in the web is given by the equation,

$$\tau = \frac{VQ_1}{2I_1 t_1} \qquad \text{[Eq 40]}$$

in which I_1 is the moment of inertia of the cross section of the wale (two channels), Q_1 is the moment of area of the cross section of the wale on one side of the neutral axis (two channels), and t_1 is the thickness of the web of a channel. The factor 2 enters because the total thickness of the two webs is $2t_1$. The maximum shear in the wale occurs at $y = 0$ and $y = L$. Its value is $V = F_1 L/2$. Consequently,

$$\tau = \frac{Q_1 \; F_1 \; L}{4 \; I_1 \; t_1} \qquad \text{[Eq 41]}$$

A shear failure of the wale may be expected if τ exceeds the shear yield stress of the steel, since large deflections and severe buckling of the web will then occur. By the von Mises theory of plasticity, the shear yield stress is equal to $\sigma_y \sqrt{3}$.

The wale may also fail if plastic hinges form at $y = 0$, $y = L/2$, and $y = L$. The bending moment in a plastic hinge is

$$m_0 = 2 \; Q_1 \; \sigma_u$$

Since the wale carries a uniform load F_1, and since moments m_0 occur at $y = 0$ and $y = L/2$, the following equation is derived by statics:

$$m_0 = \frac{F_1 \; L^2}{16} \qquad \text{[Eq 42]}$$

Local crumpling of the sheet piling, which may occur at the level of the bottom of the river adjacent to the wall, or somewhat below it, is not disastrous. It creates a hinge in the sheet piling, but the wall will not collapse until the wale fails. Crumpling causes some redistribution of pressure on the piles, but in view of the uncertainties in the behavior of the backfill, particularly with respect to areas of passive pressure, the nature of this redistribution is obscure. Consequently, it appears advisable to disregard the possibility of crumpling of the sheet piling in calculating the load F_1 on the wale. Final failure of the guide wall is to be construed as a failure of the wale or a fracture of the tie rods.

Inspecting the wale and tie rods of the guide walls is advisable, since these are the parts most likely to fail. It is not possible to predict the life of a guide wall without this information, although the admissible amount of corrosion for the web of a wale is

somewhat greater than the value of 0.20 in. proposed for the lock walls. Some underwater measurements of the corrosion of the sheet piles in the guide walls near the bottom of the river are also desirable.

The worst example of corrosion was a test pile that had lost about 0.125 in. of its thickness in 21 years. This sample suggests that some repairs may be needed in regions of high corrosion in another 21 years (i.e., by the year 2000). Uncertainty in projecting the structure's life arises primarily because some places that are inaccessible for inspection, such as the lower parts of the cross walls in the cofferdams, might be corroding faster than might be expected based on observations of exposed parts.

Corrosion Failure Limits for the Upstream Guide Wall

From Corps of Engineers data:[20]

$$H = 552 \text{ in.}, \ a \approx 444 \text{ in.}$$

The tie rods initially were 3 in. in diameter, and they are spaced at 7 ft. Hence, $L = 84$ in. From the Corps data:[21]

$$d = 348 \text{ in.}$$

The highest bending stresses in the sheet piling occur when the river is at its lowest level. This level is -2 ft, with the datum used by the Corps of Engineers.[22] Then,

$$h = 444 \text{ in.}$$

The saturation level of the backfill can vary considerably. The maximum is $s = H = 552$ in. The minimum is $s = h = 333$ in. Calculations are made for both these cases.

The sheet piling is made of U.S. Steel No. Z-32. The mean moment of inertia per foot is $I_0 = 220.4 \text{ in.}^4$ per foot. Consequently,

$$I_0 = 18.37 \text{ cu in.}$$

The distance from the neutral axis of a sheet pile to the center of a flange is $c = 5.5$ in. The initial thickness of a flange of a sheet pile is $t_0 = 0.50$ in. The factor k is not given directly by U.S. Steel Company, but it can be calculated approximately from the given data. The result is

$$k = 55 \text{ sq in.} \qquad \text{[Eq 43]}$$

The wale consists of two 12U25 channels, back-to-back. Consequently, from the U.S. Steel Handbook, $I_1 = 288 \text{ in.}^4$ initially. The moment of area Q_1 of the wale is not given directly in the U.S. Steel literature,[23] but it can be calculated from the given dimensions. The result is

$$Q_1 = 29.4 \text{ cu in.}$$

---

[20] *Plans for the Construction of Calumet River Lock and Controlling Works* Figure 20/10.
[21] *Plans for the Construction of Calumet River Lock and Controlling Works* Figure 10/5.
[22] *Plans for the Construction of Calumet River Lock and Controlling Works*, Figure 10/4.
[23] *Steel Sheet Piling Design Manual* (U.S. Steel Co., April 1972).

The initial thickness of the wale's channel web is

$$t_1 = 0.39 \text{ in.}$$

The double width of a flange of the sheet piling is

$$w = 18 \text{ in.} \qquad \text{[Eq 44]}$$

The specific weight of the dry backfill is taken to be 125 lb/cu ft. Hence,

$$\gamma = 0.0723 \text{ lb/cu in.}$$

The specific weight of the backfill immersed in water is 65 lb/cu ft.[24] Hence,

$$\gamma' = 0.0376 \text{ lb/cu in.}$$

The specific weight of water is

$$\gamma_w = 0.0361 \text{ lb/cu in.}$$

In accordance with Taylor,[25] the coefficient of active soil pressure for the backfill and the soil is conservatively taken to be

$$C = 0.45$$

The stabilizing action of the pile cap is conservatively neglected. Then $F_2 = 0$. It is assumed that $E = 30{,}000{,}000$ lb/sq in., and $\sigma_y = 36{,}000$ lb/sq in.

With these data, and $s = H$, Eq 27 yields the following value for the coefficient of passive soil pressure:

$$\bar{C} = 1.402$$

Eq 25 then yields

$$F_1 = 1327 \text{ lb/in.}$$

This is the distributed load on the wale. By Eq 29,

$$P = 84 \times 1327 = 111{,}470 \text{ lb}$$

This is the tension in a tie rod. Since the initial diameter of a tie rod is 3 in., the initial tensile stress in it is 15,770 lb/sq in. Assuming that the ultimate tensile stress of the steel σ_u is 60,000 lb/sq in., the diameter of a tie rod may be reduced by corrosion to 1.54 in. before fracture is imminent.

By Eq 32, the maximum bending moment in the sheet piles occurs at the elevation $x = 285.3$ in. This elevation is well below the bottom of the river. By the last of Eq 31, the bending moment at this elevation is M = 69, 180 lb.

---

[24] *Analysis of Calumet Sag Navigation Project-Lock.*
[25] D. W. Taylor.

With the iteration process proposed to solve Eq 38, the first approximation is $\varepsilon_1 = 0.1418$ in. The second approximation is $\varepsilon_2 = 0.1153$ in., and the third approximation is $\varepsilon_3 = 0.1192$ in. Consequently, the solution of Eq 38 is $\varepsilon = 0.119$ in. This means that the thickness of a compression flange of the Z-piles may be reduced to 0.50 - 0.119 = 0.38 in. before crumpling occurs at the location of maximum stress. However, crumpling does not signify collapse of the guide wall, especially since it occurs in the clay below the bottom of the river.

By Eq 41, the shearing stress in a web of the uncorroded wale is 7290 lb/sq in. The shear buckling stress of a web of the wale (assuming simply supported edges)[26] is

$$\tau_{cr} = 4.83\ E\ \left(\frac{t}{f}\right)^2$$

where f is the depth of the cross section of the wale between centroids of the flanges. For the upstream guide wall, f = 11.5 in. Initially, the thickness of the web of the wale is 0.39 in. If it loses 0.25 in. because of corrosion, its thickness is 0.14 in. Then,

$$\tau_{cr} = 4.83 \times 30 \times 10^6 \left(\frac{0.14}{11.5}\right)^2 = 21474 \text{ lb/sq in.}$$

Elastic buckling of the web ordinarily is not disastrous, but since the buckling stress (21,474 lb/sq in.) is close to the shear yield stress, it probably could not be exceeded very much, regardless of the web thickness. Consequently, the maximum allowable shearing stress in a web of the wale is assumed to be 21,000 lb/sq in. Since the shearing stress in the web of the uncorroded wale is 7290 lb/sq in., the thickness of the web may be reduced by corrosion to about one third of its original value before a shear failure of the web is imminent.

With σ_u = 60,000 lb/sq in., Eq 42 yields F_1' = 8000 lb/in. initially. This is the distributed load required to create plastic hinges at y = 0 and y = L/2 in the uncorroded wale. Since the actual load on the wale is F_1 = 1327 lb/in., there is little danger that the wale will fail by formation of plastic hinges.

To handle the question of plastic hinges in the wale more accurately, the length of a flange of a channel of the wale is observed to be 3.05 in. Consequently, if corrosion of the wale is uniform, simple calculations yield

$$Q_1 = 29.4 - 72.6\varepsilon$$

where Q_1 is the moment of area of the part of the cross section of the corroded wale on one side of the neutral axis. Consequently, for the corroded wale, Eq 42 yields

$$F_1' = \frac{32\ (29.4 - 72.6\varepsilon)\ (60{,}000)}{84^2}$$

If $F_1' = F_1$ = 1327 lb/in., this yields ε = 0.337 in. This means that the web of the wale may be nearly corroded away before it fails by formation of plastic hinges. Accordingly, a shear failure of the web means a critical condition.

[26] S. Timoshenko and J. Gere, *Theory of Elastic Stability*, 2nd ed. (McGraw-Hill, 1961).

The preceding calculations apply for the case in which the level of saturation in the backfill is at the top of the sheet piles. Repeating the calculations for the case in which the level of saturation in the backfill is at the same level as the surface of the water in the river (s = 444 in.) gives

$$\overline{C} = \overline{C} = 1.116, \; F_1 = 877 \text{ lb/in.}, \; P = 73{,}670 \text{ lb},$$

$$x = 286 \text{ in. for maximum bending moment, } M_{max} = 48{,}444 \text{ lb},$$

$$\varepsilon = 0.194 \text{ in. for crumbling of the sheet piles.}$$

$$F_1' = 4800 \text{ lb/in. for the uncorroded wale: } \tau = 4820 \text{ lb/sq in.}$$

It is apparent from these calculations that the level of backfill saturation has a rather strong effect on the stresses in the guide wall. The value τ = 4820 lb/sq in. is the shearing stress in the web of the uncorroded wale. Since the ultimate shearing stress of the web is about 21,000 lb/sq in., there is little danger that the wale will fail until corrosion is very far advanced.

Corrosion Failure Limits for the Downstream Guide Wall

For the downstream guide wall,[27]

$$H = 504 \text{ in.}, \; a = 420 \text{ in.}$$

The tie rods are 2.5 in. in diameter, and they are spaced at 6 ft. Accordingly, L = 72 in. From the contour lines given in Corps of Engineers data,[28]

$$d = 336 \text{ in.}$$

The minimum water level downstream from the lock is[29]

$$h = 396 \text{ in.}$$

The saturation level, s, may vary from 396 in. to 504 in.

The sheet piling is made of U.S. Steel No. Z-27. Hence,

$$w = 12 \text{ in.}, \quad I_0 = 15.35 \text{ cu in.}, \quad c = 5.81 \text{ in.}, \quad t_0 = 0.375 \text{ in.}$$

The factor k is calculated to be

$$k = 41 \text{ sq in.} \qquad \text{[Eq 45]}$$

The wale consists of two 10U20 channels, back-to-back. From the *U.S. Steel Handbook*,

$$I_1 = 2 \times 78.7 = 157.4 \text{ in.}^4, \; t_1 = 0.38 \text{ in. initially}$$

[27] *Plans for the Construction of Calumet River Lock and Controlling Works*, Figure 20/11.

[28] *Plans for the Construction of Calumet River Lock and Controlling Works*, Figure 10/5.

[29] *Plans for the Construction of Calumet River Lock and Controlling Works*, Figure 10/4.

The moment of area of the wale is calculated to be (initially)

$$Q_1 = 19.4 \text{ cu in.}$$

The constants γ, γ', γ_w, C, F_2 σ_y, σ_u are the same as for the upstream guide wall.

If the backfill is saturated to the top, s = H. For this case, Eq 27 yields

$$\bar{C} = 1.35$$

Eq 25 then yields

$$F_1 = 1038 \text{ lb/in.}$$

This is the load per inch on the wale. By Eq 29, the tension in a tie rod is

$$P = 72 \times 1038 = 74{,}700 \text{ lb}$$

Since the initial diameter of a tie rod is 2.5 in., the initial tensile stress in it is 15,200 lb/sq in.

By Eq 32, the maximum bending moment in the sheet piles occurs at elevation x = 273.5 in. Consequently, by the last of Eq 31, the maximum bending moment in the sheet piling is

$$M_{max} = 57{,}000 \text{ lb}$$

An iterative solution of Eq 38 now yields s = 0.12 in. Consequently, crumpling of the sheet piles at the elevation of maximum bending moment should be expected if the thickness of the flanges becomes less than 0.26 in. A similar calculation with x = d yields M = 46,591 lb and ε = 0.159 in. Hence, 0.159 in. of corrosion at x = d will cause crumpling of the sheet piles at the elevation x = d.

By Eq 41, the shearing stress in the web of the uncorroded wale is

$$\tau = 6060 \text{ lb/sq in.}$$

This is well below the shear yield stress of the steel, which is about 21,000 lb/sq in.

By Eq 42, F_1' = 4311 lb/in. This is the load per inch required to create plastic hinges in the wale at x = 0 and x = L/2. Since F_1 = 1038 lb/in., there is little danger of such a failure.

Similar calculations with the minimum level of saturation in the backfill (s = h) yield

$$\bar{C} = 1.05,\ F_1 = 679 \text{ lb/in.},\ P = 48{,}900 \text{ lb},$$

$$x = 270 \text{ in.},\ M_{max} = 39{,}470 \text{ lb},\ \varepsilon = 0.184 \text{ in.}$$

$$\tau = 3960 \text{ lb/sq in.},\ F_1' = 4311 \text{ lb/in.}$$

8 CORROSION MECHANISMS AND MITIGATION

There are eight main forms of corrosion: (1) uniform attack, (2) concentration cell or localized corrosion, (3) pitting corrosion, (4) galvanic (dissimilar metals) corrosion, (5) stress corrosion, (6) intergranular, (7) dezincification, and (8) erosion corrosion. The forms of corrosion damaging the O'Brien Lock and Dam project fall into the first three categories and will be considered in this chapter.

Appendix A provides the fundamental electrochemical principles associated with these corrosion mechanisms. Since the most viable corrosion mitigation technique for the O'Brien structures is cathodic protection, it is also discussed in Appendix A.

Uniform Attack

Uniform attack, or general overall corrosion, is the most common form of corrosion. It is normally characterized by a chemical or electrochemical reaction which proceeds uniformly over the entire exposed surface. The metal becomes thinner and eventually fails. For example, a piece of steel or zinc immersed in dilute sulfuric acid will normally dissolve at a uniform rate over its entire surface. A sheet iron roof will show essentially the same degree of rusting over its outside surface. In liquids, this form of corrosion involves an oxidation-reduction reaction. Anodic and cathodic areas keep shifting, so corrosion is spread more or less evenly over the metal's entire surface. This form of corrosion, although widespread at the O'Brien Lock and Dam, is not a major cause for concern; the other two forms of corrosion are more insidious and are the most probable causes of structural failure.

Concentration Cell Corrosion

Concentration cells or localized corrosion can be defined as selective removal of metal by corrosion at small specific areas or zones on a metal surface in contact with a liquid environment. The significant aspect of this form of corrosion is that it is caused by differences in the environment (heterogeneous electrolytes). These are sometimes called solution cells. If a perfectly homogeneous and pure metal surface is exposed to an environment that is not identical at all points, anodic-cathodic areas may form and result in corrosion. Concentration cells could result from any differences in the environment, but the two most common are metal ion cells and oxygen cells.

Metal ion cells occur because metal tends to dissolve or corrode at a slower rate as the concentration of its ions in the solution increases. In other words, its solution potential or electrode potential decreases in more concentrated solutions. The converse is true in more dilute solutions. Therefore, if ion concentration differentials occur across the surface of a metal sheet in contact with an aqueous electrolyte, anodic and cathodic areas will occur. Current will flow from the anode to the cathode areas, and the anodic area will corrode.

Oxygen cells occur when there is a differential in oxygen content across a metal surface. Areas low in oxygen are anodic to areas high in oxygen content; the current will flow from the anode to the cathode, and the anodic area will corrode.

At the O'Brien Lock and Dam, the water side of the sheet piling structures experiences this type of corrosion because of the low water velocity. Stagnant

conditions occur when deposits form on the surface. These deposits could be millscale, sand, dirt, or other soils. The deposit acts as a shield and creates a stagnant condition under them. The deposit can also be a permeable corrosion product. Figure 30 shows the principal elements of this type of corrosion cell, together with the corrosion current flow and resulting corrosion products.

These localized corrosion cells cause large tubercles of corrosion products to grow to a distance of 2 to 3 in. above the surface; it was this mosaic of tubercles that gave the appearance of near catastrophic corrosion damage when O'Brien was first dewatered. During the dewatering and prior to sandblasting, several of these tubercles were dissected. The cross sections showed the classical gradation of corrosion products.

Pitting Corrosion

Pitting corrosion is a form of extremely localized attack that causes holes in the metal. When the anode or anodic area remains in one spot, corrosion occurs at this site and deep penetration results. These holes could be small or large in diameter, but in most cases they are relatively small. Although the analysis showed that pitting damage in the sheet pile web was the least probable mode of failure for this structure, a pitting factor analysis was conducted during the dewatering inspection. The pitting factor is the ratio of the depth of the deepest pit to the average depth of pitting. This analysis showed no significant index of structural degradation; however, perforation caused by pitting corrosion could occur in the cofferdam cells and cause leakage.

Interlock Crevice Corrosion

Crevice corrosion occurs between the mating surfaces of the sheet pile interlocks. It begins due to the differential variation that results from this type of interface and is a form of concentration cell corrosion. The interlocks form a crevice that screens one part of the metal surface from contact with the bulk of the oxygen-bearing water, and thus from access to oxygen, while the remainder remains in contact with oxygen-saturated water. This cause of local cells is known as differential aeration, and is the most common form of concentration cell. Oxygen in liquid deep within the crevice is consumed by reaction of the metal. Oxygen content of liquid at the mouth of the crevice exposed to the bulk water is greater, so a local cell develops in which the anode or the area being attacked is the surface in contact with the oxygen-depleted liquid. It is also thought that subsequent pH changes at anode and cathode sites further stimulate local cell action as in the case of pitting corrosion.

Because of the geometry of the interlocks (Figure 22), the corrosion of the interior of the joint or "thumb and knuckle" will progress at a decreasing rate; as the analysis shows, these are the critical sections in a failure. Fortunately, however, these are also the regions that are amenable to corrosion mitigation by cathodic protection since these surfaces would be exposed to the protective current.

Mitigation

On the basis of the analyses, field measurements and laboratory mechanical properties tests, it has been concluded that so far corrosion damage has not caused the O'Brien Lock and Dam to be unsafe or unserviceable, nor are these conditions imminent.

The various forms of corrosion and the corrosion mechanisms described above can be controlled effectively by a cathodic protection system; thus, design guidelines for a system most suitable for the O'Brien structures were formulated. Chapter 9 describes the system considered optimum for this replaceable deep anode.

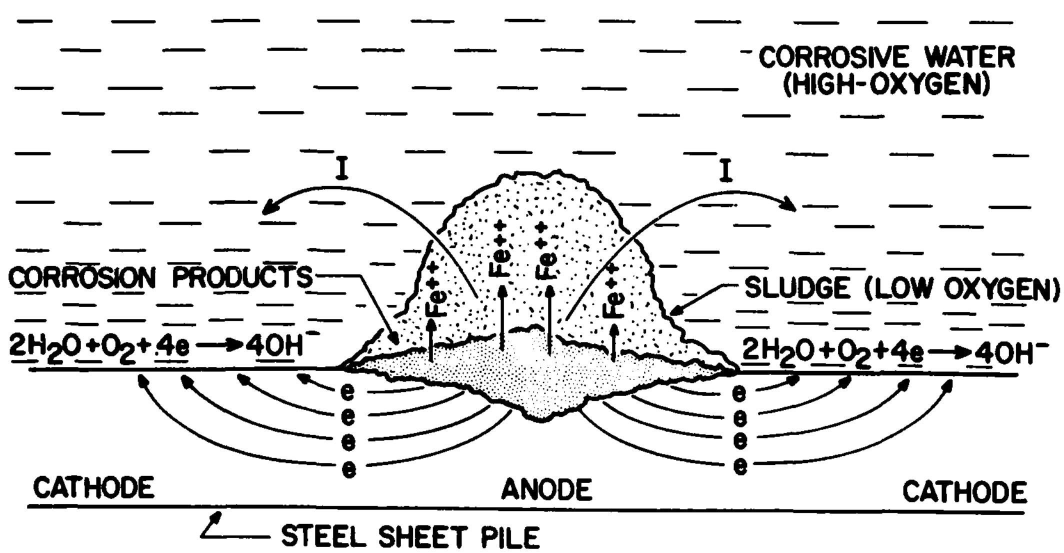

Figure 30. Concentration cell corrosion.

9 DEEP WELL ANODE SYSTEM FOR CORROSION PROTECTION OF O'BRIEN LOCK AND DAM

A deep anode groundbed is defined as one or more anodes installed vertically at a depth of 50 ft or more below grade, in a drilled hole, to cathodically protect the external surface of a metallic structure that is in contact with a common electrolyte.[30] Deep anode cathodic protection systems have been installed since 1940, using a variety of anode materials and design concepts. Deep anode cathodic protection systems, which provide the corrosion control design engineer with a viable alternative to surface groundbeds, are applicable under a variety of conditions.

There are many advantages to the use of deep anode cathodic protection systems. In areas where surface soils are subject to seasonal variations in moisture content or where freezing is a problem during the winter, deep installations place the anodes below the affected strata and allow for more constant system operation. Deep installations often provide better distribution of protective current in congested areas than do conventional (surface) groundbeds. This becomes a particular advantage where the use of distributed anodes is either not possible or impractical. By providing reduced-voltage gradients at the surface, a deep anode installation can often minimize interference with foreign utility structures. In recent years, obtaining right-of-way for conventional cathodic protection systems has, at times, become a major obstacle. Deep anode systems can be installed within the boundaries of existing easements. Maintenance problems associated with severed cables from excavations can be virtually eliminated with a deep anode design. Where surface soils have high resistivity, deep anodes can be installed in low-resistivity strata, which reduces operating costs and improves system performance. For these reasons, deep anode cathodic protection systems have been used on transmission pipelines and distribution systems, and are particularly attractive in tank farms, refineries, power plants, complex piping networks, and congested areas.

There are also disadvantages to using deep anode cathodic protection systems. The initial cost per ampere of protective current is generally higher for deep installations than for surface installations. When performing current requirement tests for design, it is difficult to accurately simulate the pattern of current distribution that the deep anodes will provide. The history of deep anode installations throughout the country indicates that the average system life is from 7 to 10 years, due to cable failures, gas blocking, connection failures, and effects, etc. Uniform compaction of the backfill material around the anodes is also hard to achieve. Some deep anode installations show rapid increases in resistance to earth as a function of time; this is attributable to either gas blocking or inadequate groundbed moisture.

The conventional approach to cathodically protecting sheet piling and bulkheads has involved the installation of impressed current systems using distributed anodes to protect the soil side surfaces and tie rods and using suspended or fixed sacrificial or impressed current to protect the water side surfaces. Though some of these systems have operated effectively over their design lives, must have failed prematurely. The anode system protecting the water side of the structure is generally the first to fail, resulting in loss of cathodic protection, costly repairs, and system downtime.

---

[30]Technical Practices Committee T-10A-7, Recommended Practice, "Design, Installation, Operation, and Maintenance of Impressed Current Deep Groundbeds," Standard RP-05-72 (National Association of Corrosion Engineers [NACE], June 1972).

Use of deep anode groundbeds will decrease the cathodic protection installation and maintenance costs, while increasing system reliability and effectiveness.

The general concept in the use of deep anode groundbeds for cathodically protecting sheet pilings deals with placing the anodes below the level of the bottom of the piling. With the anodes so placed, they are electrically remote from the metal, allowing for an even distribution of cathodic protection current to all metal surfaces. Placing the anodes below the sheet piling also minimizes shielding effects.

Replaceable Deep Anode Concept

Since the major cost of deep anode cathodic protection systems results from drilling expenditures, it becomes economically very attractive to install a deep anode system which can be salvaged if a failure occurs. This has been made possible by lubricated, calcined fluid petroleum coke, which can be held in suspension (fluidized) by pumping with water. A replaceable deep anode system is therefore possible if the hole can be maintained through proper design.

Development of this concept has led to a system design that overcomes many of the disadvantages attributable to conventional deep anode cathodic protection systems.

High-performance, replaceable, deep anode cathodic protection systems evolved over many years of testing and application. In 1972, Tatum[31] presented the concept and results of early applications at the National Association of Corrosion Engineers (NACE) National Conference. His work has led to the practical application of replaceable deep anode cathodic protection installations in a variety of industries throughout the world. Research has continued into both the method and materials.[32] By installing the deep anodes in perforated casings and extending solid casing from the anodes to grade, the hole can be maintained for future replacements, if necessary. A series of valves allows the lubricated, calcined fluid petroleum coke to be pumped first up the outside of the casing and then inside the casing. This ensures positive contact between the anode column and the surrounding earth.

System Components and Their Functions

Three basic components--the steel lead, perforated casing, and solid casing--enable installation and later replacement of the system (Figure 31). The casing diameter is sized according to the diameter of the drilled hole. Typically, a 6-in.-diameter casing is installed in a 10-in.-diameter well and a 4-in.-diameter casing in an 8-in.-diameter well.

---

[31] Joe F. Tatum, *Deep Groundbeds—Designed to Fail*, paper presented at Corrosion/74, Chicago, Illinois (NACE, March 4-8, 1974).

[32] Joe F. Tatum, *Replaceable Deep Groundbed Evaluation*, paper presented at Corrosion/74, Chicago, Illinois (NACE, March 4-8, 1974); Thomas H. Lewis, *End Effect Phenomena*, paper presented at Corrosion/78, Houston, Texas (NACE, March 6-10, 1978); Joe F. Tatum, *Platinized Anodes in Carbonaceous Backfills—A New Dimension*, paper presented at Corrosion/78, Houston, Texas (NACE, March 6-10, 1978).

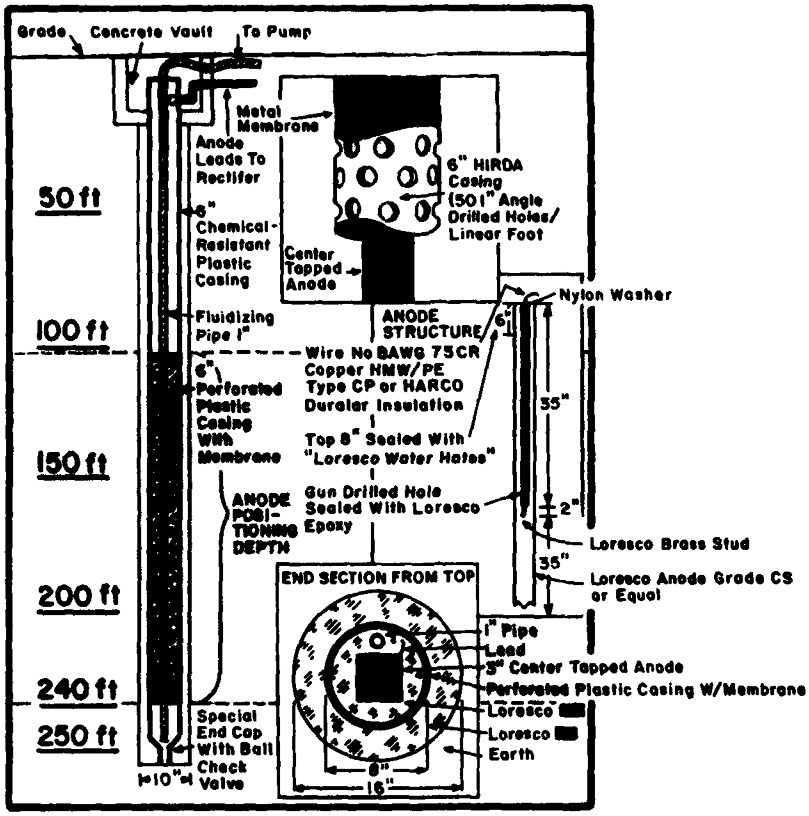

Figure 31. Deep anode cathodic protection system.

The steel lead has several functions. Made of Schedule 40 black steel pipe, the lead is equipped at the bottom with a two-way flow valve that has a 1-in., left-hand-thread, female fitting which faces the inside of the pipe. During installation of the system, a 1-in. pipe is attached to the left-hand thread in the valve. The entire casing package is lowered into the drilled hole, using this 1-in. pipe for support. The casing is assembled around the 1-in. pipe. This allows the casing to be lowered without tensile stresses on the casing itself, since all the weight is on the 1-in. pipe attached to the steel lead. Once the casing is in place, the two-way flow-valve will allow the fluid coke backfill to be pumped first through the 1-in. pipe to the outside of the casing, and then to the inside of the casing. The top of the steel lead has a transition fitting that can be attached to the perforated casing while the assembly is lowered. The weight of the steel lead can bump away any obstruction that may have fallen into the hole.

The perforated casing is made of ES-ABS (extra-strength acrylonitrile-butadiene-styrene) pipe and is installed in the area where the anodes and coke column are placed. The pipe is perforated symmetrically with 1-1/4 in. holes, drilled at a 45° angle to remove about 25 percent of the total surface area, and covered with a thin conductive membrane. The perforations allow current to pass from the anodes through the coke and finally to the earth. The angle of the holes allows the best possible contact between the calcined fluid coke on the inside and outside of the casing by preventing any voids in the

coke near the perforations that result from the angle the coke slumps out of suspension. The membrane helps prevent coke that is pumped up the outside from entering the inside of the casing. The membrane also allows the inside of the casing to be flushed with clean water to remove any contaminants that could hamper anode performance and shorten system life.

The solid casing, also made of ES-ABS, extends from the top of the perforated casing to grade. The solid casing maintains the integrity of the hole and allows access to the coke column and anodes on the inside of the casings.

Installation Practices

After the hole has been drilled and the drill bit removed, an electrical log of the holes should be established, using a 1-in.-diameter pipe, 5 in. long. Using the structure to be protected or other low-resistance ground, straight-resistance readings are recorded at five intervals as the electrode is lowered into the hole. These measurements are logged to determine the placement of the perforated casing, coke column, and anodes. Using the equations derived by Dwight[33] and Sunde,[34] the approximate groundbed resistance can be calculated from these data.

The importance of running a resistance log on the well cannot be overemphasized. During initial design, it is usually necessary to rely on the best available information regarding the area's geological stratification and mineralogy.

An electrical log of a previously drilled well close to the deep anode system is the best information on which to base the design. Often, an electric log is not available, so well logs from the State Geological Survey, local well drillers, foundation contractors, etc., will be the only sources of data on substrata. For design purposes, these data can often be quite sketchy, particularly if the only existing wells are located some distance from the site of the deep anode system. In many glacial areas, the geology can vary greatly. If a large number of deep anode systems are to be installed in an area, it may be prudent to drill a small-diameter test hole. Of course, this decision must consider the economics of additional drilling costs. By running a resistance log on the well before anode installation, field modifications in the design can be made to ensure that the anode is placed in the lowest-resistivity strata. For example, one particular well in northern Illinois was designed to a depth of 520 ft, with the anode column to be placed between 410 ft and 510 ft. A high-resistivity stratum was encountered between 480 and 510 ft, even though this was not indicated on other well logs. The high-resistivity area appeared quite dramatically on the resistance log, where the resistance-to-ground of the test electrode increased from 22 ohms at a depth of 475 ft to 200 ohms at a depth of 480 ft. Because of this anomaly, the anodes were not placed in the bottom of the hole as originally designed, but were located in the lower-resistivity strata from 372 to 472 ft. Thus, logging the well provides the information needed to modify the system design in the field to obtain the best possible groundbed.

---

[33] H. B. Dwight, "Calculations of Resistance to Ground," *AIEE Transaction*, Vol 55 (1939).

[33] E. D. Sunde, *Earth Condition Effects on Transmission Systems* (D. Van Nostrand Co., Inc., 1949), pp 66-97.

After the well has been logged, the steel lead is prepared for installation. After flushing the drilled hole with clean water, the steel lead is assembled on a 1-in.-diameter pipe, which is attached to the check valve on the bottom of the lead by the left-hand thread. When the anodes are to be installed in the bottom of the well, the perforated casing is installed immediately above the steel lead.

The lengths of perforated ABS casing are assembled with cement and sheet metal screws and lowered into the well on the 1-in.-diameter pipe. From the top of the perforated casing to grade, the necessary amount of solid ABS pipe is installed.

With all casing in place, the hole is flushed with clean water and Loresco; lubricated, calcined fluid petroleum coke can now be pumped up from the bottom of the well to fill the annular space between the casing and the sides of the hole. The amount of backfill required to fill the annulus to the proper level is determined by calculation. In a mixing vessel, the calcined petroleum coke is mixed with 5.3 to 6.5 gal of water per hundredweight and kept agitated. The intake of a pump capable of 50 gpm at 125 psi is placed in the mixing vessel containing the slurry, and the pump discharge is connected to the steel lead through the 1-in. pipe. While in continual agitation, the required amount of backfill is pumped down the 1-in. pipe through the check valve to the outside of the casing.

The bursting point of the ES-ABS pipe is 300 psi. Collapse pressure is not significant, since collapse could only occur if the drilled hole caves in before the coke is in place. Proper drilling techniques will ensure that this does not happen. When the backfill is pumped, the pressure on the inside and outside of the casing remains essentially in equilibrium. At this point, all casing is in place and the calcined petroleum coke has been pumped up the outside of the casing.

The check ball is then dropped into the casing and the 1-in. pipe is turned clockwise until the left-hand nipple is free of the steel lead. The pipe is lifted slightly to allow the check ball to seal the valve on the bottom of the lead. The inside of the casing is then flushed with clean water to ensure that any contaminants have been removed. The anodes with individual leads are lowered into place and tied off; the backfill materials are then pumped up the inside of the casing. When the required amount of coke has been pumped inside the casing, the 1-in. pipe is removed.

All anodes should have individual lead wires that terminate in a shunted junction box; this will allow the current output of the individual anodes to be monitored. Industry tests have indicated that Duralar Cable, manufactured by the Anaconda Company, is the best insulated anode lead wire commercially available. The No. 8 Anerita-Water Gauge cable consists of a stranded-copper conductor, covered by 0.02 in. of primary insulation Halar (E-CTFE fluorocopolymer), with a 0.08-in. jacket of high-molecular-weight polyethylene insulation for mechanical protection. Duralar shows good resistance to water penetration, saltwater, and notch propagation, and to temperature restrictions. Since cable failures can render deep anode cathodic protection systems inoperable, only the best materials should be used.

The final installation tasks are filling the annulus between the casing and the periphery of the drilled hole with washed gravel or cement, or drill-cutting matter from the top of the coke to grade (outside the casing only); capping the well; connecting the rectifier unit; and energizing the system.

If the system fails, the high-performance replaceable deep anode system can be rejuvenated in 1 day by two persons, using a truck, tank, pump, 1-in. hose, new anodes and wire, and perhaps an additional small amount of calcined fluid petroleum coke. The Loresco can be fluidized by pumping water into the well at a rate as low as 3 gpm. Once in suspension, the anodes can be removed and new materials lowered into place.

System Advantages

The most important advantage of the replacement deep anode system is that the anodes can be removed and replaced at minimum cost. This feature protects the investment, and provides an essentially permanent cathodic protection system.

The use of casing in the replacement system allows the area where the anodes are placed to be washed of debris and other contaminants that could reduce system performance.

Other system advantages are related to the lubricated, calcined fluid petroleum coke. Metallurgical grade 3 coal coke breeze has a specific gravity of 1.4, a bulk density of 45 lb/ft, and a porosity of 44 percent. By comparison, lubricated calcined fluid petroleum coke is 92 percent carbon, has a specific gravity of 2.0, a bulk density of 74 lb/cu ft, and a porosity of 41 percent. The heavier specific gravity of calcined fluid petroleum coke increases the pressure between the backfill column and the anode. For example, at a depth of 100 ft, the petroleum coke will produce a pressure of 40 psi, while the pressure from metallurgical grade coke will be 17 psi, or 60 percent less. Thus, calcined fluid petroleum coke produces positive backfill compaction around the anode and between the anode column and the earth.

Metallurgical grade coke used for cathodic protection installations generally contains irregularly shaped particles sized to a 3/16-in. diameter. These particles are filled with pores that increase the probability of gas entrapment. Lubricated, calcined petroleum coke has been passed through a 16-mesh screen that permits greater compaction. The calcined petroleum coke is solid and impervious, thereby enabling the porosity to function for gas relief.[35] Deep anode installations using lubricated, calcined fluid petroleum coke are therefore less subject to gas blockage.

The higher density of the petroleum coke allows most of the current to be discharged at the periphery of the backfill column, rather than at the anode/backfill interface. The small particles compact to form a much denser coke column than is possible with metallurgical grade coke. In a replaceable deep anode system, most of the current transfer from the anodes to the edge of the backfill column occurs electronically, rather than electrolytically. This has been established by both laboratory and field testing.[36] This allows for designing higher current densities than would normally be considered feasible. Graphite anodes can be designed for current outputs as high as 1000 mA/ft.[37] The petroleum coke can withstand current densities as high as 2.5 A/sq ft. The current is discharged primarily through the column electronically. This can allow a system to be designed with fewer materials than a conventional deep anode system. The net result is a higher performance capability and longer system life.

---

[35]Joe F. Tatum, *Replaceable Deep Groundbed Evaluation.*
[36]Joe F. Tatum, *Replaceable Deep Groundbed Evaluation.*
[37]Joe F. Tatum, *Replaceable Deep Groundbed Evaluation.*

The resistance-to-earth of the replaceable deep anode systems is lower than that obtained with metallurgical grade coal coke breeze. For example, two conventional deep groundbeds operating at direct current circuit resistances of 9.6 and 28 ohms, replaced with high-performance replaceable deep anode systems. The resulting circuit resistances of the replacement wells were 0.94 and 1.7 ohms, respectively.

Another advantage to the replaceable design is its suitability to the use of precious metal anodes. Small-diameter casings can be used so that the platinized materials can be salvaged if problems arise. Use of platinized anode materials in carbonaceous backfills will probably increase in the next few years.

Subsurface Strata - O'Brien Lock and Dam

Well logs for the approximate vicinity of the O'Brien Lock and Dam were gathered and analyzed to see if strata layers of low enough resistivity to install deep well anodes were present.

In the Chicago area, the Maquoketa Shale group is the rock strata of lowest resistivity. This group is made up of the Scales Shale, the Fort Atkinson Limestone, and the Brainard Shale. The Scales Shale ranges from 90 to 120 ft thick, the Fort Atkinson Limestone ranges from 5 to 50 ft thick, and Brainard Shale ranges from 10 to 100 ft thick. The thickness of Maquoketa Group ranges from 105 ft to 270 ft thick throughout the Chicago area.

An analysis of well logs closer to the O'Brien Lock and Dam indicates that the Maquoketa group is about 120 ft thick in this area, and is found between 450 ft and 570 ft below grade.

Proposed Deep Well Anode Groundbed

Installing a deep anode cathodic protection groundbed is the most effective way to mitigate corrosion activity and to increase the expected operational life of the O'Brien Lock and Dam. Since the designed operational life of the cathodic protection system is 30 to 80 years, a replaceable deep anode system is most feasible.

Analysis of the geologic strata indicates that the deep anode groundbeds must be about 600 ft deep, with the anodes placed in the bottom 120 ft. About 12 center-tapped graphite anodes could be placed in this space. The maximum current output for 12 anodes would be about 36 A. Four deep anode groundbeds would be required to provide the desired level of cathodic protection.

It is estimated that four 600-ft-deep groundbeds could be completely designed, installed, energized, and tested for $240,000.

AD-A173 016 LIFE-CYCLE ANALYSIS OF CORRODING SHEET PILE STRUCTURES 2/2
FOR A LOCK AND DAM(U) CONSTRUCTION ENGINEERING RESEARCH
LAB (ARMY) CHAMPAIGN IL F W KEARNEY SEP 86
UNCLASSIFIED CERL-TR-M-86/12 F/G 13/2 NL

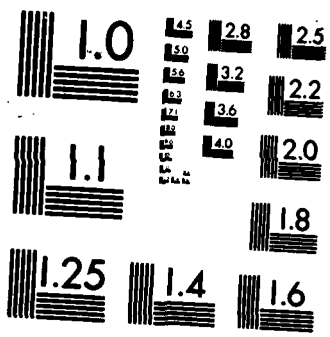

MICROCOPY RESOLUTION TEST CHART
NATIONAL BUREAU OF STANDARDS-1963-A

10 CONCLUSIONS AND RECOMMENDATIONS

The equations determining the allowable amounts of corrosion, ε_{all}, at any point in the lock walls, dam, and guide walls indicate there is a large safety factor in the O'Brien Lock and Dam. About 0.25 in. of corrosion (ε = 0.25 in.) can be tolerated anywhere without catastrophic results. However, corrosion exceeding 0.25 in. in highly stressed places may cause serious damage. Some margin of safety probably should be applied to this result, although the assumptions used for this analysis are biased toward conservatism. The assumed coefficient of soil pressure (C = 0.45) is probably high. For the guidewall computations, the reinforcement provided by the pile cap has been disregarded. The analysis is based on assumptions that render the stresses statically determinant.

The tensions required to pull the interlocks apart are calculated on the basis that the claws fail when fully plastic hinges form in the shanks and the hooks. The interlocks could be strengthened by increasing the shank thickness so it is no less than the hook thickness. Interlocks generally appear to fail by excessive yielding before the webs of the sheet piles rupture.

The point of highest stress in the lock walls is in a cross wall of the land wall near where it joins the cylindrical walls on the chamber side at the elevation of the bottom of the chamber. Sliding in the interlocks of the cross walls is a potential type of failure, but corrosion mitigates this danger. Since the interlocks have not slipped appreciably in the past, it is unlikely they will in the future.

The cross walls may be reduced in thickness to 0.11 in. before a shear rupture of a cross wall may occur. Since the initial thickness is 0.375 in., this reduction corresponds to ε = 0.26 in. This result probably is conservative, since the shear carried by the fill in the cells has been neglected.

The time required for the allowable amount of corrosion (ε_{all} = 0.20 in.) to be reached is 83 years. Thus, the webs of the sheet piles in the lock walls should serve until 2041. This is also true for the claws of the interlocks in the cofferdam walls, if the shanks and hooks in the claws corrode at the same rate as the webs. However, crevice corrosion rates for parts of the claws are not as well known as those of the webs. Thus, more data about the corrosion rates of the claws are desirable.

Inspecting the wale and tie rods of the guide walls is advisable, since these are the parts most likely to fail. It is not possible to predict the life of a guide wall without this information, although the admissible amount of corrosion for the web of a wale is somewhat greater than the value of 0.20 in. proposed for the lock walls. Some underwater measurements of the corrosion of the sheet piles in the guide walls near the bottom of the river are also desirable.

Some repairs may be needed in regions of high corrosion by the year 2000. Uncertainty in projecting the structure's life arises primarily because some places that are inaccessible for inspection, such as the lower parts of the cross walls in the cofferdams, might be corroding faster than might be expected based on observations of exposed parts.

On the basis of the analyses, field measurements, and laboratory mechanical properties tests, it has been concluded that so far that corrosion damage has not caused the O'Brien Lock and Dam to be unsafe or unserviceable, nor are these conditions imminent. Furthermore, the geometry of the sheet pile structures and the type of corrosion mechanisms involved indicate that cathodic protection could be successfully used to prevent additional corrosion damage and stabilize the structure in the present acceptable condition. The deep well anode system is ideally suited for the O'Brien project. Because of the substantial cost avoidance involved, it is recommended that this system be implemented as soon as possible.

METRIC CONVERSION FACTORS

1 in.	= 25.4 mm
1 ft	= 0.308 m
1 sq in.	= 645.2 mm^2
1 lb	= 0.453 kg
1 lb/cu in.	= 16.0185 kg/m^3
1 gal	= 3.785 L
1 psi	= 703.070 kg/m^3

REFERENCES

Analysis of Calumet Sag Navigation Project-Lock (M.J.M., August, 1956).

Beedle, L. S., T. V. Galambos, and L. Tall, *Column Strength of Constructional Steels*, Fritz Lab. Reprint No. 177 (U.S. Steel Co., undated).

Dwight, H. B., "Calculations of Resistance to Ground," *AIEE Transaction*, Vol 55 (1939).

Kearney, F., *Corrosion of Steel Pilings in Seawater: Buzzards Bay—1975-1978*, Interim Report M-275/ADA078626 (U.S. Army Construction Engineering Research Laboratory [USA-CERL], 1979).

Kumar, A., R. Lampo, and F. Kearney, *Cathodic Protection of Civil Works Structures*, Technical Report M-276/ADA080057 (USA-CERL, 1979).

Langhaar, H. L., "Buckling of Aluminum-Alloy Columns and Plates," *Jour. Aero. Sci.*, Vol 10, No. 7 (July 1943), pp 218-222.

Lewis, Thomas H., *End Effect Phenomena*, paper presented at Corrosion/78, Houston, Texas (National Association of Corrosion Engineers [NACE], March 6-10, 1978).

Plans for the Construction of Calumet River Lock and Controlling Works, (Chicago District, U.S. Army Corps of Engineers, November 1957).

Steel Sheet Piling Design Manual (U.S. Steel Co., April 1972).

Sunde, E. D., *Earth Condition Effects on Transmission Systems* (D. Van Nostrand Co., Inc., 1949), pp 66-97.

Tatum, Joe F., *Deep Groundbeds - Designed to Fail*, paper presented at Corrosion/74, Chicago, Illinois (NACE, March 4-8, 1974).

Tatum, Joe F., *Platinized Anodes in Carbonaceous Backfills - A New Dimension*, paper presented at Corrosion/78, Houston, Texas (NACE, March 6-10, 1978).

Tatum, Joe F., *Replaceable Deep Groundbed Evaluation*, paper presented at Corrosion/74, Chicago, Illinois (NACE, March 4-8, 1974).

Taylor, D. W., *Fundamentals of Soil Mechanics* (John Wiley and Sons, 1948).

Technical Practices Committee T-10A-7, Recommended Practice, "Design, Installation, Operation, and Maintenance of Impressed Current Deep Groundbeds," Standard RP-05-72 (NACE June 1972).

Terzaghi, K., "Stability and Stiffness of Cellular Cofferdams," *Trans. ASCE*, Paper 2253, (September 1944), pp 1083-1202.

Thomas J. O'Brien Lock and Controlling Works, Periodic Inspection Report No. 3 (U.S. Army Corps of Engineers, December 1978).

Timoshenko, S., and S. Woinowsky-Krieger, *Theory of Plates and Shells*, 2nd ed. (McGraw-Hill, 1959).

Timoshenko, S., and J. Gere, *Theory of Elastic Stability*, 2nd ed. (McGraw-Hill, 1961).

APPENDIX A:

CORROSION PRINCIPLES AND CATHODIC PROTECTION

General

Cathodic protection has been used in corrosion mitigation for more than 150 years. Thus, a large amount of cathodic protection knowledge, such as design data and case histories, is available. However, most of this information concerns corrosion mitigation of systems common to the industrial community and has limited application to the somewhat unique corrosion problems encountered in Corps of Engineers civil works systems such as hydraulic structures. Also, recent developments in solid-state electronics have produced a new generation of cathodic protection equipment.

Corrosion Electrochemistry

Corrosion, as considered in this study, is the deterioration of a metal or alloy by electrochemical reaction with its environment. Basically, two electrochemical reactions occur:

1. Dissolution of metal: **base metal to metal ions** plus **free electrons.** In chemical notation, this is

$$M \rightarrow M + n + ne \qquad \text{[Eq A1]}$$

where: M = the base metal

n = an integer determined by the particular metal (valence)

e = an electron.

2. Evolution of hydrogen gas: **hydrogen ions** plus **free electrons** to hydrogen gas. In chemical notation, this is

$$2H^{+} + 2e \rightarrow H_2 \qquad \text{[Eq A2]}$$

As Eqs A1 and A2 indicate, the negative electrons from the metal combine with positive ions from a conductive (electrolytic) solution at a rate dependent on the **potential** between the metal and the solution.

The reaction between hydrochloric acid and zinc illustrates the electrochemical nature of corrosion. When zinc is immersed in dilute hydrochloric acid, a vigorous reaction occurs: hydrogen gas leaves the zinc surface, and zinc ions enter the solution. Since the hydrochloric acid dissociates in aqueous solution into hydrogen and chloride ions (H^+ and Cl^-), and the chloride ions are not involved in the reaction, the overall reaction is:

$$Zn + 2H^{+} \rightarrow Zn^{+2} + H^{2} \qquad \text{[Eq A3]}$$

When zinc is placed in the acid, some hydrogen ions adjacent to it are adsorbed onto the zinc's surface. The adsorbed hydrogen ions tend to take electrons from the metal and become neutral hydrogen atoms, while the zinc surface atoms adjacent to the electrolyte tend to release two electrons and go into solution as zinc ions (Zn^{+2}). Two

hydrogen atoms combine to form a hydrogen molecule (H_2), which then combines with other hydrogen molecules and evolves from the zinc surface as a hydrogen bubble. The electrons released by the zinc travel through the metal to other surface sites where they are consumed by hydrogen ions, as shown in Figure A1. Eq A3 can be conveniently divided into two partial reactions:

Anodic

$$Zn \rightarrow Zn^{+2} + 2e \qquad \text{[Eq A4]}$$

Cathodic

$$2H^{+} + 2e \rightarrow H^{2} \qquad \text{[Eq A5]}$$

The zinc dissolution is an anodic or oxidation reaction, since it releases electrons. The neutralization of hydrogen ions is called a cathodic or reduction reaction because it consumes electrons. Neither the anodic nor the cathodic reactions occurs at definite locations. The cathodic reaction site may be any distance from the anodic dissolution site.

All metals, as well as some nonmetals, corrode similarly. Hydrochloridic acid corrodes iron and aluminum in addition to zinc. The anodic reactions for these metals are:

$$Fe \rightarrow Fe^{+2} + 2e \qquad \text{[Eq A6]}$$

$$Al \rightarrow Al^{+3} + 3e \qquad \text{[Eq A7]}$$

The cathodic reaction for hydrochloric acid is always that shown in Eq A5.

When metals like zinc, aluminum, and iron corrode in other acids, such as sulfuric, phosphoric, hydrofluoric, formic, and acetic acids, they behave just as they do in hydrochloric acid. In each case, only the hydrogen is active. The other anions, such as sulfate and phosphate, usually do not participate in the corrosion reaction, although they may react with the dissolved metallic ions to form solid precipitates (e.g., iron phosphate) on the metal surface.

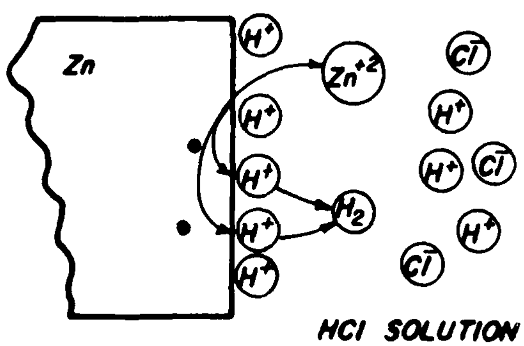

Figure A1. Electrochemical reactions during corrosion of zinc in air-free hydrochloric acid.

In addition to the hydrogen ion, several other chemical species in an electrolyte (e.g., oxygen, ferric ion [Fe^{+3}], cupric ion [Cu^{+2}]) can participate in electron-consuming cathodic reactions. The common cathodic reactions are:

1. Hydrogen evolution

$$2H^{+} + 2e \rightarrow H_2 \qquad \text{[Eq A8]}$$

2. Oxygen reduction (acid solution)

$$O_2 + 4H^{+} + 4e \rightarrow 2H_2O \qquad \text{[Eq A9]}$$

3. Oxygen reduction (neutral or basic solutions)

$$O_2 + 2H_2O + 4e \rightarrow 4OH^{-} \qquad \text{[Eq A10]}$$

4. Metal-ion reduction

$$M^{+2} + e \rightarrow M^{+} \qquad \text{[Eq A11]}$$

$$(\text{e.g., } Cu^{+2} + e \rightarrow Cu^{+}$$

$$\text{or } Fe^{+3} + e \rightarrow F^{+2})$$

5. Metal deposition

$$M^{+} + e \rightarrow M \qquad \text{[Eq A12]}$$

Since acids or acidic media are common, hydrogen evolution is a frequent cathodic reaction. Oxygen reduction is also very common, since many aqueous solutions in contact with air contain some dissolved oxygen molecules that can provide this reaction. Metal-ion reduction and metal deposition are less common reactions usually found in chemical process streams. Metal-ion reduction occurs in solutions contaminated with metallic ions having two or more possible ionic states (e.g., Cu^{+} or Cu^{+2} and Fe^{+2} or Fe^{+3}). Metal ions in solution tend to take up electrons and deposit on the metal electrode surface.

More than one anodic and one cathodic reaction may occur during corrosion. When an alloy corrodes, its component metals go into solution as ions. If more than one cathodic reaction occurs, the rate of anodic dissolution of the metal equals the sum of all cathodic reactions. Thus, acid solutions containing dissolved oxygen are more corrosive than air-free acids.

The concept of partial reactions can be used to interpret virtually all corrosion problems. When iron, in the form of a steel piling or a dam gate, is immersed in freshwater or seawater exposed to the atmosphere, the anodic reaction is:

$$Fe \rightarrow Fe^{+2} + 2e \qquad \text{[Eq A13]}$$

Oxygen reduction is the main cathodic reaction:

$$O_2 + 2H_2O + 4e \rightarrow 4OH^{-} \qquad \text{[Eq A14]}$$

Since freshwater and seawater are nearly neutral, the sodium and chloride ions (Na^+ and Cl^-) do not participate in the reaction. The overall reaction, obtained by adding Eqs A2 and A9, is

$$2Fe + 2H_2O + O_2 \rightarrow Fe^{+2} + 4OH^- = 2Fe(OH)_2 \qquad \text{[Eq A15]}$$

The ferrous ion and the hydroxide ion may combine to form insoluble ferrous hydroxide ($Fe(OH)_2$) if the ionic concentrations exceed certain limits. Ferrous hydroxide is not stable; however, it reacts with oxygen or water molecules to form ferric hydroxide:

$$2Fe(OH)_2 + H_2O + \frac{1}{2} O_2 \rightarrow 2Fe(OH)_3 \qquad \text{[Eq A16]}$$

The final product is the familiar brown rust or ferric hydroxide.

If the dissolved oxygen in the water is eliminated, the corrosion rate of iron drops sharply. This result is logical, since oxygen reduction is the main cathodic reaction. Coating the iron or steel surface with paint or some other nonconducting film can reduce the rates of both anodic and cathodic reactions and thus retard corrosion. Similarly, corrosion inhibitors added to the electrolyte form a surface layer that interferes with either or both of the anodic and cathodic reactions. In cathodic protection, external electrical devices "pump" the electrons required for the cathodic reaction to the metal surface. Consequently, iron dissolution, which also releases electrons to the metal surface, is greatly reduced by the counterflow of electrons that this external voltage supplies.

Cathodic Protection Principles

So far, the discussion of electrochemical reactions and corrosion cells has thus far dealt primarily with isolated corrosion cells and the nature of electrochemical reactions. The fundamental principle of cathodic protection is the application of a **counter potential** to prevent the electrochemical interchange that occurs in corrosion. In cathodic protection, the metal to be protected is made negative (cathodic) with respect to a "protecting" electrode (anode). This externally applied electric current can be supplied in two ways: by an external power source (impressed current) or by a metal that is more electrochemically positive than the protected metal (sacrificial anode). Although the examples below consider only a single cell, the surface of a submerged piece of steel (or any other metal) consists of many such cells, which may be microscopic in size.

Because the current flow between anode and cathode causes polarization, the potential difference (driving force) between the two electrodes is invariably less than the open-circuit potential with no net current flowing across the electrode-electrolyte interface. Figure A2 shows how potential varies with current density. As a net current flows, the potential of the anode becomes more noble (positive), and the potential of the cathode becomes more active (negative). The potential difference between the two effectively decreases as greater amounts of current flow through the cell. The magnitude of polarization (difference in potential for an electrode passing a net current compared to that for a state of no net current) depends mainly on current density or current per unit electrode area. If the corrosion cell circuit contains metallic electrodes and an electrolyte of high conductivity, and if no high-resistance reaction produces films on the metal surfaces, then electrical resistance is minimal, and anode and cathode potentials achieve very nearly the same value. This situation often occurs with iron or

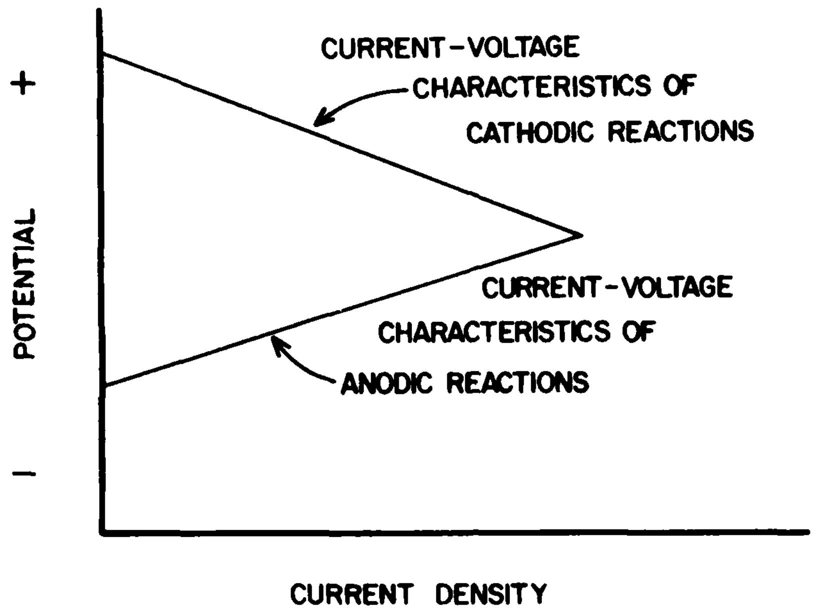

Figure A2. Relationship of potential to net current.

steel in seawater, which has high conductivity. In a high-resistance electrolyte, such as a freshwater low in chlorides, a potential difference between anode and cathode is maintained. Figures A3 and A4 illustrate potential variation in low- and high-resistance electrolytes.

Cathodic protection essentially introduces a direct current from an outside source that alters polarization and reduces or halts current flow from the metal into the electrolyte at the anodic sites. Introducing this current requires a modification of the circuitry of the electrochemical or corrosion cell. One type of modification, called impressed-current cathodic protection (Figure A5), involves electrically coupling a submerged, corroding metal structure or component consisting of many microelectrodes or "local action cells" to the negative terminal of a direct current power supply or rectifier and bonding the positive terminal to an auxiliary piece of submerged metal. This auxiliary metal is commonly termed an impressed-current anode.

Although any conducting solid can illustrate basic cathodic protection theory, in practice the chemical makeup of the anode material determines the protection system's efficiency. An anode material naturally positive to the structure requiring protection will produce the same result as a direct current power source and anode system; i.e., it will supply current through the electrolyte to the metal structure. Use of a naturally positive anode material (Figure A6) is called sacrificial-anode cathodic protection.

In both impressed-current and sacrificial-anode protection systems, positive current flows through the electrolyte to the structure to be protected. This metal structure thus becomes the cathode in a galvanic couple; it is polarized cathodically (negatively), and its corrosion rate is reduced.

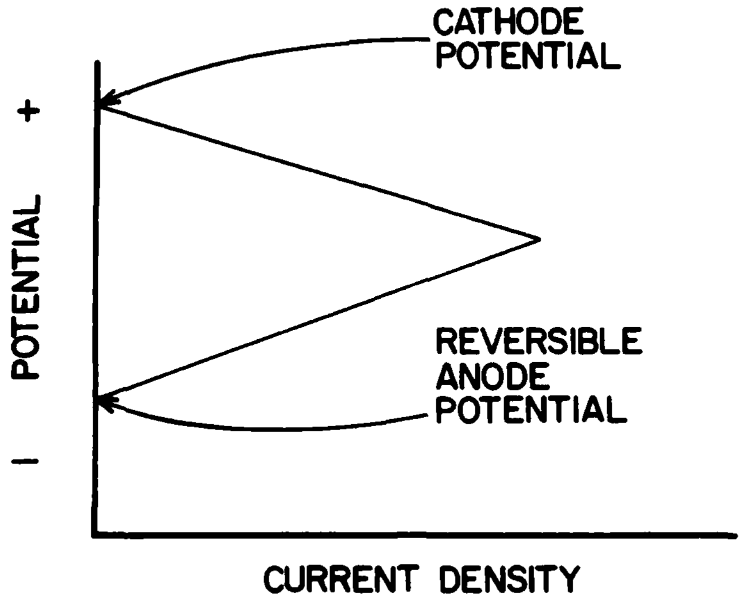

Figure A3. Variation of potential in a low-resistance electrolyte.

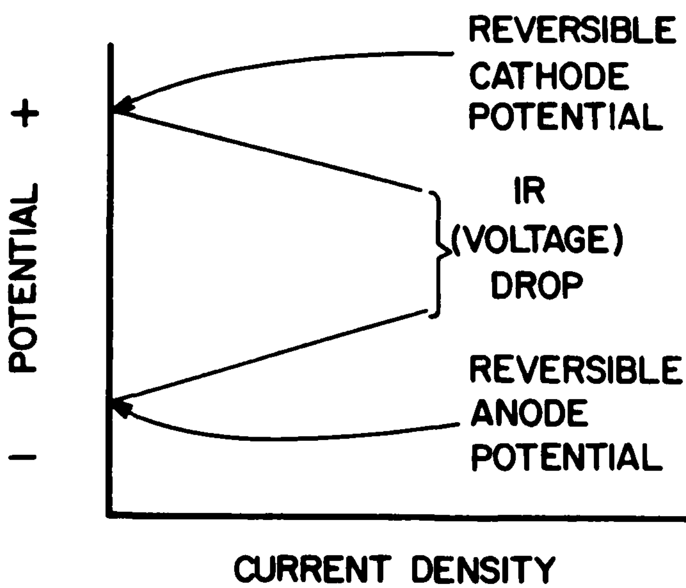

Figure A4. Variation of potential in a high-resistance electrolyte.

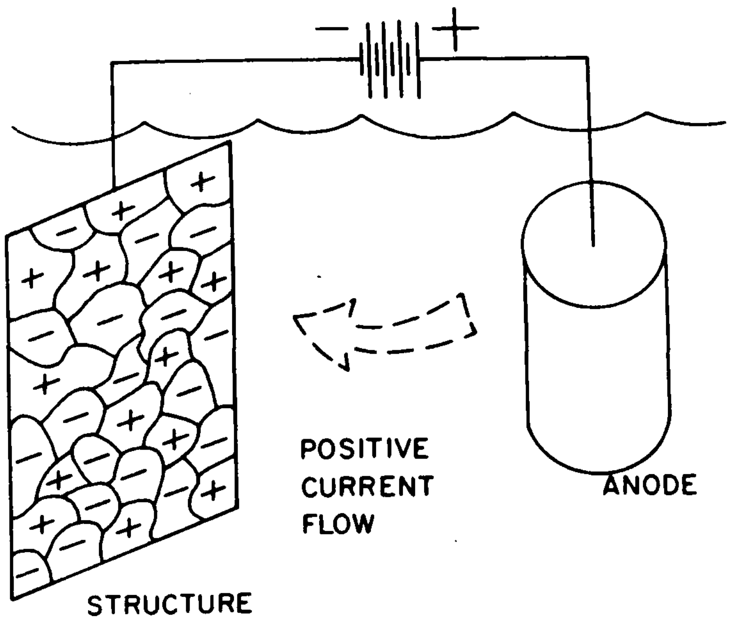

Figure A5. Impressed-current cathodic protection.

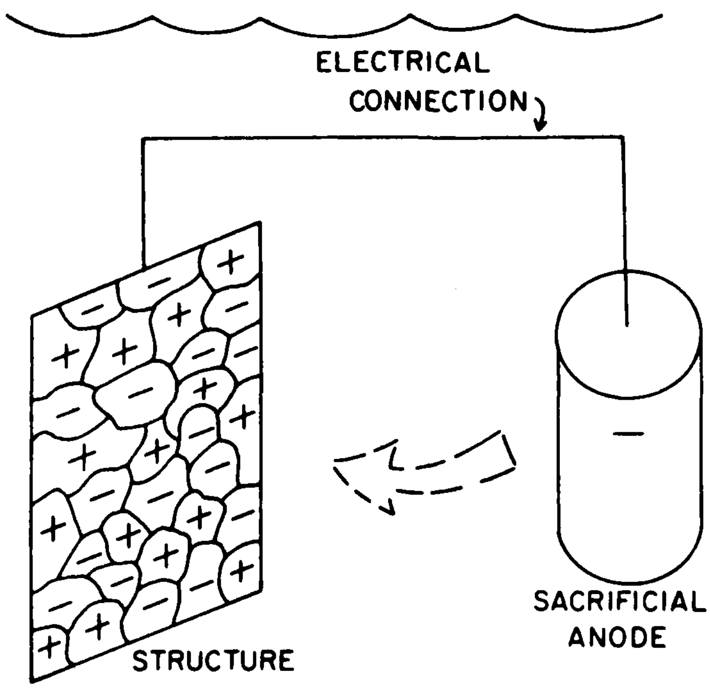

Figure A6. Sacrificial-anode cathodic protection.

The electrolyte's resistivity largely determines which anodes to use. Anode-alloy chemistry and installation procedures are important in both high- and low-resistivity electrolytes. Table A1 indicates what levels of resisitivity are classified as low, moderate, and high.

High-resistivity electrolytes generally require an impressed-current system employing anode materials like duriron, graphite, or a nobler metal. If anode selection is properly based on the environment, such impressed-current anodes will have a longer life than galvanic anodes. In low-resistivity electrolytes, galvanic anodes such as aluminum, zinc, and magnesium are often more economical.

The limited driving voltage of galvanic anodes can produce only a small amount of current in high-resistivity electrolytes, so these anodes are generally used only in salty and brackish water. Magnesium anodes, which have more negative corrosion potential than aluminum or zinc, have been used in freshwater, but the large number of anodes needed to produce the required current in this situation may cause high installation costs.

An advantage of using galvanic anodes in high-resistivity electrolytes is that they present little danger of overprotection (creation of a structure potential that is too negative). Potential changes of steel structures in freshwaters, as effected by galvanic anodes, rarely exceed -0.90 V with respect to a copper-copper sulfate reference electrode. A practical example is the use of magnesium on intake gates in the Columbia and Missouri Rivers. These gates are set in slots in concrete and have stainless steel rollers on each end. Excessive current on the rollers from overprotection might cause hydrogen embrittlement, and stray current might damage the concrete.

Galvanic anodes are more practical than impressed-current anodes for high-resistivity electrolytes when a rectifier system will not be properly maintained, either because of inaccessibility or environmental exigencies. Where power is not available for a rectifier system, galvanic anodes may be the only alternative.

On the other hand, although galvanic anodes are quite efficient for low-resistivity electrolytes and are generally easy to install and maintain, a rectifier system may sometimes be more economical.

Table A1

Classification of Electrolyte Resistivity

Resistivity (ohm-cm)	Classification
Below 2500	Very low
2500 to 7500	Low
7500 to 10,000	Moderate
Above 10,000	Progressively higher

Achieving uniform cathodic-current density, and hence, uniformly and adequately protecting an irregularly shaped structure such as a miter gate, can be a formidable problem. The current tends to concentrate on that portion of the structure closest to the anode. Because the resistivity of natural waters is generally at least a million times greater than that of structural steel, the current flows along the shortest anode-to-structure distance. On some experimental gates at the O'Brien Lock and Dam whose coating had badly deteriorated, current distribution was poor, even several months after the current was applied, although the distribution gradually improved and became adequate. Deposition of a carbonate film, which increases the resistance of structure surfaces on which it forms, causes this improvement and makes greater current density available for surfaces farther from the anode.

A paint coating in reasonably good condition largely eliminates shielding problems. In fact, a paint coating is generally necessary for cathodic protection systems on hydraulic structures.

The essential element of cathodic protection is the external current source which opposes the corrosion potential of the metal to be protected **at every point** of the exposed surface. This potential must be maintained over changes in structural geometry. To implement this, a design approach based on the continuum aspects of electric field analysis was investigated. This approach provides a practical overview that uses some versatile techniques such as curvilinear-square field mapping and superposition synthesis.

A field is defined as a region of space that possesses at each point some definite physical quantity that is a continuous function of the space coordinates. For example, the region in the vicinity of two surfaces that are maintained at a constant temperature difference may be thought of as a temperature field, since each point possesses a scalar quantity (temperature) and a vector quantity (temperature gradient). A map of this field would indicate various isotherms and heat flow lines. Similarly, maps of electric fields consist of lines of equal potential called equipotential lines, and flux lines connecting points on a current source, such as an anode, to a "sink," which would be the protected metal surface.

Large electrolyte tanks were constructed for performing laboratory electric field mapping of structural models. Three button anodes and a plane cathode sheet were placed in the 5-ft-long by 10-ft-wide by 4-ft-deep electrolyte tanks, as shown in Figure A7. A suitable halfcell (copper/copper sulfate or silver/silver chloride) was mounted on a microphone boom and moved to follow a particular equipotential line; sufficient coordinate points were noted to construct the field plots. The anodes were energized and the electric field plots were made. Figure A8 shows a field plot being made in one of the electrolyte tanks.

Figure A9 shows the electric field plot for a field resulting from energizing one of the anodes. In this case, the anode-to-cathode potential was adjusted to give a protective value of -0.850 V (with respect to a copper/copper sulfate reference electrode) at the cathode sheet. This plot shows the constant voltage contours.

This plot was made with no conducting materials in the electrolyte. The only interfering conductors were the metal walls of the electrolyte tank; this effect is observed by the deviation of the contour of the 1-V equipotential line. Figures A10 through A12 are field plots of a single anode energized in the electrolyte tank with a 1.5-sq-ft metal specimen intervening between the anode and cathode sheet.

Figure A10 shows the effect of fringing or shadowing associated with a plate of this size at right angles to the electric flux lines from the anode to the cathode sheet. Figure A11 shows the distortion of the field when the interfering specimen is oriented 45 degrees to the flux lines. Figure A12 is the field obtained when the interfering element is oriented parallel to the electric flux lines.

These field plots show that the relatively small interfering conductive object severely distorted the field; thus, even with a large surface area, such as the skin side of a miter gate, cathodic protection is affected drastically by the placement of an extraneous conductor whose area is only 5 to 10 percent of the gate area.

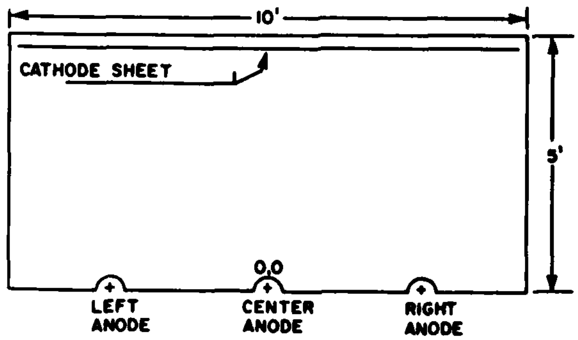

Figure A7. Typical electrolyte tank for model studies.

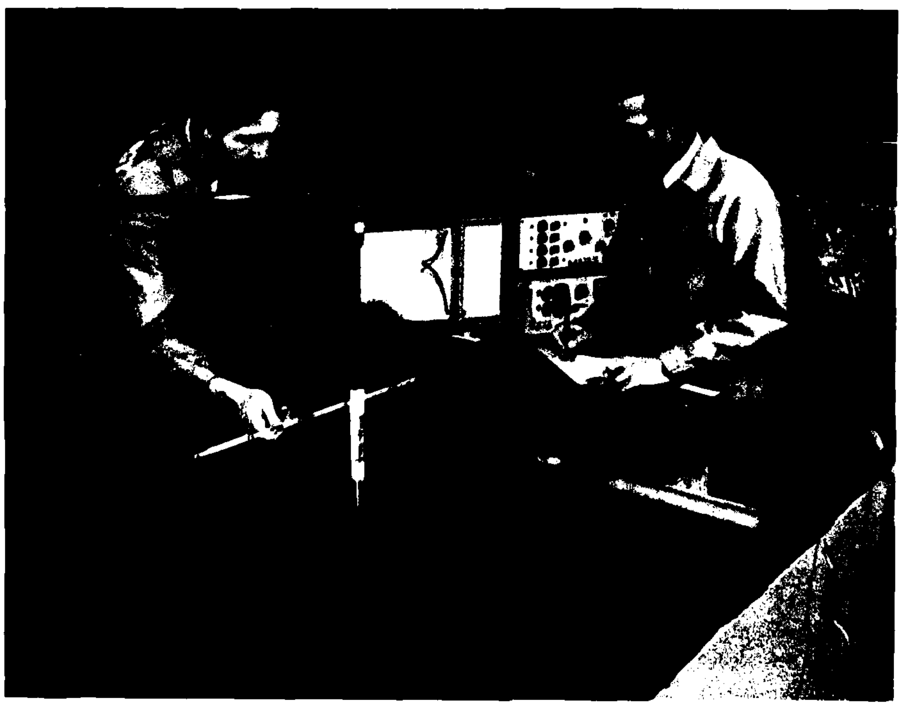

Figure A8. Field mapping in electrolyte tank.

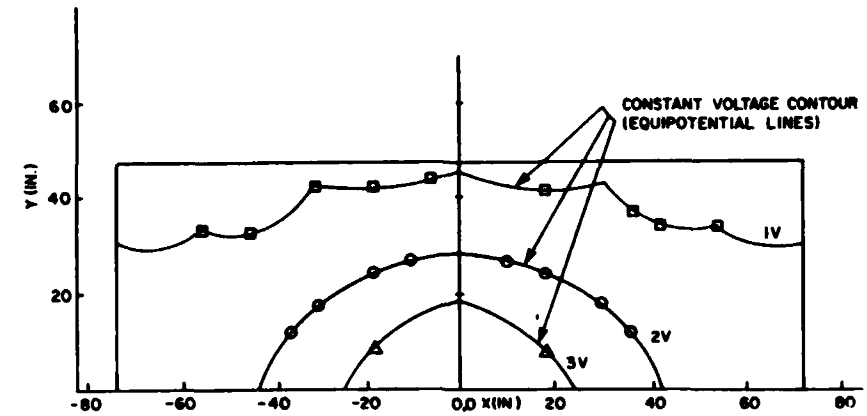

Figure A9. Electric field plot: single button anode energized.

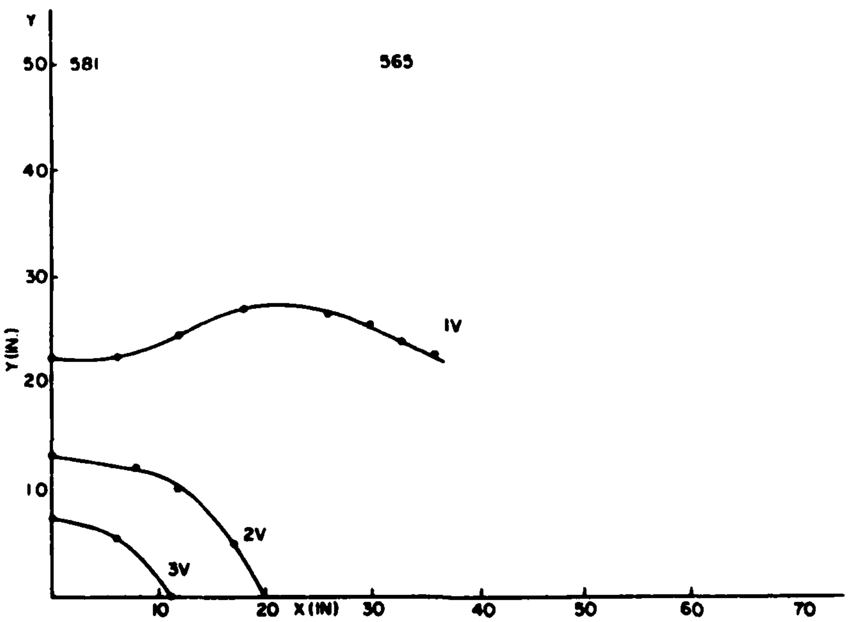

Figure A10. Small anode: shadowing.

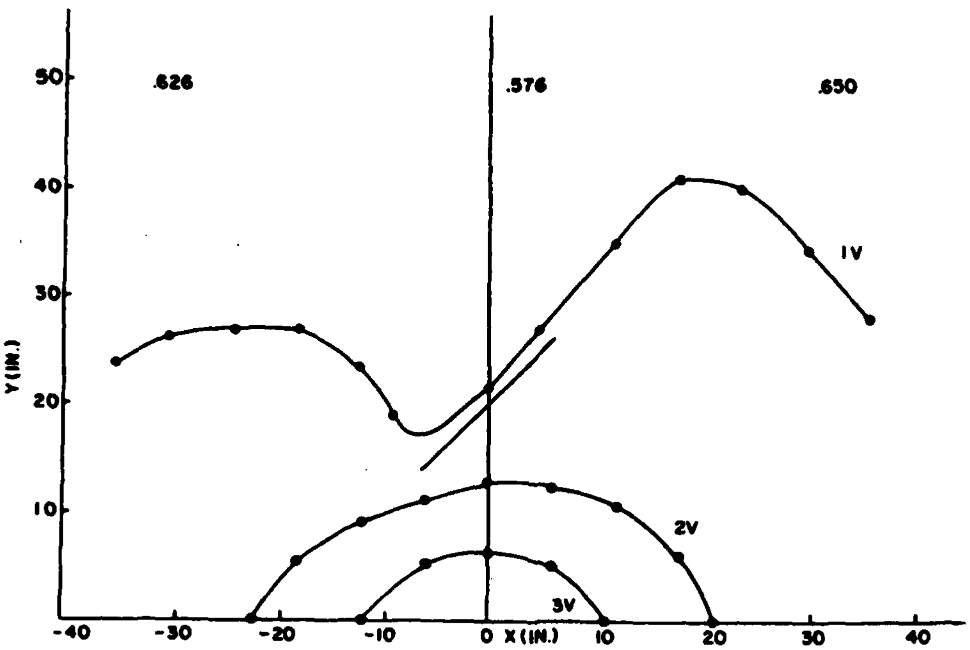

Figure A11. Shadowing: plate at 45 degrees.

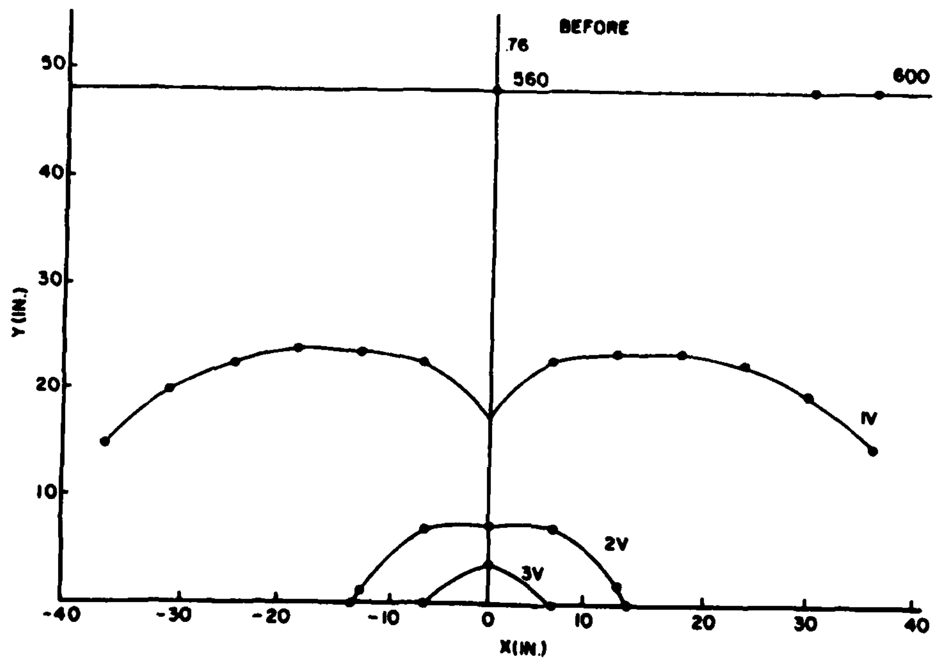

Figure A12. Shadowing: plate at 90 degrees.

APPENDIX B:

NONDESTRUCTIVE EVALUATION PROCEDURES—POLARIZATION MEASUREMENTS, ULTRASONIC TESTING

Polarization Measurements

The use of a continuous and instantaneous recording corrosion rate instrument reads and measures indirect corrosion current. It is impractical to place a measuring instrument or device under water on a retaining wall or lock surface, and since no net current occurs naturally, direct corrosion current readings are not possible. A corrosion rate instrument takes advantage of the fact that there is a measurable relationship between the direct corrosion current and the effect of an externally applied current on a metal's surface.

The most commonly used corrosion rate instrument uses a sensor probe consisting of three electrodes made up of the same metallurgical composition as the metallic structure under study. This sensor probe is placed in the water near, for example, the retaining wall where it will not be in the way or be damaged. The corrosion rate meter measures the corrosion rate by producing direct mils-per-year readings in the water where the structure is located. These readings can be recorded on a strip chart recorder, thereby providing an automatic system requiring little supervision. Figure 8 (p 19) shows the system used at the O'Brien Lock and Dam.

Ultrasonic Inspection

Ultrasonic inspection is a rapid, efficient, nondestructive method of detecting, locating and measuring defects in weldments and/or base materials. Ultrasonic inspection is gradually replacing radiography for inspecting welds during construction and maintenance because it is faster, cheaper, and safer. The ultrasonic range starts at 18,000 Hz but is usually stated as beginning at 20,000 hertz. Ultrasonic flaw detection is usually in the range of 1 and 5 MHz.

Ultrasonics uses low-energy, high-frequency mechanical vibrations, or sound waves. These sound waves are directed into the material by a handheld device called a transducer or search unit. The transducer converts the electrical pulses generated by the ultrasonic inspection unit into sound vibrations by means of a piezoelectric element, usually a ceramic wafer placed in contact with the material being tested. The sound vibrations travel into the test object and are reflected from geometric boundaries or from other boundaries formed by cracks, lack of fusion, slag inclusions, porosity, etc. Many of the vibrations are scattered and absorbed by the material; however, others are reflected to the transducer. The received sound is converted into electrical signals by the piezoelectric element and displayed on a cathode ray tube.

The sound vibrations emitted by the transducer or search unit must be coupled to the material being inspected by water, oil, grease, or glycerin to exclude all air. The emitted vibrations have properties similar to a beam of light. The vibrations will diverge from the transducer, be reflected at angles equal to the incident angle, and become weaker as distance from the transducer increases.

Two important considerations in selecting a transducer are its diameter and operating frequency. The higher the frequency, the greater the sensitivity will be;

however, this advantage may be offset if lower frequencies are needed to penetrate coarse-grained or very thick materials. The higher the frequency, the higher the sensitivity, with a decrease in penetration power. Correspondingly, the lower the frequency, the greater the penetrating power, with a decrease in sensitivity. Generally, the method for determining the right frequency is to choose the lowest frequency that satisfactorily indicates the smallest defect to be rejected. The Structural Welding Code, D.1, has specific charts and tables on ultrasonic inspection. A frequency of 2.25 MHz is recommended for weld inspection. Transducer size is determined by the scanning procedure, surface accessibility, etc. For example, small-diameter transducers will result in greater beam spread and will therefore have less capability of pinpointing a reflecting surface.

Most ultrasonic inspection of welds uses a straight beam or angle beam transducer. The straight beam transducer uses a longitudinal wave, which directs the sound into the material perpendicular to the surface. This method locates subsurface defects such as laminations or porosity on material of about 1/2 in. thick or larger (see Figure B1)

The angle beam transducer is a straight beam transducer mounted in a plastic wedge of a specific angle. The sound wave is introduced into the material of 45, 60, or 70 degrees, depending on the material thickness. This angle beam is a shear wave that travels at about one-half the speed of longitudinal waves. Most weld inspection is done with an angle beam transducer, as shown in Figure B2.

Most straight and angle beam techniques use the pulse-echo method where one transducer, or search unit, is both the transmitter and receiver of the ultrasonic sound waves. The transducer emits a burst of sound waves, then waits for reflected waves similar to sonar. The electrical signal striking the transducer, which is usually not more than 1 microsecond, makes the transducer vibrate during the driving period. The pulse duration is short, so that returning or reflected echoes from defects or boundaries lying close to the surface will appear as a separate indication, as shown in Figure B3. Such a presentation is called an A-scan and is a "time versus amplitude display." From the pip or pulse location on the cathode ray tube time line and its height of amplitude, the relative depth and size of the discontinuity can be estimated.

Ultrasonics are specifically applicable to inspecting sheet piling or lock gates to determine material thickness. Using an ultrasonic unit designed for measuring thickness, and knowing what the metal's thickness was at the time of construction, the inspector can easily determine how much material has corroded or eroded. For example, if the sheet piling was 0.375 in. thick when it was installed and the ultrasonic unit indicates that the present thickness is 0.125 in., 0.250 in. of the material has corroded or eroded. With this information, the corrosion engineer can determine the corrosion rate of the material and its approximate remaining service life.

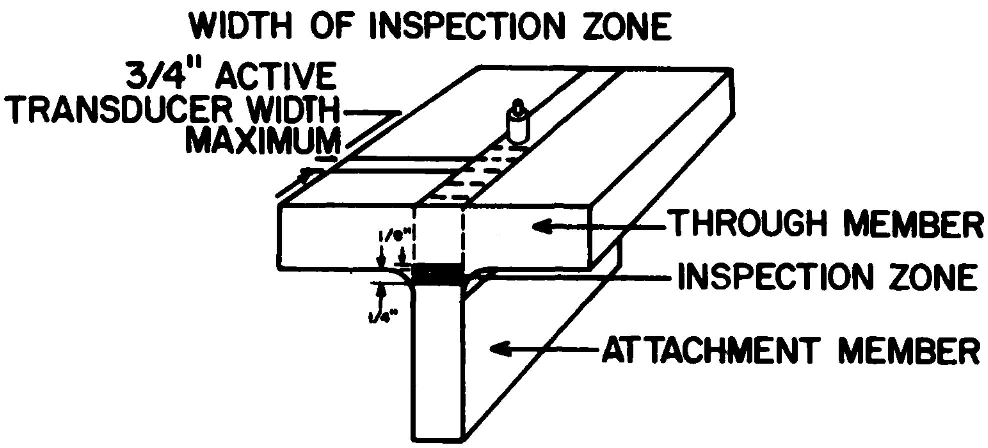

Figure B1. **Straight beam inspection techniques used in scanning a tee weld.**

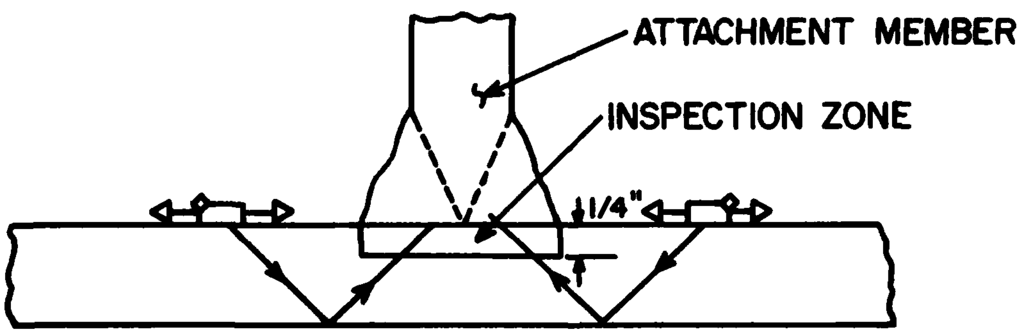

Figure B2. **Angle beam inspection technique used in scanning a tee weld.**

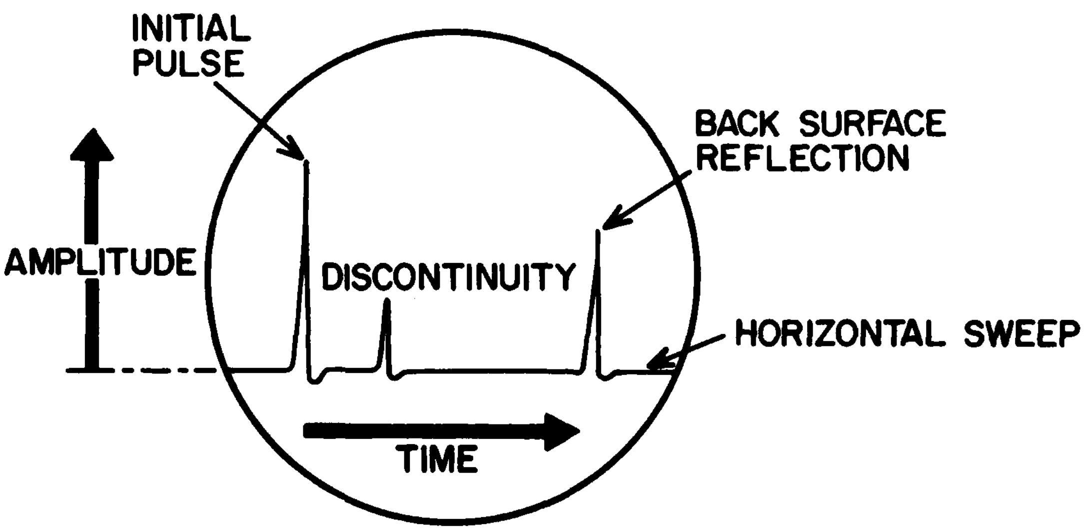

Figure B3. A-scan presentation on cathode ray tube.

APPENDIX C:

NOTATIONS

Elevations are measured from the level of the bottom of the sheet piling.

C	coefficient of active soil pressure
$\bar{C}$	coefficient of passive soil pressure
E	Young's modulus
F	shear force in a cross wall at the bottom of the chamber
F_1	reaction of the wall on the guide wall per unit length (Figure 29)
F_i	value of F_1 that will cause plastic hinges in the wall
F_2	reaction of the pile cap on the guide wall per unit length
H	elevation of the top of the fill
I	mean moment of inertia of the cross section of a unit width of the guide wall
I_o	initial value of I (before corrosion)
I_1	moment of inertia of a cross section of wall
K_1	edge fixity factor for a plate in the sheet piling
L	distance between successive cross walls or between successive tie rods
$M = M_x$	bending moment in a unit width of the guide wall
M_x, M_y, M_{xy}	bending and twisting moments in the orthotropic plate representing the guide wall (Timoshenko and Woinowsky-Krieger)
N_1, N_2	reactions (lb/in.) in elements of a claw of the sheet piling (Figure 22)
N_u	ultimate horizontal tension in the sheet piling (lb/in.)

N_x, N_y, N_{xy}	reactions in the orthotropic plate representing the guide wall (Timoshenko and Woinowsky-Krieger)
P	tension in a tie rod of the guide wall
σ_1	moment of area of the part of the cross section of the wall on one side of the neutral axis
σ_x, σ_y	transverse shears in the orthotropic plate representing the guide wall (Timoshenko and Woinowsky-Krieger)
R	radius of a cylindrical wall (Figure 23)
S=F/b'	shear flow in a cross wall at bottom of the chamber
a	elevation of the wall on a guide wall
b	outside width of a cofferdam (Figures 23 and 24)
b'	mean width of a cofferdam (b' = 0.96) (Figure 23)
c	distance from the neutral axis to the center of the outside wall of the sheet piling in a guide wall (Figure 28)
d	elevation of the bottom of the chamber or the river bottom adjacent to the wall
e_1, e_2, e_3	eccentricities in a claw of the sheet piling (Figure 22)
n	elevation of the surface of the water in the chamber or the river
k	constant in the equation, $I = I_o - k\varepsilon$
p (x)	net pressure at elevation x tending to overturn the land wall of the lock
q (x)	net pressure on a sheet pile at elevation x
x	elevation of surface of pore water in the fill
t	thickness of a web of the sheet piling, or of a bar representing a part of a claw. Also, it is the thickness of the outside flange of a sheet pile in the guide wall
T	horizontal tension

t_o	initial value of t (before corrosion)
t_1, t_2	thickness of a shank and a hook in a claw of the sheet piling (Figure 22). Also, t_1 is the thickness of the web of a channel of the wall.
w	width of a flat part of the sheet piling in the guide wall between centroids
x	elevation of an arbitrary point
y	a horizontal coordinate along a wall
V	specific weight of dry fill
V'	specific weight of fill submerged in water
V_w	specific weight of water
ε	reduction of thickness of a part due to corrosion
ε_{all}	the maximum allowable value of ε
σ_{cr}	compression stress to cause crumpling of the sheet piling
σ_y	yield stress of the steel
σ_u	ultimate tensile stress of the steel

USA-CERL DISTRIBUTION

Chief of Engineers
ATTN: Tech Monitor
ATTN: DAEN-IMS-L (2)
ATTN: DAEN-CCP
ATTN: DAEN-CW
ATTN: DAEN-CWE
ATTN: DAEN-CWM-R
ATTN: DAEN-CWO
ATTN: DAEN-CWP
ATTN: DAEN-EC
ATTN: DAEN-ECC
ATTN: DAEN-ECE
ATTN: DAEN-ECR
ATTN: DAEN-RD
ATTN: DAEN-RDC
ATTN: DAEN-RDM
ATTN: DAEN-RM
ATTN: DAEN-ZCE
ATTN: DAEN-ZCF
ATTN: DAEN-ZCI
ATTN: DAEN-ZCM
ATTN: DAEN-ZCZ

FESA, ATTN: Library 22060
ATTN: DET III 79906

US Army Engineer Districts
ATTN: Library (41)

US Army Engineer Divisions
ATTN: Library (14)

US Army Europe
AEAEN-ODCS/Engr 09403
ISAE 09081
V Corps
ATTN: DEH (11)
VII Corps
ATTN: DEH (15)
21st Support Command
ATTN: DEH (12)
USA Berlin
ATTN: DEH (11)
USASETAF
ATTN: DEH (10)
Allied Command Europe (ACE)
ATTN: DEH (3)

8th USA, Korea (19)

USA Japan (USARJ)
ATTN: AJEN-DEH 96343
ATTN: DEH-Honshu 96343
ATTN: DEH-Okinawa 96331

416th Engineer Command 60623
ATTN: Facilities Engineer

US Military Academy 10966
ATTN: Facilities Engineer
ATTN: Dept of Geography & Computer Science
ATTN: DSCPER/MAEN-A

AMMRC, ATTN DRXMR-WE 02172

USA ARRCOM 61299
ATTN: DRCIS-RI I
ATTN: DRSAR-IS

AMC - Dir., Inst., & Servc
ATTN: DEH (23)

DLA ATTN: DLA-WI 22314

DNA ATTN: NADS 20305

HSC
ATTN: HSLO F 78234
ATTN: Facilities Engineer
Fitzsimons AMC 80240
Walter Reed AMC 20012

INSCOM Ch, Instl. Div
ATTN: Facilities Engineer (3)

ROK/US Combined Forces Command 96301
ATTN: EUSA-HHC-CFC/Engr

MDW, ATTN: DEH (3)

MTMC
ATTN: MTMC-SA 20315
ATTN: Facilities Engineer (3)

NARADCOM, ATTN: DRDNA-F 01760

TARCOM, Fac. Div. 48090

TSARCOM, ATTN: STSAS-F 63120

USACC, ATTN: Facilities Engr (2)

WESTCOM
ATTN: DEH, Ft. Shafter 96858
ATTN: APEN-IM

SHAPE 09055
ATTN: Surv. Section, CCB-OPS
Infrastructure Branch, LANDA

HQ USEUCOM 09128
ATTN: ECJ 4/7-LOE

FORT BELVOIR, VA 22060 (7)
ATTN: Canadian Liaison Officer
ATTN: British Liaison Officer
ATTN: Australian Liaison Officer
ATTN: French Liaison Officer
ATTN: German Liaison Officer
ATTN: Water Resources Support Ctr
ATTN: Engr Studies Center
ATTN: Engr Topographic Lab.
ATTN: ATZA-DTE-SU
ATTN: ATZA-DTE-EM
ATTN: R&D Command

CRREL, ATTN: Library 03755

WES, ATTN: Library 39180

HQ, XVIII Airborn Corps
and Fort Bragg
ATTN: AFZA-FE-EE 28307

Area Engineer, AEDC-Area Office
Arnold Air Force Station, TN 37389

Chanute AFB, IL 61868
3345 CES/DE, Stop 27

Norton AFB, CA 92409
ATTN: AFRCE-MX/DEE

AFESC, Tyndall AFB, FL 32403

NAVFAC
ATTN: Engineering Command (7)
ATTN: Division Offices (6)
ATTN: Naval Public Works Center (9)
ATTN: Naval Civil Engr Lab. (3)

ATTN: Library, Code L08A NCEL 93043

Defense Technical Info. Center 22314
ATTN: DDA (2)

Engr Societies Library, NY 10017

Natl Guard Bureau Instl. Div 20310

US Govt Print Office 22304
Receiving Sect/Depository Copies (2)

US Army Env. Hygiene Agency
ATTN: HSHB-E 21010

National Bureau of Standards 20899

325
08/86

Metallurgy Team Distribution

Chief of Engineers
ATTN: DAEN-ECZ-A
ATTN: DAEN-ECB

US Army Engineer District
Philadelphia 19106
ATTN: Chief NAPEN-D
Balitmore 21203
ATTN: Chief, Engr Div
Norfolk 23510
ATTN: Chief, NAOEN-D
Wilmington 28401
ATTN: Chief, SAWEN-D
Charleston 29402
ATTN: Chief, Engr Div
Savannah 31402
ATTN: Chief, SASAS-L
Jacksonville 32232
ATTN: Const Div
Mobile 36652
ATTN: Chief, SAMEN-C
ATTN: Chief, SAMEN-D
Memphis 38103
ATTN: Chief, LMMED-DM
Vicksburg 39180
ATTN: Chief, Engr Div
Louisville 40201
ATTN: Chief, Engr Div
St. Paul 55101
ATTN: Chief, ED-D
Omaha 68102
ATTN: Chief, Engr Div
New Orleans 70160
ATTN: Chief, LMNED-DG
Little Rock 72203
ATTN: Chief, Engr Div
San Francisco 94105
ATTN: Chief, Engr Div
Sacramento 95814
ATTN: Chief, SPKED-D
Portland 97208
ATTN: Chief, DB-6
Seattle 98124
ATTN: Chief, NPSCO
Walla Walla 99362
ATTN: Chief, Engr Div
Alaska 99503
ATTN: Chief, NPASA-R

US Army Engineer Division
New England 02154
ATTN: Chief, NEDED-T
North Atlantic 10007
ATTN: Chief, NADEN-T
South Atlantic 30303
ATTN: Chief, SADEN-TS
Huntsville 35807
ATTN: Chief, HNDED-CS
ATTN: Chief, HNDED-SR
Ohio River 45201
ATTN: Chief, Engr Div
Southwestern 75202
ATTN: SWDED-TM
Pacific Ocean 96858
ATTN: Chief, Engr Div
North Pacific 97208
ATTN: Chief, Engr Div

West Point, NY 10996
ATTN: Library

Fort Leavenworth, KS 66027
ATTN: ATZLCA-SA

Fort McPherson, GA 30330
ATTN: AFEN-CD

Fort Monroe, VA 23651
ATTN: ATEN-AD (3)

6th US Army 94129
ATTN: AFKC-EN

7th US Army 90407
ATTN: AETTM-HRD-EHD

US Army Science & Technology 96328
Center - Far East Office

Tyndall AFB, FL 32403
AFESC/PRT

Dept of Transportation Library 20590

END

12-86

DTIC